Inaugural dissertation

for

obtaining the doctoral degree

of the

Combined Faculty of Mathematics, Engineering and Natural Sciences

of the

Ruprecht – Karls - University

Heidelberg

Presented by

M. Sc. Feyza Gül Özbay Kurt

Born in: Texas, USA

Oral examination: 22.09.2023

Targeting MDSC-mediated immunosuppression in melanoma

Referees:

apl. Prof. Dr. Viktor Umansky

Prof. Dr. Adelheid Cerwenka

Summary

Immunotherapeutic strategies for malignant melanoma have made significant progress but are still challenged by the development of resistance in a subset of patients. One of the factors contributing to this resistance is the accumulation of myeloid-derived suppressor cells (MDSC) in the melanoma microenvironment. MDSC are a heterogeneous population of myeloid cells that can inhibit anti-tumor T cell responses, thereby promoting immunosuppression and facilitating tumor progression. TLR4 and RAGE signaling are considered as important regulators of MDSC accumulation and acquisition of their immunosuppressive functions. Damage-associated molecular patterns (DAMPs) such as S100A8/9, high mobility group box 1 (HMGB1), and heat shock proteins (HSPs) that act as ligands for TLR4 or RAGE were reported to drive MDSC accumulation and to be significantly expressed in the tumor microenvironment (TME) of solid tumors. However, a precise role of TLR4 and RAGE signaling in the acquisition of immunosuppressive properties by MDSC requires further elucidation. The present study aims to evaluate the impact of endogenous TLR4 ligands and TLR4 signaling on MDSC-mediated immune suppression in malignant melanoma.

MDSC were purified from the peripheral blood of late-stage melanoma patients and were generated *in vitro* from healthy donor-derived monocytes. Normal monocytes were treated with recombinant (r) HSP90α for 24h or with rS100A9 and rHMGB1 in the presence of GM-CSF for 72 h. The immunosuppressive capacity of MDSC and stimulated monocytes were assessed in T cell inhibition assays. In addition, TLR4 inhibitor (Resatorvid) and RAGE inhibitor (FPS-ZM1) were tested in these assays. Expression of immunosuppression related markers and pathways involved in the MDSC stimulation were assessed by flow cytometry, Western Blot, and gene expression profiling. The levels of S100A8/9 and HMGB1 were measured in the plasma of melanoma patients by ELISA. The Cancer Genome Atlas (TCGA) data analysis was performed to evaluate the association between the expression of immunosuppressive markers and S100A9 and HMGB1 in the TME of melanoma.

Stimulation of monocytes with HSP90α, S100A9 and HMGB1 resulted in the acquisition of suppressive activity against T cells via increased production of reactive oxygen species (ROS) and nitric oxide (NO) as well as upregulated expression of programmed death ligand-1 (PD-L1) and indoleamine 2,3-dioxygenase (IDO). Increased plasma levels of S100A8/9 was found to be correlated with the expression of immunosuppressive markers on MDSC in the peripheral blood of melanoma patients. Importantly, the blockade of TLR4 signaling and, to a lesser extent

RAGE signaling, resulted in a substantial attenuation of T cell inhibition. The supernatant of *in vitro* generated MDSC contained a significantly higher levels of S100A8/9 and HMGB1 than in that from patient derived MDSC Furthermore, elevated plasma levels of S100A8/9 were found to be associated with a poor progression free survival (PFS) in melanoma patients.

In conclusion, this study highlights the crucial role of TLR4 and, to a lesser extent RAGE signaling, as well as TLR4 ligands S100A9 and HMGB1 in the acquisition of immunosuppressive properties by MDSC in malignant melanoma. These findings suggest that targeting TLR4 signaling pathway may represent a promising therapeutic strategy to overcome MDSC-mediated immune suppression and enhance the efficacy of melanoma immunotherapy.

Zusammenfassung

Immuntherapien zur Behandlung des malignen Melanoms haben erhebliche Fortschritte gemacht, das Therapieansprechen wird jedoch bei einer großen Patientengruppe durch die Entwicklung von Resistenzen beeinträchtigt. Einer der Faktoren, die zu einer solchen Resistenz beitragen, ist die Akkumulation von myeloiden Suppressorzellen (MDSC) in der Mikroumgebung des Melanoms. Bei MDSC handelt es sich um eine heterogene Population myeloider Zellen, die die T-Zell-Antwort gegen den Tumor hemmen und so die Immunsuppression fördern können, wodurch das Voranschreiten der Tumorerkrankung begünstigt wird. Signalkaskaden, die durch Toll-like Rezeptor 4 (TLR4) und Receptor for advanced glycosylation end products (RAGE) ausgelöst werden, gelten als wichtige Regulationsmechanismen für die Akkumulation von MDSC und den Erwerb ihrer immunsuppressiven Funktionen. Studien haben gezeigt, dass schadensassoziierte molekulare Muster (engl. damage-associated molecular patterns, DAMPs) wie S100A8/9, High Mobility Group Box 1 (HMGB1), und Hitzeschockproteine (engl. heat shock proteins, HSPs) als Liganden für TLR4 oder RAGE fungieren und so die Akkumulation von MDSC begünstigen können. Es wurde ebenfalls herausgefunden, dass jene Moleküle in der Tumormikroumgebung (TME) von soliden Tumoren in signifikanter Menge vorhanden sind. Die genaue Rolle der TLR4- und RAGE-Signalwege bei der Erlangung immunsuppressiver Eigenschaften durch MDSC ist jedoch noch nicht ausreichend geklärt. Die vorliegende Studie hat das Ziel, die Bedeutung endogener TLR4-Liganden und des TLR4-Signalwegs für die MDSC-vermittelte Immunsuppression beim malignen Melanom zu untersuchen.

MDSC wurden aus dem peripheren Blut von Melanompatienten (Stadium IV) isoliert oder *in vitro* aus Monozyten von gesunden Spendern generiert. Hierfür wurden die Monozyten 24 Stunden lang mit rekombinantem (r) HSP90α oder 72 Stunden lang mit rS100A9 und rHMGB1 in Gegenwart von GM-CSF behandelt. Die immunsuppressive Kapazität der MDSC und der stimulierten Monozyten wurde in T-Zell-Inhibitionstests untersucht. Darüber hinaus wurden die Effekte eines TLR4-Inhibitors (Resatorvid) und eines RAGE-Inhibitors (FPS-ZM1) in T-Zell-Suppressionstests getestet. Die Expression von Markern, die mit der Immunsuppression und mit Signalwegen, die an der MDSC-Stimulation beteiligt sind, in Zusammenhang stehen, wurde mittels Durchflusszytometrie, Western Blotting und Genexpressionsanalyse untersucht. Die Konzentrationen von S100A8/9 und HMGB1 wurden im Plasma von Melanompatienten mittels ELISA gemessen. Eine TCGA-Datenanalyse wurde durchgeführt, um den Zusammenhang zwischen der Expression von immunsuppressiven Markern und S100A9 sowie HMGB1 im TME des Melanoms zu bewerten.

Die Stimulation von Monozyten mit HSP90α, S100A9 und HMGB1 führte durch eine erhöhte Produktion von reaktiven Sauerstoffspezies (ROS) und Stickstoffmonoxid (NO) sowie zu einer Hochregulation von PD-L1 und Indolamin-2,3-Dioxygenase (IDO) zur Erlangung einer suppressiven Aktivität gegenüber T-Zellen. Es konnte weiterhin festgestellt werden, dass erhöhte Plasmaspiegel von S100A8/9 mit der Expression von immunsuppressiven Markern auf MDSC im peripheren Blut von Melanompatienten korrelierten. Die Blockade des TLR4-Signalwegs führte zu einer erheblich verminderten der T-Zell-Inhibitiion; in geringerem Maße war dies auch für die Blockade des RAGE-Signalwegs zutreffend. Der Überstand von in vitro erzeugten MDSC enthielt signifikant höhere Konzentrationen von S100A8/9 und HMGB1 als der Überstand von MDSC, die von Patienten stammen. Darüber hinaus wurde festgestellt, dass erhöhte Plasmaspiegel von S100A8/9 mit einem schlechteren progressionsfreien Überleben (PFS) bei Melanompatienten korrelierten.

Zusammenfassend zeigt diese Studie die entscheidende Rolle von TLR4, in geringerem Maße auch von RAGE, sowie deren Interaktion mit endogenen TLR4-Liganden wie S100A9 und HMGB1 bei der Erlangung immunsuppressiver Eigenschaften durch MDSC beim malignen Melanom auf. Die Ergebnisse deuten darauf hin, dass die Beeinflussung des TLR4-Signalwegs eine vielversprechende therapeutische Strategie zur Überwindung der MDSC-vermittelten Immunsuppression und zur Verbesserung der Wirksamkeit der Melanom-Immuntherapie darstellen könnte.

Table of contents

List of abbreviations

ALEs   Advanced lipoxidation end products

AP-1   Transcription factor activator protein-1

ARG1   Arginase 1

ATRA   All-trans retinoic acid

BCA   Bicinchoninic acid

Bcl2   B-cell lymphoma 2

bFGF   Basic fibroblast growth factor

BTLA   B and T lymphocyte attenuator

C/EBP-β   CCAAT/enhancer binding proteins

CAF   Cancer-associated fibroblasts

CMP   Common myeloid progenitors

CTLA-4   Cytotoxic T-lymphocyte-associated protein 4

DAMPs   Damage-associated molecular patterns

DCs   Dendritic cells

DMSO   Dimethyl sulfoxide

DPBS   Dulbecco's phosphate-buffered saline

ELISA   Enzyme-linked immunosorbent assay

Evs   Extracellular vesicles

FACS   Fluorescence-activated cell sorting

FAO   Fatty acid oxidation

FATP2   Fatty acid transport protein 2

G-CSF   Granulocyte colony-stimulating factor

GITR   Glucocorticoid-induced TNFR-related protein

M-MDSC   Monocytic-MDSC

mAbs   Monoclonal antibodies

MACS   Magnetic-activated cell sorting

MAPK   Mitogen-activated protein kinases

MDSC   Myeloid-derived suppressor cells

miRNAs   MicroRNAs

MMP9   Matrix metalloproteinase 9

MyD88   Myeloid differentiation primary response 88

NF-κB   Nuclear factor kappa B

NF1   Neurofibromin 1

NK   Natural killer

NO   Nitric oxide

ORA   Over Representation Analysis

OS   Overall survival

P/S   Penicillin/streptomycin

PAMPs   Pathogen-associated molecular patterns

PBMCs   Peripheral blood mononuclear cells

PD-1   Programmed cell death protein 1

PD-L1   Programmed cell death ligand-1

PDE5   Phosphodiesterase-5

PGE2   Prostaglandin E2

PI3K   Phosphatidylinositol 3-kinase

PMN-MDSC   Polymorphonuclear-MDSC

PFS   Progression-free survival

RAGE   Receptor for advanced glycation end products

ROS   Reactive oxygen species

SLAM   Signaling lymphocytic activation molecule

STAT-3   Signal transducer and activator of transcription 3

T-VEC   Talimogen laherparepvec

TAM   Tumor-associated macrophages

TBS   Tris Buffered Saline

TCGA   The Cancer Genome Atlas

TGF-β   Transforming growth factor-β

Th1   T helper cell

Tim-3   Lymphocyte activation gene-3

TIRAP   TIR domain-containing adapter protein

TLR4   Toll-like receptor 4

TME   Tumor microenvironment

TNF-α   Tumor necrosis factor alpha

TRAF6   TNF receptor-associated factor 6

TRAIL   TNF-related apoptosis-inducing ligand

TRAM   TRIF related adaptor molecule

Treg   Regulatory T cells

TRIF   TIR domain containing adapter-inducing IFNβ

UV   Ultraviolet

VEGF   Vascular endothelial growth factor

VEGF   Vascular endothelial growth factor

VISTA   V-domain Ig suppressor of T cell activation

5-FU   5-fluorouracil

List of tables

List of figures

List of own publications during the thesis work

<u>Özbay Kurt, F.G</u>.; Lasser S.; Arkhypov I.; Utikal J.;Umansky V. Enhancing immunotherapy response in melanoma: myeloid-derived suppressor cells as a therapeutic target. J Clin Invest. 2023, 133 (13), e170762.

<u>Özbay Kurt, F.G</u>.; Lepper, A.; Gerhards, C.; Roemer, M.; Lasser, S.; Arkhypov, I.; Bitsch, R.; Bugert, P.; Altevogt, P.; Gouttefangeas, C.; Neumaier M.; Utikal J.; Umansky V. Booster dose of mRNA vaccine augments waning T cell and antibody responses against SARS-CoV-2. Front. Immunol.2022, 13, 1012526.

Arkhypov, I.*; **<u>Ozbay Kurt, F.G</u>**.*; Bitsch, R.; Novak, D.; Petrova, V.; Lasser, S.; Hielscher, T.; Groth, C.; Lepper, A.; Hu, X; Li, Wi; Utikal, J; Altevogt P; Umansky, V. HSP90alpha induces immunosuppressive myeloid cells in melanoma via TLR4 signaling. J. Immunother Cancer 2022, 10, e005551.

Bitsch R, Kurzay A, **<u>Ozbay Kurt F</u>**, De La Torre C, Lasser S, Lepper A, Siebenmorgen A, Muller V, Altevogt P, Utikal J, Umansky V. STAT3 inhibitor napabucasin abrogates MDSC immunosuppressive capacity and prolongs survival of melanoma-bearing mice. J Immunother Cancer. 2022.https:// doi. org/ 10. 1136/ jitc- 2021- 004384.

Kursunel MA, Taskiran EZ, Tavukcuoglu E, Yanik H, Demirag F, Karaosmanoglu B, **<u>Ozbay F.G.;</u>** Uner A; Esendagli D; Kizilgoz D; Yilmaz U; Esendagli G. Small Cell Lung Cancer Stem Cells Display Mesenchymal Properties and Exploit Immune Checkpoint Pathways in Activated Cytotoxic T Lymphocytes. Cancer Immunol Immunother (2021).doi: 10.1007/s00262-021-02998-1.

Groth C, Weber R, Lasser S, **<u>Özbay FG</u>**, Kurzay A, Petrova V,Altevogt P, Utikal J, Umansky V. Tumor promoting capacity of polymorphonuclear myeloid-derived suppressor cells and their neutralization. Int J Cancer. 2021 Nov 1;149(9):1628–1638.doi:10.1002/ijc.33731.

*Equally contributed

1 Introduction

1.1 Cancer Immunoediting

The concept of cancer immunoediting emphasizes how the immune system performs a dual function, serving as a defender of the host while also sculpting the tumors (1). Cancer immunoediting comprises three phases: elimination, equilibrium, and escape (2). Initially, immune surveillance eliminates tumor cells (elimination), but some remaining cells become dormant and coexist with immune cells (equilibrium). Eventually, these cells develop mechanisms to evade immune reactions (escape) (2). These three phases of cancer immunoediting exhibit the complex interplay between the cancer cells and immune system during different stages of tumor development and progression (3).

1.1.1. Elimination

The first phase of cancer immunoediting is "elimination" where the adaptive and innate immune systems synergize to detect and eradicate early tumors when they are not yet clinically detectable (4). Tumor antigens and stress-induced molecules such as surface calreticulin presented by MHC class I molecules and NKG2D ligands on tumor cells are recognized by CD8$^+$ effector cells and natural killer (NK) cells, respectively (4). Tumor antigens can be also taken up and cross-presented by dendritic cells (DCs) to T cells. Activated T and NK cells release interferon (IFN)-γ, which exerts anti-tumor effects by suppressing tumor cell proliferation and angiogenesis (5).

CD8 T cells can promote tumor cell apoptosis through secreting granzymes and perforin or interacting with TNF-related apoptosis-inducing ligand (TRAIL) and Fas receptors on tumor cells (6). Moreover, co-stimulatory molecules such as CD137, glucocorticoid-induced TNFR-related protein (GITR), OX40, and CD28 expressed by effector T cells can enhance their proliferation and survival (7). Danger signals released by dying tumor cells or damaged tissues include type I IFNs, which activate immune cells and provide anti-tumor immune response. Type I IFNs, IFN-α/β, were reported to activate DCs and to improve the cytotoxic activity of NK cells by inducing TRAIL (8). Furthermore, tumor-derived type I IFNs foster the development of memory CD8 T cells by inducing interleukin (IL)-15 (9). Additionally, classically activated (M1) macrophages and granulocytes play role in promoting anti-tumor immunity by releasing IL-1, IL-12, tumor necrosis factor (TNF)-α, and reactive oxygen species (ROS) (10, 11). In the elimination phase, the immune cells destroy tumor cells, showing an increased expression of

tumor antigens, Fas and TRAIL receptors, and MHC class I molecules on tumor cells (5). Moreover, tumor microenvironment (TME) exhibits an abundance of perforin, granzymes, IL-12, IL-1, TNF-α, and IFN-α/β/γ further enhancing the anti-tumor activity (12).

1.1.2. Equilibrium

If the immune system fails to eliminate growing tumor cells, the cancer enters equilibrium phase. During this phase, tumor outgrowth is immunologically restrained yet not eradicated (13). The interaction between tumor cells and the adaptive immune system is maintained in a durable equilibrium over a long period, which spans years or even decades (14). Within this phase, certain tumor cells undergo genetic and epigenetic alterations, resulting in the emergence of tumor cell variants, which can evade immune recognition (such as defects in antigen-presentation or antigen loss) and promote immunosuppression (via programmed cell death ligand-1 (PD-L1) expression) (5). A delicate equilibrium is maintained between anti-tumor cytokines such as IL-12 and IFN-γ and cytokines that facilitate tumor growth including IL-10 and IL-23 (15).

1.1.3. Escape

When tumor cells undergo genetic mutations or are influenced by other stimuli, they shift from equilibrium phase to the escape phase. In the escape phase, tumor cells express various immunosuppressive ligands to inhibit the function of effector T cells and evade immune cell attack (16). The growth and proliferation of tumors are no longer restricted by the immune system. As a result, the accumulation of rapidly proliferating tumor cells along with other stromal cells facilitates the development of a more complex immunosuppressive microenvironment, further disrupting the balance between the immune system and tumor cells (17). Despite notable advancements in cancer detection, tumors in the elimination and equilibrium phases are generally difficult to detect. Therefore, when tumors are clinically diagnosed, the majority of them have already entered the escape phase (13). Tumor cell escape can be mediated through different mechanisms such as diminished immune recognition by the loss of tumor antigens, co-stimulatory or MHC class I molecules, via elevated resistance mediated by augmented expression of signal transducer and activator of transcription 3 (STAT-3) or anti-apoptotic protein B-cell lymphoma 2 (Bcl2), and by the development of an immunosuppressive tumor microenvironment orchestrated by cytokines such as vascular endothelial growth factor (VEGF) and transforming growth factor-β (TGF-β) as well as by immunoregulatory molecules like indoleamine 2,3-dioxygenase (IDO),

programmed cell death protein 1 (PD-1)/PD-L1, T cell immunoglobulin and mucin domain-containing protein 3 (Tim-3)/galectin-9, and lymphocyte activation gene-3 (LAG-3) (18, 19). Additionally, other factors have been identified such as CD73, adenosine receptors, and novel B7 family checkpoint molecules like V-domain Ig suppressor of T cell activation (VISTA) and B and T lymphocyte attenuator (BTLA) that contribute to tumor-induced immunosuppression (5, 20). Recruitment of immunosuppressive cells is one of the escape mechanisms that tumors develop. Regulatory T cells (Treg) alternatively activated (M2) macrophages, and myeloid-derived suppressor cells (MDSC) are among the immunosuppressive cells, which support the immunosuppressive microenvironment by inhibiting the function of effector T and NK cells (21, 22).
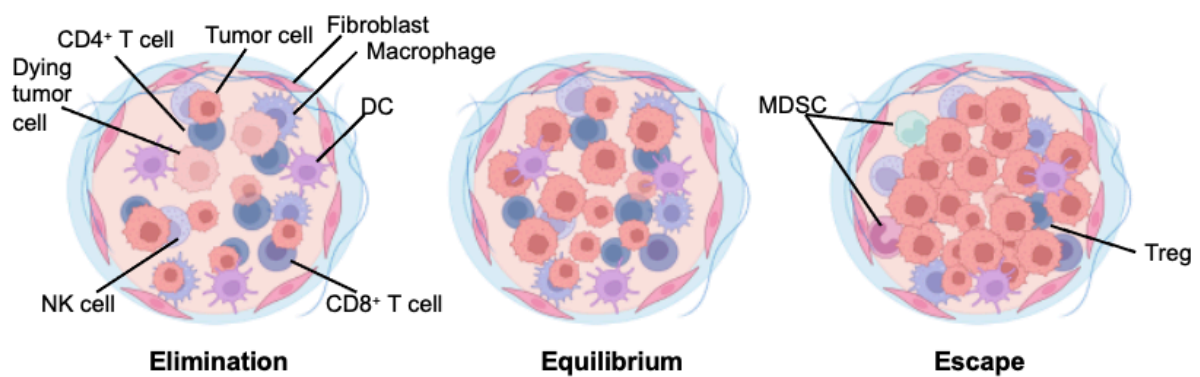
Figure 1. Three stages of cancer immunoediting: elimination, equilibrium, and escape.

1.1.4 Cancer immunoediting in immunotherapy

The process of cancer immunoediting occurs not only during the natural progression of tumors but also in response to immunotherapy (13). Tumors can be driven back to the elimination phase by effective immunotherapy, which can be reflected as a complete response. On the other hand, if the immunotherapy fails to completely overcome the immunosuppression in the TME, tumors can be forced into an equilibrium phase characterized by a partial response (5, 23). The emergence of certain tumor cell clones with the capacity to elude or suppress the immune responses can lead to secondary escape, which is clinically recognized as acquired resistance to therapy (24). The optimal strategies to achieve effective tumor elimination include therapeutic combinations to induce immune activation and T cell priming, inhibiting immunosuppressive signals in the TME, and maintaining a robust presence of T cells with the TME (25).

Cancers are characterized by an increased mutation rate (5). Tumors with high mutational burden express immunogenic neoantigens, which can be recognized by T cells, and patients with these tumors are more likely to give response to immune checkpoint inhibitors (ICI) (26). Cancers with high somatic tumor mutation burdens comprise cutaneous melanomas, urothelial carcinomas, lung carcinomas, and microsatellite instability-high colorectal carcinomas (27). The frequency of patients with these cancers that respond to ICI is higher than the proportion of patients carrying other epithelial cancers with lower tumor mutation burden (5, 27). However, in cancers with relatively low mutation burden including pancreatic and breast cancer, tumor-reactive T cells have been detected (28). This observation indicates that several confounding factors could modulate the therapy response, including epigenetic variations among tumors in different individuals, which can impact the expression of neoantigens, the existence of immunosuppressive factors in the TME, and the random generation of neoantigens (2, 29). Patients who have tumors with a transcriptional signature characterized by increased inflammation (hot tumor) and enriched in genes associated with IFNγ response demonstrate better prognosis and a better response to immunotherapies compared to those with a tumor showing lower inflammation (cold tumor) (30). The latter tumors can be classified into two phenotypes i) immune-desert tumors, which lack T cells within the tumor tissue and the TME and ii) immune cell-excluded tumors, where T cells are present in the tumor stroma but absent in the tumor (31, 32). The second phenotype indicates the absence of anti-tumor immune response and patients with these tumor types generally exhibit unfavorable responses to anticancer immunotherapies (5).

TME can determine the resistance to immunotherapies (21, 23). Tumors characterized by high tumor mutational burden and T cell-inflamed gene signature exploit several mechanisms to escape from therapy (28). These mechanisms involve loss of tumor antigen expression, insensitivity to interferons or cytokine dysregulation, and adaptive immune resistance (upregulation of PD-L1 expression in tumor infiltrating immune cells and tumor cells in response to IFNγ). The immunosuppressive environment created by Treg, MDSC, tumor-associated macrophages (TAM), and immunosuppressive cytokines can dampen the anti-tumor immune responses (33). Hence, it is critical to gain a better understanding of the specific immunosuppressive mechanisms employed by each tumor to identify suitable combinations of anticancer immunotherapies (16). Therapeutic combinations are necessary to be optimized to promote immune activation and T cell priming, to inhibit immunosuppressive pathways, leading to the accumulation of T cells in the TME (23, 33).

1.2 Malignant melanoma

Melanoma arises from the malignant transformation of melanocytes located in various locations within the body, including the skin, conjunctiva, mucosal surfaces, and uveal structures (34). Although it comprises only 1 % of all skin malignant tumors, it is considered the most aggressive and lethal type of skin cancer (35). Melanoma primarily arises from exposure to ultraviolet (UV) light emitted by the sun, which induces DNA damage, triggering cell cycle arrest and apoptosis. However, in cancer cells, apoptosis is circumvented and cell division persists at an accelerated pace despite DNA damage (36). The development of malignant melanoma is primarily driven by oncogenic factors, leading to the constant activation of the mitogen-activated protein kinases (MAPK) pathway, which involves mutations in genes such as BRAF (40-50% of cases), NRAS (20-30% of cases), and neurofibromin 1 (NF1) (10-15% of cases (37).

1.2.1 Therapeutic strategies in malignant melanoma

The primary treatment strategy for melanoma is surgical resection. However, successful outcomes are only achieved in patients with earlier stage melanoma with minimal metastasis (38). Systemic therapy is generally employed for the treatment of unresectable metastatic melanoma. Radiotherapy has been used to treat melanoma, both locally and systemically, yet it has shown resistance and an elevated risk of secondary cancers like leukemia (39). Another commonly used systemic therapy is chemotherapy, which induces cytotoxicity. The effectiveness of chemotherapy, however, is suppressed by the development of resistance and it can also result in substantial toxicity to healthy tissues (40).

Currently, targeted therapies including a combination of selective inhibitors targeting mutant BRAF (dabrafenib, encorafenib, or vemurafenib) and MEK inhibitors (trametinib, binimetinib, or cobimetinib) are currently employed to treat metastatic melanoma (37). These inhibitors have demonstrated lower toxicity and increased overall survival (OS) compared to classical chemotherapy (41). However, the effectiveness of MEK and BRAF inhibitors is limited due to the development of resistance in a significant number of patients (42).

Melanoma possesses a high mutational burden and exhibits extensive immune infiltration, making it an ideal candidate for immunotherapy (43). Currently approved immunotherapeutic approaches include targeting PD-1 with antibodies nivolumab and pembrolizumab, targeting cytotoxic T-lymphocyte-associated protein 4 (CTLA-4) with antibody ipilimumab, or employing

a combination of antibodies against PD-1 and CTLA-4 (44). Although ICI showed a high response rate and improved clinical outcomes (45), the development of resistance mechanisms reduced the treatment effectiveness (46). Resistance to ICI primarily arises from insufficient generation or dysfunction of anti-tumor effector T cells and from an inadequate formation of memory T cells (47).

T-VEC, a modified oncolytic herpes virus, was designed to replicate solely within melanoma cells and was approved for intratumoral injection in non-resectable melanoma lesions (48). Its mechanism involves the lysis of melanoma cells while triggering the secretion of granulocyte-macrophage colony-stimulating factor (GM-CSF) by melanoma cells, thereby promoting the accumulation of host immune cells (49). In a phase III clinical trial testing the efficacy of T-VEC, patients with late-stage melanoma demonstrated an improved durable response rate (50).

1.3 Myeloid-derived suppressor cells (MDSC)

MDSC are myeloid cells that can be immature or mature and possess immunosuppressive functions (51, 52). They accumulate in chronic inflammatory conditions like autoimmune diseases, cancer, and chronic infections (52). Under normal circumstances, hematopoietic progenitor cells (HPC) differentiate into common myeloid progenitors (CMP) in the bone marrow. These progenitors then give rise to immature myeloid cells, which eventually develop into macrophages, DCs, and granulocytes (35). Pathological conditions including chronic inflammation and cancer disrupt the normal differentiation process and lead to the accumulation of immature myeloid cells (53). These MDSC exhibit weak phagocytic activity, display anti-inflammatory and immunosuppressive functions as well as immature characteristics (54). Mature myeloid cells can be converted into MDSC by tumor-derived extracellular vesicles (EVs) (55). For example, melanoma-derived EVs induced the differentiation of monocytes into immunosuppressive MDSC through specific miRNA molecules (55) and toll-like receptor 4 (TLR4) signaling (56). MDSC can be categorized into two major subsets: polymorphonuclear (PMN-MDSC), which resemble granulocytes, and monocytic (M-MDSC), resembling monocytes. In humans, a small subset of more immature myeloid cells known as early-stage (e)-MDSC was described (57). In mice, M-MDSCs are defined as $CD11b^+Ly6G^-Ly6C^{hi}$ and PMN-MDSCs as $CD11b^+Ly6G^+Ly6C^{lo}$. In humans, M-MDSC express CD14, CD33, and CD11b, but lack CD15 and have low or no expression of human leukocyte antigen (HLA)-DR, while PMN-MDSC are negative for CD14 and show

CD15, CD33, CD11b as well as low or no HLA-DR expression. Additionally, e-MDSC are defined as HLADR$^-$CD33$^+$CD14-CD15$^-$ cells (54).

Human M-MDSC can be separated from monocytes by evaluating the level of HLA-DR expression. Unlike neutrophils, which are separated using a higher density gradient, PMN-MDSC are found in the low-density phase after gradient centrifugation (54). Lectin-like oxidized low-density lipoprotein receptor (LOX-1), was found to be a potential marker to distinguish human PMN-MDSC from normal neutrophils (58). Additionally, co-expression of CD84, one of the member of signaling lymphocytic activation molecule (SLAM) family, and JAML, a member of the junctional adhesion molecule (JAM) family, has been demonstrated on human MDSC correlating with their suppressive (59). Despite the presence of MDSC markers and their defined phenotypes, the identification of MDSC still relies on assessing their suppressive activity due to the shared gene expression patterns with conventional monocytes or neutrophils (51).

1.3.1 MDSC accumulation and recruitment

Two partially overlapping signals are necessary for the accumulation and activation of MDSC (Figure 2) (51). The first group of signals includes tumor cell-derived mediators like stem cell factor (SCF), GM-CSF, granulocyte colony-stimulating factor (G-CSF), monocyte colony-stimulating factor (M-CSF), and vascular endothelial growth factor (VEGF). These mediators stimulate myelopoiesis and promote the expansion of MDSC by activating STAT and janus kinase (JAK) proteins (60). Transcription factors such as STAT3, STAT4, CCAAT/enhancer binding proteins (C/EBP-β), Notch, and interferon regulatory factor (IRF) 8 contribute to MDSC accumulation (61).

The second group of signals consists of inflammatory cytokines produced mainly by host cells in the TME, such as IL-6, IL-4, IL-1β, and prostaglandin E2 (PGE2). Additional molecules like TLR agonists and damage-associated molecular patterns (DAMPs) like tumor-derived heat shock proteins (HSPs), high mobility group box 1 (HMGB1), S100 calcium-binding proteins, and complement component C5a also contribute to MDSC generation (62). Prolonged secretion of these mediators can activate MDSCs and enhance their immunosuppressive activity (62). Transcription factors STAT1, nuclear factor kappa B (NF-κB), and STAT6 are also involved in this process (63). High levels of cytokines such as IL-1β, TGF-β, IL-10, and TNF-α contribute to the acquisition of immunosuppressive features by MDSC (64). TNF-α induces STAT3 phosphorylation, leading to the differentiation of myeloid progenitor cells into MDSC

(64). STAT3 also induces pro-inflammatory proteins S100A8/9, which promote MDSC accumulation (65). Inhibition of S100A8/9 has been shown to reduce MDSC accumulation and restrain tumor growth in various mouse tumor models (66, 67).

Chemokines derived from both tumor and stromal cells recruit MDSCs to the TME. CXCL5, CXCL6, CXCL12, CXCL8, CXCL1, CCL2, CCL3, CCL4, and CCL5 have been identified as important chemokines for MDSC recruitment (68). However, these chemokines also play a crucial role in recruiting conventional neutrophils and monocytes, which poses challenges for specifically targeting MDSC (69). Hypoxia in the TME is another significant factor that stimulates MDSC recruitment (70). Hypoxia-inducible factor (HIF)-1α was reported to involve in generating M2 macrophages from monocytes within tumors (71).

Studies suggest that the subsets of MDSC and tumor types determine, which chemokines facilitate MDSC migration into the tumor site (72). CCR2 signaling mediates the recruitment of M-MDSC, promoting the suppression of CD8 T cell infiltration in melanoma patients (73). CCR5 ligands CCL4, CCL3, and CCL5 also contribute to M-MDSC migration (74). On the other hand, PMN-MDSC are primarily recruited by CXC chemokines, including CXCL5, CXCL6, CXCL1, CXCL2, and CXCL12 produced by tumor cells (75, 76). Deletion of CXCR2 expressed by PMN-MDSC in melanoma-bearing mice impairs PMN-MDSC accumulation and leads to the inhibition of tumor growth (77).

1.3.2 MDSC immunosuppressive mechanisms

MDSC employ a range of mechanisms to effectively suppress immune responses mediated by T cells, B cells, and NK cells, thereby facilitating tumor progression (Figure 2). These mechanisms encompass several key processes and molecular interactions (64). One major mechanism of T cell suppression involves the expression of negative immune checkpoint molecules such as PD-L1 (64) that induces T cell anergy via interaction with PD-1 on these cells, impairing their ability to mount effective immune responses (70). Furthermore, MDSC have the capacity to deplete essential amino acids required for T cell activation, such as cysteine, tryptophan, and L-arginine (78). This depletion is mediated by the upregulation of enzymes like arginase 1 (ARG1), inducible nitric oxide synthase (iNOS), and IDO, which lead to T cell dysfunction and anergy (79, 80). MDSC also exert their suppressive functions through the production of ROS and nitric oxide (NO). Elevated levels of ROS and NO in the TME impairs T cell responsiveness and promotes T cell apoptosis (81, 82). Moreover, MDSC can induce Treg expansion through the secretion of TGF-β and IL-10 (83).

MDSC extend their suppressive effects also to other immune cells. For instance, they inhibit the function of NK cells by producing TGF-β, which suppresses NK cell cytotoxicity and promotes downregulation of NKG2D expression (84, 85). Furthermore, MDSC impair antigen cross presentation by DC (86) and promote M2 macrophage differentiation through downregulating MHC-II expression and IL-12 secretion by macrophages (87).

Metabolic changes play a crucial role in the acquisition of MDSC suppressive activity. MDSC undergo changes in lipid metabolism, which contribute to their differentiation and immunosuppressive activities (88). Polyunsaturated fatty acid-enriched diets were reported to promote the generation and suppressive activity of MDSC (89). Furthermore, MDSC show resistance to ferroptosis, a form of programmed cell death induced by iron-dependent lipid peroxidation (90). MDSC upregulate glycolytic pathways supporting their survival by preventing ROS-mediated apoptosis (91).

MDSC contribute to tumor angiogenesis and metastasis through the production of matrix metalloproteinase 9 (MMP9) and angiogenic factors such as VEGF and basic fibroblast growth factor (bFGF), which promote the generation of new blood vessels (92).
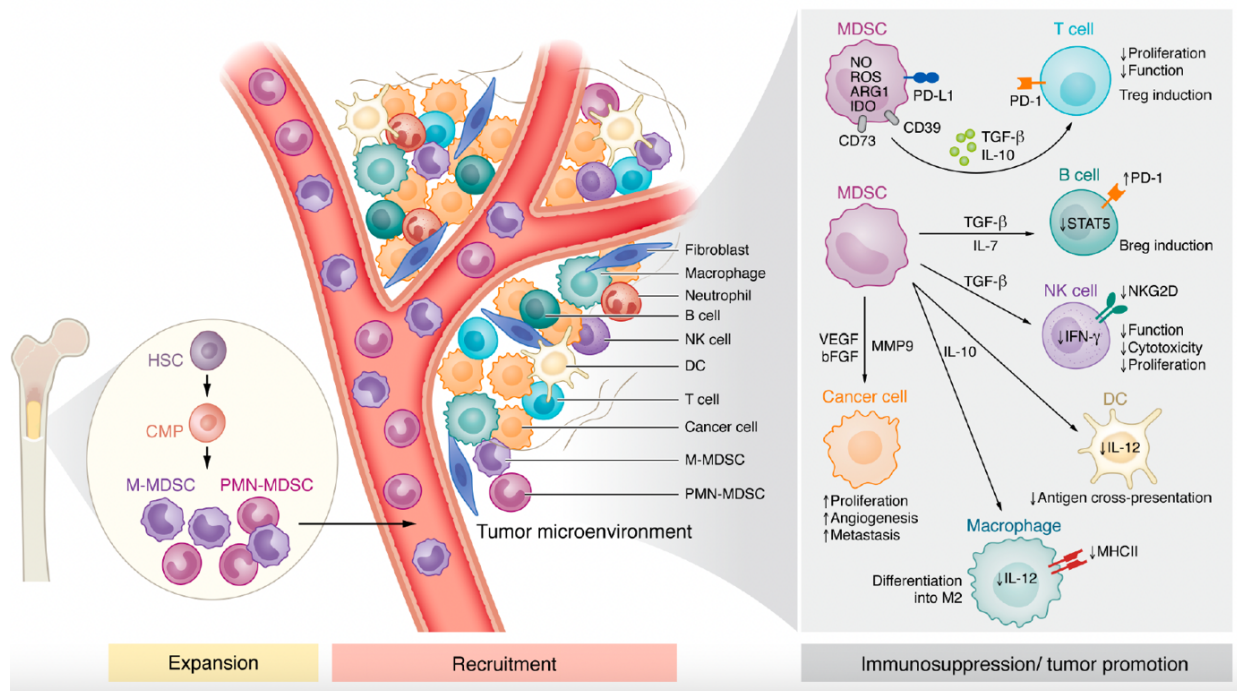
Figure 2. The accumulation, recruitment, and immunosuppressive/tumor promoting functions of MDSC. Dysregulated myelopoiesis is induced by the release of inflammatory mediators from tumor and immune cells, leading to the accumulation of MDSC in the bone marrow. Through the interaction of CCR or CXCR with their respective chemokine ligands, MDSC expand and migrate to the TME. Within the TME, they contribute to immunosuppression and tumor promotion by employing several mechanisms (93).

9

1.4 MDSC in melanoma

Targeting tumor-infiltrating immune cells holds promise for enhancing ICI effectiveness since TME plays a crucial role in the efficacy of ICI (94). Melanoma cells produced various factors that induce the generation and enrichment of immunosuppressive cells, including MDSC, Tregs, cancer-associated fibroblasts (CAF), and TAM (95, 96). Among them, MDSC are considered major contributors to the immunosuppressive microenvironment in melanoma (94). Chronic inflammation has been associated with the initiation and progression of melanoma (97). Melanoma cells produce several inflammatory mediators, which promote the secretion of cytokines, growth factors, and chemokines by fibroblasts and immune cells. This stimulates further production of chemokines by tumor cells, enhancing thereby tumor progression (98). The long-term secretion of inflammatory cytokines gives rise to MDSC accumulation and activation, and the conversion of normal cells into immunosuppressive MDSC (99).

Elevated number of peripheral M-MDSC and PMN-MDSC were reported to be associated with high tumor burden in melanoma patients (100, 101). Moreover, increased numbers of M-MDSC in advanced melanoma patients were reported to correlate with a high level of inflammatory mediators such as IFN-γ and IL-1β, which induces MDSC accumulation and activation (102).

Several studies have demonstrated the involvement of microRNAs (miRNAs) in the expansion and activation of MDSC (103). Elevated expression of specific miRNAs has been correlated with shorter progression-free survival (PFS) in patients undergoing treatment with immunotherapeutic agents such as ipilimumab and nivolumab (55).

1.4.1 MDSC targeting for melanoma immunotherapy

Numerous preclinical and clinical studies have been conducted to assess the effectiveness and safety of inhibiting MDSC as a single therapy or in combination with other therapies to enhance anti-tumor responses and overcome resistance to therapies (104, 105). The current treatment strategies can be categorized into five groups: i) depleting MDSC, ii) inhibiting their expansion and recruitment, iii) blocking their suppressive functions, iv) promoting MDSC differentiation into mature myeloid cells, and v) inhibiting MDSC metabolism (Table 1) (69, 106).

Depleting MDSC: Chemotherapeutic agents like gemcitabine, 5-fluorouracil (5-FU), paclitaxel, and doxorubicin have been reported to promote a significant reduction in MDSC frequencies (106). For instance, low-dose paclitaxel reduces tumor-infiltrating MDSC and their immunosuppressive activity, resulting in inhibition of tumor progression (107). Additionally, the monoclonal antibody gemtuzumab ozogamicin (GO) depletes MDSC, reinvigorates T-cell immunity, and reinforces immunotherapy efficacy in various tumors, including melanoma (108). Tyrosine kinase inhibitor sunitinib, which targets both MDSC and tumor cells, reduces MDSC frequencies in patients with renal cell carcinoma (109). Additionally, DS-8273a, an agonistic monoclonal antibody against DR5, eliminates MDSC without affecting mature myeloid cells and restrains disease progression in patients with advanced malignancies (46).

Inhibiting MDSC expansion and recruitment: Tumor-derived growth factors such as SCF, GM-CSF, CSF, and VEGF, have been shown to promote MDSC expansion (110). Inhibiting the SCF pathway has reduced MDSC expansion and tumor angiogenesis in a mouse model of colon cancer (111). Blocking GM-CSF/G-CSF signaling has restrained MDSC accumulation and enhanced anti-tumor immune responses (112). CSF-1/CSF-1R blockade has also inhibited MDSC expansion, although a clinical trial with the CSF-1R inhibitor ARRY-382 was reported to be unsuccessful (113). However, a phase I/II clinical trial with PD-0360324, CSF-1R inhibitor, is still ongoing (NCT02554812).

Targeting chemokine receptors and their ligands can inhibit MDSC recruitment to the tumor site. Anti-CXCR2 therapy was reported to reduce PMN-MDSC accumulation in the tumor microenvironment and prolong the survival of melanoma-bearing mice (77). The CXCR1/2 inhibitor SX-682 is currently tested in a phase I trial with pembrolizumab in metastatic melanoma patients (NCT03161431).

Histone deacetylase (HDAC) inhibitors and DNA methyltransferases can regulate anti-tumor immunity (114). HDAC inhibition was demonstrated to reduce MDSC recruitment to the tumor site, enhance T cell activation, and thereby improve anti-tumor immune responses (115). Entinostat, an HDAC inhibitor, used in combination with pembrolizumab, promoted durable anti-tumor responses in patients with metastatic uveal melanoma (116).

Blocking MDSC suppressive functions: Disrupting the COX-2/PGE2 pathway and using phosphodiesterase-5 (PDE5) inhibitors like vardenafil, sildenafil, and tadalafil inhibit MDSC immunosuppressive capabilities (69). Sildenafil reduces the expression of ARG1 and iNOS in MDSC, thereby hampering their immunosuppressive functions (117). Sildenafil was also

reported to prolong the survival of melanoma bearing mice by reducing the level of MDSC and their activity, resulting in restored CD8 T cell function in the TME (118). In an open-label trial, tadalafil treatment led to MDSC inhibition and activated CD8 T cells in metastasis lesions in melanoma patients resistant to ICI (119).

STAT3 has emerged as a promising target to restrain MDSC immunosuppressive functions (120). Various approaches aiming to inhibit STAT3 have been evaluated in both preclinical models and clinical trials (121, 122). However, their implementation in advanced solid tumors has resulted in intolerable toxicities or limited efficacy (123). It was shown that STAT3 inhibition using napabucasin reduces the immunosuppressive activity of MDSC and improves the survival of melanoma bearing mice (124).

Blocking IDO is another approach to hinder MDSC suppressive functions (106). A phase III trial combining epacadostat with pembrolizumab in advanced melanoma patients was reported to be unsuccessful (NCT02752074). However, an IDO vaccine was demonstrated to deplete immunosuppressive myeloid populations and improve anti-tumor responses in melanoma-bearing mice (125). Furthermore, a phase I/II clinical trial in metastatic melanoma patients using an immune-modulatory vaccine (IO102/IO103) against PD-L1 and IDO demonstrated a high response rate and improved PFS (126).

Blocking phosphatidylinositol 3-kinase (PI3K) was demonstrated to convert immune suppressive MDSC into immune-promoting phenotypes (92). The ongoing phase I clinical trial with IPI-549, a PI3K inhibitor, in combination with nivolumab, shows improved clinical activity in late-stage melanoma patients resistant to anti-PD-L1 therapy (NCT02637531).

Promoting MDSC differentiation: All-trans retinoic acid (ATRA) has been shown to stimulate the maturation of myeloid cells, including MDSC, into less immunosuppressive variants (127, 128). Combination therapy with ATRA and pembrolizumab has shown a high response rate and favorable tolerability in late-stage melanoma patients (129).

Inhibiting MDSC metabolism: Interrupting the metabolism of MDSC can inhibit their immunosuppressive functions. Inhibitors of fatty acid transport protein 2 (FATP2) and fatty acid oxidation (FAO) have been reported to be effective in blocking the activity of MDSCs and delaying tumor growth in mouse models, respectively (130, 131). The CD39/CD73/A2AR signaling pathway and the inhibition of adenosine receptors have been studied as potential strategy to overcome MDSC-mediated immunosuppression (132).

Table 1. Therapeutic strategies for targeting MDSC.

Treatment strategies	Agents
1. Depleting MDSC	1. Chemo-therapeutic agents (5-Fluoroacil, paclitaxel, gemcitabine, doxorubicin) 2. TKIs (sunitinib, ibrutinib) 3. TRAIL-R2 agonistic antibody (DS-8273a) 4. Anti-CD33 antibodies (GO)
2. Blocking MDSC suppressive functions	1. STAT3 inhibitors (AZD9150, napabucasin) 2. ARG inhibitors (CB-1158), COX-2 inhibitors (celecoxib) 3. TLRs agonists (resiquimod) 4. PDE5 inhibitors (slldenafil, vardenafil, tadalafil) 5. IDO inhibitors (epacadostat, navoximod, EOS200271, BMS-986205), IDO vaccine (I0102/I0103) 6.PI3K inhibitor (IPI-549)
3. Inhibiting MDSC expansion and recruitment	1. CXCR1/2 inhibitors (AZD5069, SX-682) 2. CCR5 inhibitors (maraviroc) 3. S100A8, A9 inhibitors (tasquinimod) 4. HDAC inhibitors (entinostat, TSA) 5. CSF1/R inhibitors (plexidartinib, ARRY-382, PD-0360324) 6. VEGFR inhibitors (sunitinib), anti-VEGF antibody (bevacizumab)
4. Promotion of MDSC differentiation	1. ATRA

	2. Vitamin D3, E
5. Inhibition of MDSC metabolism	1. FATP2 inhibitor (lipofermata)
	2. FAO inhibitor (etomoxir)
	3. CD39/CD73 inhibitor (oleclumab) A2AR/A2BR antagonists (AB928)

1.5 TLR4 and RAGE signaling pathways in cancer

1.5.1 TLR4 signaling in cancer

TLR4, the first identified toll-like receptor family member, can recognize pathogen-associated molecular patterns (PAMPs) and DAMPs (133). Studies reported an overexpression of TLR4 and myeloid differentiation primary response 88 (MyD88) in cancer, indicating the potential role of the TLR4 signaling pathway in the TME (134). Both immune and tumor cells express TLR4. Many TLR4 ligands such as HSPs, HMGB1, surfactant protein A, and S100 proteins were identified in the TME (135).

TLR4 can signal either via MyD88-dependent or TIR domain-containing adapter-inducing IFN-β (TRIF)-dependent pathway, which is MyD88-independent (136). Studies with MyD88 deficient macrophages indicated that MYD88 dependent signaling pathway is responsible for pro-inflammatory cytokine production, whereas the MYD88-independent pathway was shown to induce Type I IFNs and IFN-inducible genes (137, 138). Upon stimulation with LPS, MYD88 subunit of TLR4 complex recruits and activates IL-1 receptor-associated kinase 4 (IRAK-4) that triggers the recruitment and activation of IRAK-1, leading to the activation of TNF receptor-associated factor 6 (TRAF6) (139). The latter is responsible for the activation of TAK1, which promotes the activation of MAPK and NF-κB signaling, resulting in the production of pro-inflammatory cytokines (140). In the MyD88-independent pathway, TRIF plays crucial role in the activation of IRF3 transcription factor, NFκB, and MAPK (141). IRF3 and NF-κB trigger the

transcription of diverse target genes, which encompass the genes responsible for the synthesis of type I IFNs, mediating thereby effective antiviral and antibacterial response (141).

The activation of TLR4 in TME was demonstrated to boost anti-tumor immunity, including DC maturation and antigen presentation but also lead to the immune escape and tumor progression by stimulating tumor cells (142). TLR4 ligands were shown to promote T helper cell (Th1) mediated anti-tumor immunity via the MyD88-dependent pathway (143). On the other hand, TLR4 ligands released from TME trigger an inflammatory response, resulting in the recruitment of M2 macrophages and MDSC (144, 145).

1.5.2 RAGE signaling in cancer

Receptor for advanced glycation end products (RAGE) is a transmembrane receptor for both PAMPs and DAMPs, belonging to the immunoglobulin superfamily. (146). RAGE was shown to interact with multiple ligands, including AGEs, members of the S100/Calgranulins family, HMGB1, β-sheet fibrils, advanced lipoxidation end products (ALEs), adhesion molecules, complement components, lipopolysaccharide, and many others (147). Ligand-RAGE interaction induces many signal transduction cascades such as Erk1/2 MAPK, Ras-extracellular signal-regulated kinase, Cdc42/Rac, stress-activated protein kinase/c-Jun-NH2– terminal kinase, and p38-MAPK. Additionally, RAGE triggers NF-κB activation, which leads to the induction of antiapoptotic genes crucial for cell survival, including A1, A20, XIAP, Bcl-XL, and Bcl-2 (148).

RAGE expression was reported to be elevated in several malignancies such as gastric, breast, prostate, colorectal, and liver cancer (149). Moreover, RAGE expression was reported to be correlated with tumor progression (149-151). Studies also demonstrated that increased RAGE expression hinders cell death in cancer cells exposed to chemotherapy and hypoxia (150, 152). Additionally, RAGE has been demonstrated to contribute to the generation of MDSC (153). Administration of anti-RAGE antibodies to mice with metastatic lesions was reported to decrease the level of MDSC in the circulation, draining lymph nodes, and spleen (151). Although the blockade of RAGE resulted in diminished levels of MDSC, it did not reduce their suppressive activity (151).

1.6 TLR4 and RAGE ligands

1.6.1 HSP90α

HSP90 is a crucial cellular chaperone with isoforms HSP90α and HSP90β92 (160). It has distinct isoforms localized in mitochondria (Trap1) and endoplasmic reticulum (Grp94) (154). It is localized on the cell surface and can be secreted from the cytoplasm (extracellular HSP90). In addition to protein folding, HSP90 plays roles in DNA repair, immune response, neuronal signaling, and cancer development through chaperoning oncogenes (155, 156). HSP90 has been studied as a therapeutic target in oncology due to its overexpression in tumor cells, including melanoma cells (157). Cancer cells release HSP90, which interacts with several co-chaperons to form complexes serving specific functions including the folding and activation of extracellular targets as well as the stimulation of cell surface receptors (155). It has been recently suggested that HSP90-mediated activities play a crucial role in tumor growth and progression (158-160). HSP90, acting as a DAMP, interacts with TLR4 and induces the formation of several inflammatory mediators (157). Inhibition of HSP90 was reported to increase T cell recognition of melanoma cells, prevent the induction of immunosuppressive myeloid cells, and enhance the efficacy of immunotherapy in mouse melanoma models (56). Extracellular HSP90α was implicated in promoting cancer cell invasiveness, migration, and facilitating metastasis formation (160). Accumulation of HSP90α in plasma was proposed as a potential biomarker for various cancers and a prognostic indicator for immunotherapy (159).

1.6.2 S100A8/S100A9 and HMGB1

Calprotectin A and B (S100A8 and S100A9), S100 family members, are intracellular calcium-binding proteins and endogenous DAMPs (161, 162). When stimulated by various factors, including pro-inflammatory cytokines such as TNF, neutrophils, and monocytes release S100A8/9 (163). In addition, these proteins can also be released by tumor cells undergoing necrosis after hypoxia (164). These proteins predominantly exist as a heterodimer of S100A8/9 but can also form homodimers and tetramers (162). It was demonstrated that neutrophils, immature macrophages, and tumor cells express S100A8 and S100A9 (164). In numerous diseases (including cancer), these proteins play an important role in promoting and sustaining inflammation (163). Under normal conditions, they are present at very low levels

in the serum. However, their levels are remarkably elevated in cancer and positively correlated with tumor progression and metastasis (161, 164).

Several reports demonstrated the involvement of S100A8/9 in the differentiation, accumulation, and suppressive capacity of MDSC (63, 65, 165, 166). NF-κB activation by the interaction of S100A8/9 and TLR4/RAGE induces the production of proinflammatory cytokines that can drive MDSC accumulation (65).

Amphoterin, also known as HMGB1, is a non-histone protein that plays diverse roles in DNA repair, differentiation, neural development, transcription, and extracellular signaling (167). It acts as DAMP and alarmin. Its release occurs passively during necrotic cell death or actively through translocation and exocytosis (167). HMGB1 was shown to be associated with cancer (168). An elevated level of HMGB1 was reported to be associated with poor prognosis and reduced survival of cancer patients (169). Like S100A8/9, HMGB1 was also reported to drive the accumulation and suppressive functions of MDSC in cancer (170, 171). Mice with renal cell carcinoma treated with anti-HMGB1 antibody displayed reduced tumor growth and MDSC levels. However, the effectiveness of such anti-tumor therapy was diminished when MDSC were depleted, indicating that MDSC are the primary targets for HMGB1 (171).

Both S100A8/9 and HMGB1 bind either to the cell membrane receptor TLR4 or to RAGE, initiating a complex signal transduction pathway, which leads to the generation of ROS, NO, and pro-inflammatory cytokines IL-1β, IL-6, and TNFα (153). TLR4 and RAGE pathways intersect at kinase signaling stages, leading to the translocation of NF-κB and the production of several inflammatory mediators (Figure 3) (153). The role of S100A8/9 and HMGB1 on tumor progression has been demonstrated (153, 164). Similarly, the involvement of these proteins in regulating the development, accumulation, and function of MDSCs has been well established. However, it is not yet clear whether S100A8/A9 and HMGB1 exclusively activate MDSC via TLR4 or if they also activate MDSCs through RAGE (153).
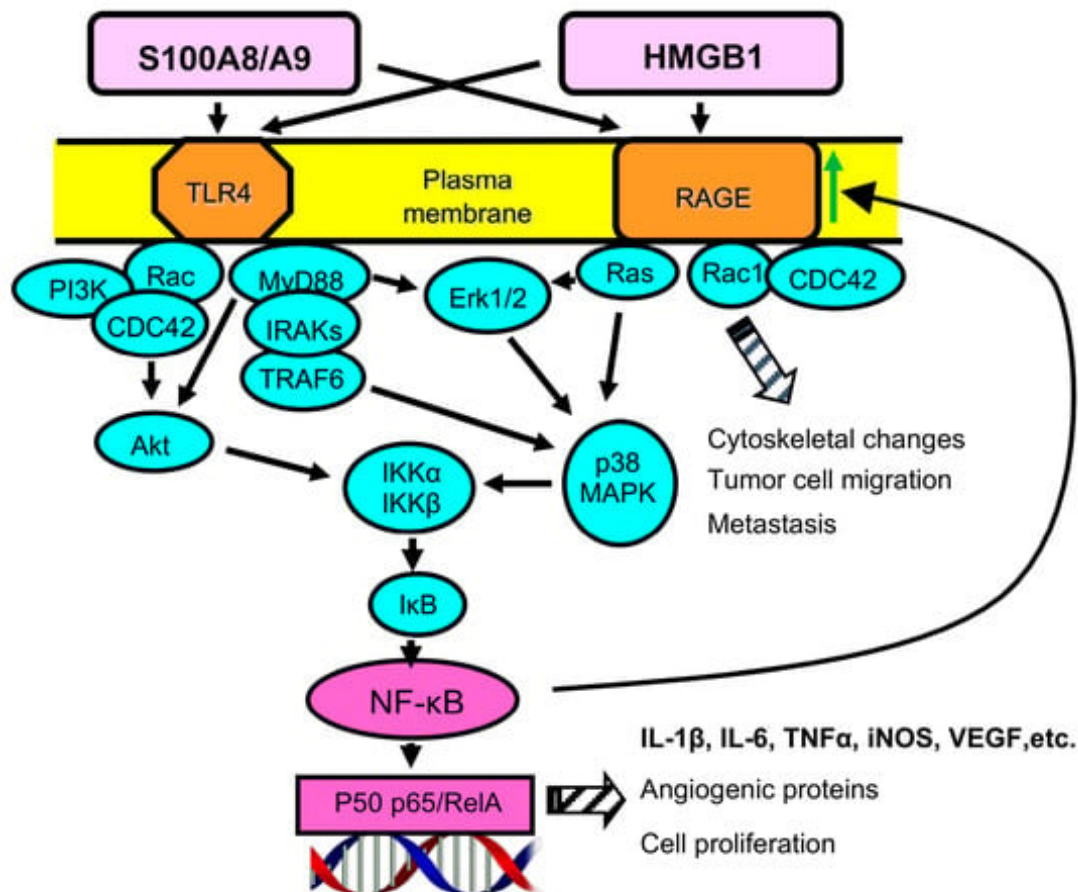
Figure 3. S100A8/9 and HMGB1 act as the primary ligands for TLR4 and RAGE. Upon binding of HMGB1 and S100A8/A9 to either TLR4 or RAGE, a complex intracellular signaling cascade is triggered, resulting in the translocation of NF-kB to the nucleus. In the nucleus, NF-kB promotes the synthesis of pro-inflammatory mediators, pro-angiogenic proteins, and activates cell proliferation. This activation of NF-kB creates a feedback loop, leading to the increased expression of RAGE (indicated by a green arrow). Additionally, S100A8/A9 and HMGB1 may individually facilitate crosstalk between TLR4 and RAGE, thereby activating both signal transduction pathways (153).

2 Aim of the study

Understanding the regulatory factors and signaling pathways that control the survival, generation, and activation of MDSC is crucial for developing immunotherapeutic strategies targeting MDSC since it has been shown that inhibiting these cells can delay tumor progression (62). Studies demonstrated that TLR4 ligands play a role in the activation of

MDSC (56, 165). In contrast, other groups reported that TLR4 signaling can diminish the immunosuppressive functions of MDSC (144). Therefore, the role of TLR4 signaling on MDSC and its effect on tumor progression remain to be better defined. Similarly, the involvement of RAGE signaling in MDSC accumulation has not been fully elucidated (153). My study aims to investigate the role of TLR4 and RAGE signaling in MDSC-mediated immunosuppression in melanoma and to find potential MDSC targeting mechanisms. Deciphering the effect of TLR4 and RAGE signaling on MDSC will help to optimize the role of TLR4 and RAGE antagonists in anti-tumor therapy and provide a novel insight into the development of cancer immunotherapies.

To determine the role of endogenous DAMPS including HSP90α, S100A8/A9, and HMGB1 in the generation and suppressive activity of MDSC, healthy donor-derived monocytes were stimulated with these recombinant proteins. TLR4 inhibitor (Resatorvid) and RAGE antagonist (FPS-ZM1) were tested in the stimulated monocytes to identify, which pathway is used exclusively to promote the activation of MDSC. Moreover, those inhibitors were also tested in MDSC derived from melanoma patients or generated *in vitro*. Markers and pathways involved in the MDSC immunosuppression were assessed by flow cytometry, Western blot, and gene expression profiling. TCGA data analysis was performed to evaluate the association between the expression of immunosuppressive markers and HSP90α, S100A9, and HMGB1 in the TME of melanoma. Finally, the potential prognostic value of these proteins and their possible association with the MDSC activity was investigated in the plasma of melanoma patients.

3 Material

3.1 Technical equipment

Device	Manufacturer
Balance BP 3100P	Sartorius
Cell culture incubator Hera cell 150	Heraeus
Centrifuge Biofuge primo R	Heraeus
Centrifuge Labofuge 400R	Heraeus
Centrifuge MEGAFUGE 40R	Heraeus
Counting chamber C-Chip Neubauer	Carl Roth

Electrophoresis chamber Mini-PROTEAN® 3 Cell	BioRad
Flow cytometer BD FACSAria™ IIU	Becton Dickinson
Flow cytometer BD FACSLyric™	Becton Dickinson
Fridge	Liebherr
Ice machine	Manitowoc
Imaging System Fusion SL	Viber Lourmat
Laminar flow hood Hera safe	Heraeus
Light microscope DM IL	Leica
Magnetic bead column holder MACS® multistand	Miltenyi Biotec
Microplate reader Tecan infinite M200	Tecan
Mr. Frosty™ freezing container	Thermo Fisher
N_2 tank BIOSAFE®	Cryotherm
Pipettes Transferpette	Eppendorf
Refrigerator (-20 °C)	Liebherr
Refrigerator (-80 °C)	Heraeus
Wet blotting chamber	BioRad
Vortexer REAX Top	Heidolph
Heating block	Peqlab
Magnetic stirrer RCT basic	IKA Werke
Vortexer REAX top	Heidolph
Water bath DC3	HAAKE, GFL
Sunlab® Mini vortex mixer	NeoLab

3.2 Technical equipment

Software	Manufacturer / Reference
FACSuite™	Beckton Dickinson

FlowJo V10	Becton Dickinson	
GraphPad Prism	GraphPad Software	
iControl	Tecan	
IPA	QIAGEN	
cBioPortal (v5.3.6)	Cerami et al., 2012 & Gao et al., 2013	

3.3 Consumables

Consumable	Manufacturer	Order number
15 mL tube	Sarstedt	62.554.502
5 mL polystyrene tubes	StemCell Technologies	38007
50 mL tube	Sarstedt	62.547.254
12 well plate	Sarstedt	83.3921.500
96-well plate F	Sarstedt	82.1581
96-well plate R	Sarstedt	82.1582
MACS® LS colums	Miltenyi Biotec	130-042-401
Needles 27G ¾	Becton Dickinson	302200
Pre-separation filters, 30 µM	Miltenyi Biotec	130-041-407

Consumable	Manufacturer	Order number
Pipette Filter Tips 10 µL	Sarstedt	70.1116.210
Pipette Filter Tips 1000 µL	Sarstedt	70.762.211
Pipette Filter Tips 200 µL	Sarstedt	70.760.211
Pipette tips 10 µL	Sarstedt	70.1130.600
Pipette tips 1000 µL	Sarstedt	70.760.452
Pipette tips 200 µL	Sarstedt	70.762.100

Immun-Blot PVDF/Filter Paper Sandwiches	BioRad	1620238
4-15% mini-protean tgx stain-free protein gels	BioRad	4568085
Reaction tube 1.5 mL	Eppendorf	0030120086
Reaction tube 2.0 mL	Eppendorf	0030120094
Serological pipette 10 mL	Sarstedt	86.1254.001
Serological pipette 25 mL	Sarstedt	86.1685.001
Serological pipette 5 mL	Sarstedt	86.1253.001
Syringe 1 mL	Becton Dickinson	300013
Syringe 10 mL	Becton Dickinson	309110
Transfer pipette	Sarstedt	86.1171
Leucosep tube 50 mL	Greiner	227290

3.4 Chemicals, solvents, and reagents

Reagent	Manufacturer	Order no.
2-β-mercaptoethanol (50 mM)	Thermo Fisher	31350-010
4x NuPAGE LDS sample buffer	Thermo Fisher	NP0007
7AAD	Becton Dickinson	559925
Annexin V APC	Biolegend	640920
Annexin V Binding Buffer	Biolegend	422201
Human Albumin 20%	CSL Behring GMBH	
CellROX^{TM} Deep Red reagent	Thermo Fisher	C10422
Cell proliferation dye eFluor 450	Thermo Fisher	65-0842-85
DAF-FM DA (NO detection reagent)	Cayman Chemical	18767
Dimethyl sulfoxide (DMSO)	Carl Roth	A994.1
1x Dulbecco's phosphate-buffered saline (DPBS)	PAN-Biotech	P04-36500

Ethanol	Carl Roth	9065.1
Heat inactivated FBS	Thermo Fisher	10500-06
Fixable viability stain 700	Becton Dickinson	564997
Fixable viability stain 510	Becton Dickinson	564406
Fluorescence mounting medium	Sigma-Aldrich	F4680
HEPES (1 M)	Thermo Fisher	15630080
Pancoll 1.077 g/ml	PAN-Biotech	P04-60500
MEM non-essential amino acids	Thermo Fisher	11140050
Methanol	Carl Roth	4627.4
NaN$_3$	Carl Roth	K305.1
Penicillin/streptomycin (P/S)	Thermo Fisher	15140-122
Protease inhibitor cocktail 50x	Promega	G6521
Pierce® RIPA Buffer 100 ml	Sigma Aldrich	20-188
RNase out	Thermo Fisher	10777019
RPMI 1640 medium	Thermo Fisher	11875101
RPMI 1640 Medium for SILAC	Thermo Fisher	88365
Sodium pyruvate	Thermo Fisher	11360-03
Tris(hydroxymethyl)-aminomethan (Tris)	Carl Roth	0188.3
Trypan blue solution	Sigma-Aldrich	T8154
Tween 20	Sigma-Aldrich	P9416
UltraPure™ 0.5 M EDTA	Thermo Fisher	15575020
10x Tris/Glycine Buffer	BioRad	1610734
10x Tris/Glycine/SDS	BioRad	1610732
10x Tris Buffered Saline (TBS)	BioRad	1706435
Phosflow™ Fix Buffer I	Becton Dickinson	557870
Phosflow Perm Buffer III	Becton Dickinson	558050
FcR blocking reagent	Miltenyi Biotec	130-059-901

Sodium orthovanadate	Jena Bioscience	AK-102V-L	
Sodium fluoride	Jena Bioscience	CSS-290	
SuperSignal West Pico PLUS Chemiluminescent Substrate	Thermo Fisher	34580	
PageRuler prestained protein ladder 10kDa to 180kDa, order no	Thermo Fisher	26617	

3.5 Antibodies

3.5.1 Primary antibodies

Specificity	Source	Manufacturer	Order no.	Dilution
GAPDH	rabbit	Cell signaling technology	2118S	1:1000
β-Actin	rabbit	Cell signaling technology	4970S	1:1000
pSTAT3	mouse	Cell signaling technology	4113S	1:2000
STAT3	mouse	Cell signaling technology	9139S	1:1000
P38 MAPK	rabbit	Cell signaling technology	8690S	1:1000
P-P38 MAPK	rabbit	Cell signaling technology	4511S	1:1000
PNFKB p65	rabbit	Cell signaling technology	3033S	1:1000
NFKB p65	rabbit	Cell signaling technology	8242S	1:1000
IDO-1	rabbit	Cell signaling technology	D5J4E	1:1000
CD28, unlabelled monoclonal antibody		Beckman Coulter	IM1376	1 :100
CD3 monoclonal antibody (OKT3), functional grade		eBioscience	16-0037-85	1 :1000

3.5.2 Peroxidase-conjugated antibodies

Specificity	Manufacturer	Order no.	Dilution
Horseradish peroxidase (HRP)-conjugated goat anti-mouse	Jackson Immuno Research	115-035-003	1:10000
Peroxidase AffiniPure Goat Anti-Rabbit IgG (H+L)	Jackson Immuno Research	115-035-003	1:10000

3.5.3 Fluorescent-conjugated antibodies

Specificity	Fluorophore	Clone	Manufacturer	Order no.	Dilution
p38 MAPK (pT180/pY182)	PE	36/p38	Becton Dickinson	562065	1:30
PD-L1	BV421	MIH1	Becton Dickinson	563738	1:100
NFκB (pS529)	PE	K10-895.12.50	Becton Dickinson	558423	1:30
STAT3 (Py705)	PE	4/P-STAT3	Becton Dickinson	562072	1:30
CD14	FITC	MΦP9	Becton Dickinson	347493	1:25
IgG1	BV421	X40	Becton Dickinson	659453	1:100
IgG1	PE	MOPC-21	Becton Dickinson	554680	1:200
HLA-DR	V500	G46-6	Becton Dickinson	561224	1:100
CD33	PE	WM53	Becton Dickinson	555450	1:25
CD33	PE-Cy7	WM53	Biolegend	3034034	1:100
CD66b	PerCP-Cy5.5	G10F5	Becton Dickinson	562254	1:100
LIN (CD3, CD19, CD20, CD56)	APC		Biolegend	363601	1:100
CD80	PE-Cy7	L307.4	Becton Dickinson	561135	1:100

CD86	APC	FUN-1	Becton Dickinson	560956	1:100
TLR4	PE	TF901	Becton Dickinson	564215	1:100
RAGE	PE	EPR21171	Abcam	ab237363	1:500
IgG	PE	EPR25A	Abcam	ab209478	1:500
Annexin V	APC		Biolegend	640920	1:20

3.5.4 Inhibitors

Name	Company	Order no.	Concentration
TLR4 inhibitor, TAK-242	Sigma	243984-11-4	5 μg/mL
RAGE antagonist, FPS-ZM1	Sigma	553030	30 nM

3.6 TLR4/RAGE ligands, cytokines, and growth factors

Factor	Order no.	Company
GM-CSF	130-093-865	Miltenyi Biotec
IL-6	130-093-931	Miltenyi Biotec
LPS	tlr-3pelps	Invivogen
Recombinant human HMGB1 protein	ab167718	Abcam
Recombinant human S100A9 protein	ab95909	Abcam

3.7 Commercial kits

Kit	Manufacturer	Order no.
CD3 Microbeads, human	Miltenyi Biotec	130-050-101

CD14 Microbeads, human	Miltenyi Biotec	130-050-201
Human HSP90α ELISA kit	Novus Biologicals	NBP2-29914
Human HMGB1 ELISA kit	Novus Biologicals	NBP2-62766
Human S100A8/9 ELISA kit	R&D Systems	DS8900
Pierce® BCA Protein Assay Kit	Thermo Fisher	23225
Pierce® ECL Substrate	Thermo Fisher	32106
RNase-Free DNase Set	QIAGEN	79254
RNeasy Mini Kit	QIAGEN	74104

3.8 Buffers and media

Buffer/medium   **Composition**

RIPA lysis buffer   1956 μL 1x RIPA buffer

                                     (1:10 dilution with distilled

                                      water of 10x Pierce® RIPA Buffer)

                                      40 μL (1x from 50x protease inhibitor cocktail

                                      2 μL (1x) from 1000x NaF

                                      2 μL (1mM) from 1M Sodium orthovanadate

1x Running buffer   100 mL 10x Tris/Glycine/SDS buffer
                                     (25 mM Tris, 192 mM glycine and 0.1% SDS)
                                     900mL distilled water

1x Transfer buffer   100 mL 10x Tris/Glycine buffer
                                     (25 mM Tris, 192 mM glycine)

200 mL HPLC grade methanol

700 mL distilled water

1x TBST buffer	100 mL (1x) 10x Tris buffer
	1 mL Tween®20 (final concentration 0.1%)
	900 mL distilled water

Buffer/medium	Composition
MDSC medium	500 mL RPMI Medium
	10 % heat inactivated FBS
	1 % P/S
	10 mM HEPES
	1 mM Sodium Pyruvate
	50 µM β-mercaptoethanol
	1 mM MEM non-essential amino acids
Arginine-low Medium	88 mL RPMI 1640 Medium for SILAC
	10 % FBS
	1 % Penicilin/Streptamycin
	0.04 mg/mL L-Lysine hydrochloride
	0.15 mM L-Arginine
FACS buffer	1x PBS
	2 % heat inactivated FBS
	0.2 % NaN_3
MACS buffer	1x PBS
	0.5 % human albumin
	2 mM EDTA

4 Methods

4.1 Cell counting

To determine the cell count, a 10 µL sample of a single cell suspension was diluted 1:10 in Trypan blue. The solution was then transferred to a Neubauer chamber and only viable cells, which did not take up Trypan blue, were counted. The total number of viable cells per mL was calculated using the following formula:

$$alive\ cell\ number\ per\ mL$$
$$= \frac{counted\ number\ of\ Trypan\ blue\ negative\ cells}{number\ of\ counted\ squares} * 10^4$$
$$* dilution\ factor$$

4.2 Isolation of primary human cells

4.2.1 Human samples and density gradient separation

PBMCs (peripheral blood mononuclear cells) were isolated from either healthy donors' buffy coats (provided by the German Red Cross Blood Service Baden-Württemberg-Hessen) or whole blood from healthy donors or melanoma patients using Pancoll 1.077 g/mL separation medium. Stage III-IV melanoma patients (n=61) who did not receive any systemic therapy for three months were enrolled in this study. The study was approved by the ethics committee of University Medical Center Mannheim (2010-318N-MA). Patients gave informed consent prior to enrollment. The isolation process involved layering 25 mL of the buffy coat (diluted 1:1 with sterile PBS) or blood (without any dilution) onto a 15 mL Pancoll gradient separation medium, followed by centrifugation at 400 x g for 30 minutes without brake. This resulted in distinct layers: the upper fraction contained plasma, a layer represented PBMCs, followed by Pancoll, and the lower part contained erythrocytes and granulocytes. The plasma was collected by leaving a 5-10 mm space above the PBMC layer and stored at -80°C. The PBMC layer was carefully collected without any Pancoll contamination for subsequent isolation of monocytes, T cells, or MDSC.

4.2.2 Magnetic-activated cell sorting (MACS)

CD14 monocytes and CD3 T cells were isolated from PBMCs using magnetic beads following the instructions provided by the manufacturer (Miltenyi). PBMCs were washed with PBS and then resuspended in 80 μL of MACS buffer per 10^7 cells. For every 10^7 cells, 20 μL of CD14 or CD3 MicroBeads were added, mixed, and incubated for 15 minutes at 4°C. Subsequently, the cells were washed with 1-2 mL of buffer and centrifuged at 300 x g for 10 minutes. The supernatant was aspirated, and the cell pellet was resuspended in 500 μL of buffer. Simultaneously, an LS column was placed in the magnetic field of a MACS separator and cleaned with 3 mL of buffer. The cell suspension was then applied to the column, followed by three times washing steps with 3 mL of buffer. Afterward, the column was removed from the separator and placed in a 50 mL tube. By gently pushing the plunger into the column, CD14 monocytes labeled with magnetic beads were flushed out. The cells were subsequently centrifuged at 300 x g for 5 minutes, and the cell pellet was resuspended in complete RPMI-1640 medium. The efficiency of the MACS procedure or the purity of the cells was evaluated by staining them with a fluorochrome-conjugated anti-human CD14 monoclonal antibody and analyzed using flow cytometry.

4.2.3 Fluorescence-activated cell sorting (FACS)

PBMCs were labeled with anti-human CD33-PE, HLA-DR-V500, CD66b-PerCPCy5.5, and LIN (CD3, CD19, CD20, CD56)-APC monoclonal antibodies (mAbs). Monocytes (CD33$^+$HLA-DR$^+$) and M-MDSC (CD33$^+$HLA-DR$^-$) were purified using fluorescence-activated cell sorting (FACS) performed by the Flow Core Team at the University Medical Center Mannheim, Germany, using BD FACSAriaTM IIU cell sorter. Accudrop beads were employed to determine appropriate FACS settings to perform sorting. The initial step in flow cytometric analysis is eliminating debris by plotting the size (FSC-A) against granularity (SSC-A). Then, single cells were gated in forward scatter height (FSC-H) versus area (FSC-A). The target population was then identified as Monocytes (CD33$^+$HLA-DR$^+$) and M-MDSC (CD33$^+$HLA-DR$^-$). Gating strategy is shown in Figure 4. Sorting was performed at room temperature (RT) and cells were collected into 10 mL prewarmed Arginase low medium. Sorted cells were centrifuged at 300 x g for 5 minutes and resuspended in medium for further analysis.
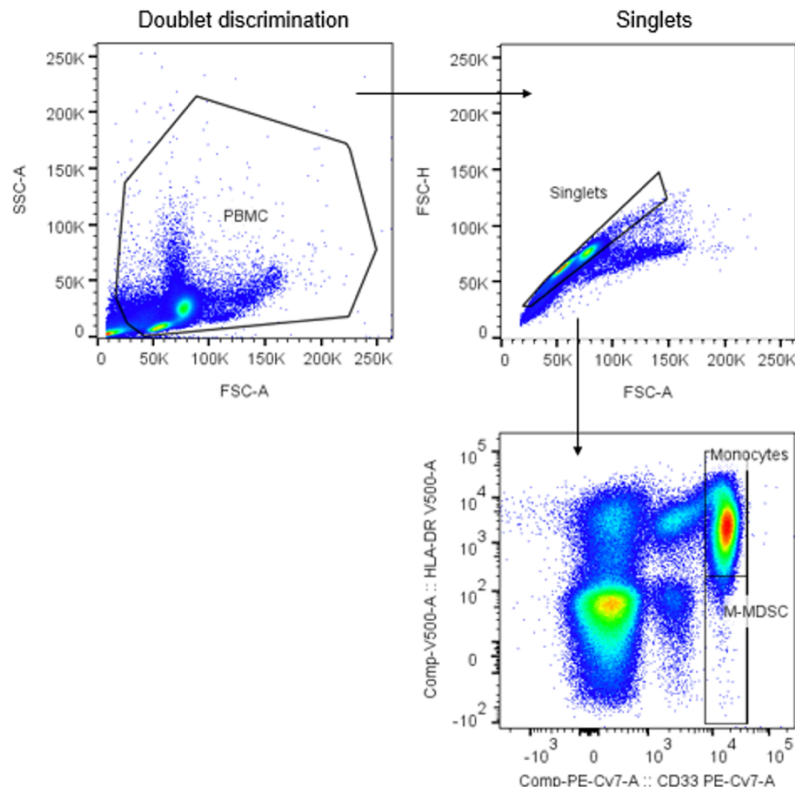
Figure 4. Gating strategy for monocytes (CD33+HLA-DR+) and M-MDSC (CD33+HLA-DR-) isolation from PBMC of melanoma patients.

4.3 Stimulation of monocytes with TLR4 ligands

Monocytes were cultured in the MDSC medium and then subjected to treatment with rHSP90α at a concentration of 2 µg/mL per 10^6 cells or LPS (100 ng/mL) or left untreated as a control for 24 in the presence or absence of Resatorvid (5 μM). Additionally, healthy donor-derived CD14 monocytes were pre-treated with inhibitors Resatorvid (5μM) or FPS-ZM1 (30nM) or DMSO (as control) for 1h, then they were stimulated with either rHMGB1 (5 µg/mL) or rS100A9 (10 µg/mL) in the presence of GM-CSF (40 ng/mL) for 72h. Only GM-CSF (40 ng/mL) stimulated monocytes were used as control.

4.4 MDSC generation *in vitro*

Briefly, monocytes from healthy donors were isolated as described in section 4.2.2, and $1x10^6$ cells were cultured in 1 mL MDSC medium supplemented with 50 ng/mL GM-CSF and 50 ng/mL IL-6 (for MDSC generation) or 50 ng/mL GM-CSF only (as a control) for 4 days in a 12-well plate at 37 °C and 5 % CO_2. At day 4, the plate was centrifuged at 300 x g for 5 minutes, supernatant was collected, and stored at -80°C until further use. Generated MDSC exhibit a mixed growth pattern, with some cells growing in suspension and others adhering to the culture surface, resembling the heterogeneous MDSC population. The cells growing in suspension were simply collected in a 50 mL tube, and then adherent cells were detached using a cell scraper and added into the mixture. Cells were washed with PBS, centrifuged for 5 minutes at 300 x g, and resuspended in the appropriate medium or buffer for further experiments.

.

4.5 Microarray analysis

4.5.1 RNA isolation

Total RNA was extracted from $2x10^6$ cells stimulated monocytes or *in vitro* generated MDSC using the RNeasy Mini kit from Qiagen. To remove DNA contamination, an on-column DNase digestion step was performed using the RNase-free DNase set from Qiagen by following the manufacturer's instructions. The RNA was eluted in 25 µL of RNase-free water. Afterward, RNA concentration was determined using a Nanoquant plate by Tecan Infinite M200 microplate reader. The RNA was then stored at -80 °C until further use.

4.5.2 Microarray and Bioinformatics

Gene expression analysis was conducted using the Affymetrix Clariom S human assay (Thermo Fisher Scientific) following the manufacturer's instructions at the Microarray Unit of the Genomics and Proteomics core facility, German Cancer Research Center (DKFZ). The data were submitted to Dr. Thomas Hielscher (DKFZ NGS core facility) and Dr. Carolina De la Torre (ZMF Mannheim) for bioinformatics and statistics. Two different bioinformatics methods were used for the analysis of microarray data. i) The Affymetrix CEL files were normalized using the RMA method and the expression values were log2-transformed.

Differentially expressed genes in the experimental groups were identified using the empirical Bayes approach (172) based on moderated t-statistics implemented in the Bioconductor package limma (173) considering batch effects. Gene set enrichment analysis (GSEA) was performed using the camera test (174). Pathway analysis utilized the KEGG (http://www.genome.jp/kegg), Reactome (https://reactome.org/), and Gene Ontology (GO) (http://geneontology.org/) databases. The results from pathway tests were visualized using an enrichment map. The analysis was conducted with the R Statistical Software (V.4.0; R Core Team 2020) with the EnhancedVolcano add-on package, and the p-values were adjusted for multiple testing using the Benjamini-Hochberg correction. ii) A customized version of CDF (Custom CDF Version 25) that incorporated ENTREZ-based gene definitions was utilized to annotate the arrays. To normalize the raw fluorescence intensity values and correct for background effects using the oligo package, quantile normalization and RMA background correction were employed. The identification of differentially expressed genes was performed using the limma package (173). Genes were considered significant if they had an adjusted p-value < 0.05 and a log fold change (logFC) greater than absolute value 1. For assessing the distribution bias of defined gene sets within a ranked gene list, GSEA was employed using the fgsea package. Additionally, Over Representation Analysis (ORA) using the genekitr package was conducted specifically on the differentially expressed genes. Pathways associated with various cellular functions, such as cell cycle or apoptosis, were obtained from publicly available external databases including KEGG and GO.

4.6 Protein isolation

Monocytes ($2.5\text{x}10^6$) stimulated with recombinant proteins or left untreated were washed with PBS and centrifuged at 300 x g for 5 minutes. Afterward, the cell pellet was resuspended in 300 µL RIPA buffer containing 1x protease inhibitor cocktail. Cells were incubated for 30 minutes on ice on a shaking platform. Next, lysates were centrifuged at 13000 rpm for 10 minutes at 4 °C. The supernatant (protein lysates) was transferred to new pre-cooled 1.5 ml tubes and stored at -80 °C.

4.7 Bicinchoninic acid (BCA) assay

Pierce® BCA Protein Assay Kit was used to determine the protein concentration. The albumin standard was diluted in PBS to achieve final concentrations of 2000 µg/mL, 1500 µg/mL, 1000

µg/mL, 750 µg/mL, 250 µg/mL, 125 µg/mL, and 25 µg/mL of protein. To measure the protein concentration, 10 µL of each sample, standard dilution, and a blank were pipetted in duplicates into a 96-well flat bottom plate. BCA reagent A and BCA reagent B were mixed at 50:1 and added into each well (200 µL/ well). The plate was then incubated in the dark at 37 °C on a shaker for 30 minutes. After incubation, the absorbance at 562 nm was determined using the Tecan Infinite M200 microplate reader. Protein concentration was determined by drawing standard curve. For each assay, a fresh mixture of 5% beta-mercaptoethanol and 4x NuPAGE LDS sample buffer were prepared. The protein lysates were then combined with the mixture in a ratio of 3:1 (protein lysates: 4x LDS sample buffer, v/v). The resulting mixture was denatured at 100°C on a heat block for 5 minutes. Afterward, the samples were placed on ice for 5 minutes and immediately stored at -20°C.

4.8 Gel electrophoresis

Samples (5 to 20 µL) and protein ladder (7 µL) were loaded on a 4-15% mini-protean tgx stain-free protein gels. Gels were placed in a gel electrophoresis tank filled with freshly prepared 1x running buffer (1x Tris/Glycine/SDS buffer). Electrophoresis was performed at 75 V for approximately 2.5 h, until the solvent front reached the lower end of the gel.

4.9 Western blot and immunostaining

After SDS-PAGE, the gels were removed and placed into the 1x transfer buffer (1x Tris/Glycine). The membrane was activated for 1 min in 100 % methanol on a shaker to enable protein binding and an effective transfer. Afterward, PVDF membranes, filter papers, and sponges were soaked in freshly prepared cold 1x transfer buffer. Two filter papers were placed on two sponges, with the gel and membrane positioned in between. To ensure the movement of negatively charged proteins towards the anode, the membrane was placed close to the anode (+). A roller was used to remove air bubbles. The cassette was then placed in the transfer tank. With the aid of a stirring magnet, protein transfer was conducted at 75V for 90 minutes in a cold room (+4-8°C).

After the completion of the transfer, the membranes were incubated at room temperature in 1x TBST containing 5% skimmed milk at 100 rpm on a shaker. Then, the membranes were washed with 1x TBST on a shaker for 10 min. Diluted primary antibodies (Section 1.5.1) were prepared in 1x TBST containing 5% BSA or skimmed milk (depending on the manufacturers`

recommendations) and added to the membranes. The membranes were incubated overnight on a shaker at 100 rpm in a cold room. Next day, the primary antibodies were removed, and the membranes were washed three times in total 30 min with 1x TBST at room temperature while shaking (100 rpm). Subsequently, diluted horseradish peroxidase (HRP)-conjugated secondary antibodies prepared in 1x TBST containing 5% skimmed milk were added to the membranes and incubated at room temperature on a shaker at 100 rpm. The membranes were washed three times in total 30 min with 1x TBST at RT, shaking (100 rpm). To prepare the substrate working solution, equal parts of the substrate and stable Peroxide components from SuperSignal West Pico PLUS Chemiluminescent Substrate kit were combined (for a mini blot, 5 mL of substrate was mixed with 5 mL of stable peroxide). The membrane was incubated with the substrate working solution for 3-5 minutes. An absorbent tissue was used to remove any excess liquid and any bubbles between the blot and the membrane protector was gently eliminated. Finally, chemiluminescence was detected using the Fusion SL detection device. Western Blot was performed in collaboration with Ece Tavukcuoglu.
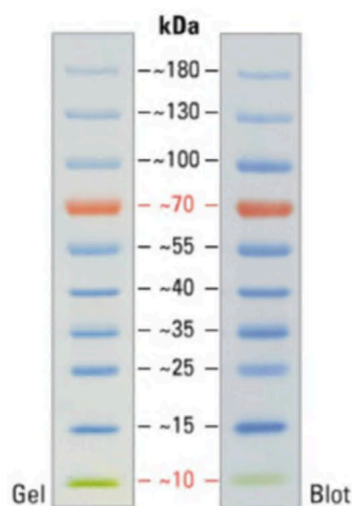
Figure 5. SDS-PAGE band profile of Thermo Scientific PageRuler prestained protein ladder.

4.10 Flow cytometry analysis

4.10.1 Extracellular staining

Cells (2×10^5-1×10^6) were transferred into a 96 well round bottom plate or 5 mL flow tubes followed by washing at 300 x g for 5 min at 4 °C with PBS. The pellet was resuspended in 100 µL FACS buffer containing a master mix of the conjugated antibodies with 1:200 Fc block. The cells were further incubated for 30 min at 4 °C in the dark and washed (300 x g, 5 min, 4 °C) with PBS. Then they were resuspended in 100 µl of FACS buffer for subsequent analysis on the BD FACSLyric^{TM} flow cytometer.

4.10.2 Apoptosis assay

Stimulated monocytes or generated MDSC were stained with antibodies for extracellular markers as described above. Afterwards, cells were washed and resuspended in 100 µL (1×10^5 cells) of Annexin V binding buffer. Annexin V and 7-AAD were added according to the manufacturer's instructions. Cells were then incubated for 15 minutes at RT, resuspended in 400 µL of Annexin V binding buffer and analyzed by flow cytometry. Gating strategy used to determine apoptotic and necrotic cells is shown in Figure 6.
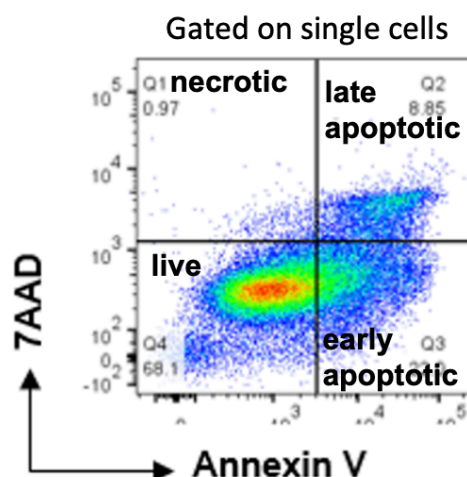
Figure 6. Gating strategy to determine early (annexin V$^+$7AAD$^-$) and late apoptotic (annexin V$^+$7AAD$^+$), necrotic (annexin V$^-$7AAD$^+$) and live (annexin V$^-$7AAD$^-$) cells.

4.10.3 ROS and NO detection by flow cytometry

To detect ROS, the CellROX^{TM} Deep Red reagent was diluted 1:500, while for NO detection, the DAF-FM DA reagent was diluted 1:1000 in serum free RPMI medium. The cell pellet (5×10^5) was then resuspended in 100 μL of the respective diluted reagent mix and incubated in the dark at 37 °C for 30 minutes. Afterward, the cells were washed with 1000 μL of PBS, centrifuged at 300 x g and resuspended in 100 μL of PBS. For NO staining, the cells were rested further 15 min at 37 °C before analysis. Following the staining, the cells were immediately measured using the BD FACSLyric^{TM} flow cytometer.

4.10.4 Intracellular staining to detect phosphoproteins

Phosflow Fix buffer I were prewarmed at 37 °C for 5 minutes prior to the staining. After extracellular staining was completed, the cells (5×10^5) were fixed with 100 μL Phosflow Fix buffer I for 10 minutes at 37 °C. Afterward, cells were washed with FACS buffer and centrifuged at 300 x g for 5 minutes. Cells were permeabilized in 200 μL BD phosflow Perm Buffer III for 20 minutes on ice followed by washing twice with 1 mL FACS buffer and resuspension in 100 μL of FACS buffer containing the antibodies for intracellular staining. Then, cells were washed with 1 mL FACS buffer, centrifuged at 300 x g for 5 minutes, and resuspended in 100 μL of FACS buffer. The analysis was performed at the BD FACSLyric^{TM} flow cytometer.

4.11 Enzyme-linked immunosorbent assay (ELISA)

ELISA was performed with the plasma from melanoma patients and healthy donors, obtained after density gradient centrifugation of whole blood as described in Section 4.2.1. The measurements of HSP90α, HMGB1, and S100A8/9 were carried out using ELISA kits from Novus Biologicals (HSP90α and HMGB1) and R&D Systems (S100A8/9) following the manufacturer's protocols. In summary, plasma samples and protein standards were loaded into 96-well plates that were pre-coated with anti-HSP90α or anti-HMGB1 or anti-S100A8/9 antibodies for capturing. The plates were then incubated with biotinylated antibodies followed by adding of streptavidin-conjugated horseradish peroxidase and a substrate solution. Finally, the enzyme reactions were stopped, and optical density (OD value) of each well were measured with TECAN Infinite M200 microplate reader set to 450 nm.

4.12 Suppression of T cell proliferation assay

This assay was performed according to the standardized protocol (57). CD14 monocytes were isolated from PBMCs of healthy donors and then stimulated as described in Sections 4.2.2 and 4.3. After 24 h (for rHSP90α stimulated monocytes) or 72 h (for rHMGB1 and rS100A9 stimulated monocytes and generated MDSC), CD3 T cells were isolated from PBMCs of another healthy donor using human anti-CD3 magnetic beads (as described in Section 4.2.2) and labeled with 20 μM cell proliferation dye eFluor 450 according to the manufacturer's instructions. To stimulate T cells, a 96-well round bottom cell culture plate was coated with human anti-CD3 (1 μg/mL, clone OKT-3) and human anti-CD28 antibodies (2 μg/mL, clone CD28.2) for 3 h at 37°C. Afterwards, stimulated monocytes were washed and co-cultured with CD3 T cells at 1:1 or 1:2 T cell: monocyte ratio in arginine low medium in pre-coated 96-well plate. After 96 hours, the plate was centrifuged at 300 x g for 5 minutes, supernatants were collected into 1.5 mL Eppendorf tubes, and stored at -80°C until further use. Cell pellets were resuspended in 100 μL FACS buffer and T cell proliferation was assessed by measuring the dilution of the proliferation dye using BD FACSLyric™ flow cytometer. The percentage of divided T cells were normalized to the respective control of stimulated T cells alone.

4.13 TCGA data analysis

RNA sequencing data of metastatic melanoma patient samples were obtained from the Cancer Genome Atlas (TCGA) database through cBioPortal (http://www.cbioportal.org). The normalized RNA-seq by expectation maximization (RSEM) read counts for the genes of interest were extracted from the TCGA cBioportal (175). We analyzed the data to examine the changes in MDSC markers in patients with S100A9-low or HMGB1-low versus S100A9-high or HMGB1-high melanoma across all samples (n=20). These samples were divided into two groups, the top quartile, and the bottom quartile, based on their expression levels of S100A9 or HMGB1. Subsequently, an unpaired Student's t-test was conducted to analyze the difference in mean expression of MDSC-related markers in the low and high percentile melanoma samples for the specific gene of interest. The results are presented as a bar plot displaying the genes of interest in y axis and p values in x axis.

4.14   Statistical analysis

Statistical analysis was conducted using GraphPad Prism software with a minimum of three biological replicates. Two groups were compared using paired or unpaired two-tailed Student's t-test, depending on the nature of the data, assuming a Gaussian distribution. Survival curves were generated using the Kaplan-Meier method, and statistical comparison was performed using the Log-rank (Mantel-Cox) test. For microarray analysis, bioinformatics and statistics were carried out as described previously (Section 4.5.2).

5   Results

5.1   Effect of TLR4 and RAGE ligands on MDSC accumulation

5.1.1 Determining concentrations of Resatorvid and FPS-ZM1

In this study, I used two different inhibitors, Resatorvid (TAK-242) and FPS-ZM1, to block TLR4 and RAGE signaling, respectively. Resatorvid blocks the interaction between the TLR4 dimer and its adaptor proteins, TIR domain-containing adapter protein (TIRAP) and TIR domain containing adapter-inducing IFNβ (TRIF) related adaptor molecule (TRAM), leading to the inhibition of NF-κB activation (176). FPS-ZM1, a RAGE antagonist, is a blocker of RAGE V domain-mediated ligand binding (K_i = 25, 148, and 230 nM, against Aβ40, HMGB1, and S100B, respectively binding to RAGE) (177). Investigating the optimal concentration of Resatorvid and FPS-ZM1 was essential for studying the effect of these inhibitors on MDSC-mediated immunosuppression. Therefore, I tried to find out an optimal concentration, in which the inhibitors do not exert cytotoxicity against T cells but also effectively inhibit TLR4 signaling and RAGE signaling in monocytes.

Resatorvid was shown to block LPS-induced production of IL-6, NO, TNF-α in mouse macrophages with IC50 of 1.3 nM, 1.9 nM, and 1.8 nM, respectively (178). In our experiments, Resatorvid inhibited PD-L1 expression mediated by TLR4 agonist LPS at higher concentrations (range 2.5 μM-10 μM) (Figure 8A). The gating strategy to determine PD-L1 expression on stimulated monocytes were shown in Figure 7B. Then, I tested different concentrations of Resatorvid on T cell proliferation. Even at the highest concentration (10 μM),

it did not alter T cell proliferation (Figure 8B). Furthermore, I stimulated monocytes with S100A9 in the presence of 5 μM Resatorvid and found that it did not induce cell death.
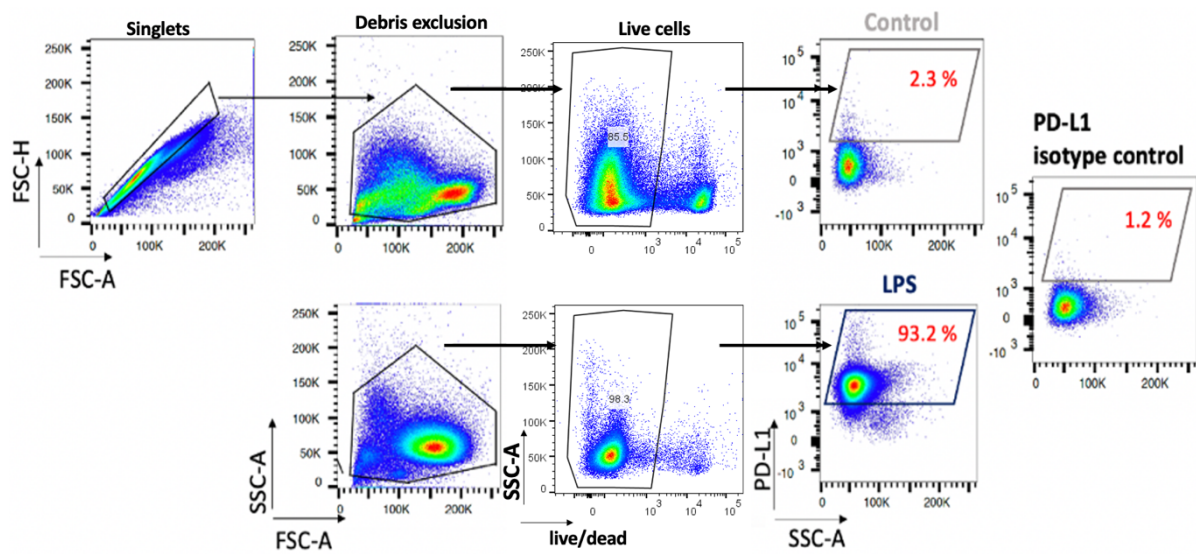
Figure 7. Gating strategy to compare PD-L1 expression on LPS treated monocytes (LPS) and monocytes incubated for 24h in complete RPMI medium (control). Monocytes were incubated with LPS or without LPS in complete RPMI medium (control) for 24h. They were further stained with fluorescently labeled antibodies and analyzed by flow cytometry. Single cells were gated, debris and dead cells were excluded. PD-L1+ were gated according to the respective isotype control.
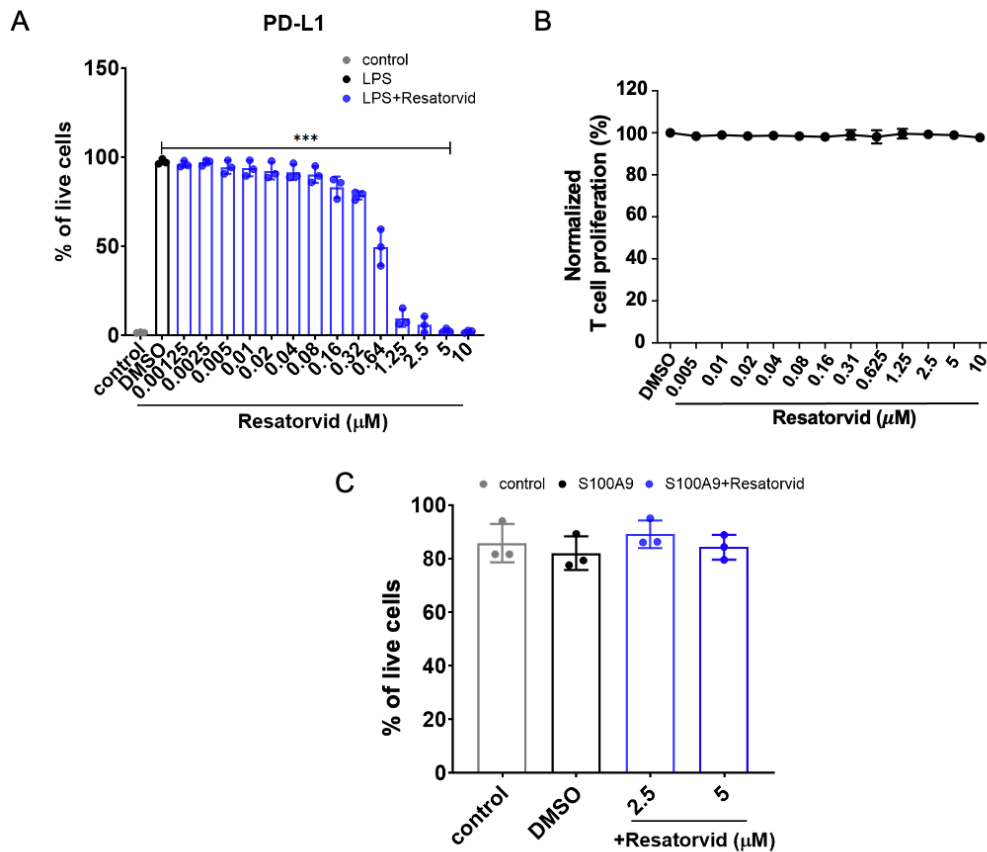
Figure 8. Investigating the optimal Resatorvid concentration for further experiments. Healthy donor-derived monocytes were treated with LPS (100ng/mL) and Resatorvid or DMSO at different concentrations for 24h. (A) Frequency of PD-L1+ monocytes on LPS treated monocytes (LPS) and monocytes incubated for 24h in complete RPMI medium (control) are shown. (B) CD3+ T cells from healthy donor peripheral blood were purified by MACS and labelled with cell proliferation dye eFluor450. They were further co-cultured in a 96 well-plate pre-coated with anti-CD3 and anti-CD28 antibodies in the presence of different concentrations of Resatorvid (0.005-10 μM) or DMSO. Following 96h of incubation, T cell proliferation was determined by eFluor450 dilution measurement by flow cytometry. Proliferation of T cells was normalized to 100 %, and normalized values are shown. (C) Frequency of dead monocytes incubated for 72 h with GM-CSF (40 ng/mL) in the absence (control) or presence of S100A9 (10 μg/mL) (S100A9) with Resatorvid (S100A9+Resatorvid) are shown. Data are presented as mean $\pm$ SD. n=3, *p<0.05, **p<0.01, ***p<0.001.

To determine the optimal concentration for FPS-ZM1, ROS production capacity of monocytes stimulated with S100A9 in the presence or absence of FPS-ZM1 was assessed (Figure 9A).

FPS-ZM1 could downregulate ROS production by monocytes at concentrations ranging from 30 to 60 nM. However, FPS-ZM1 at 40-60 nM significantly decreased the proliferation of T cells (Figure 9B). In addition, FPS-ZM1 at 30 nM did not induce a significant increase in the frequency of dead monocytes after 72 h of stimulation of monocytes.

Thus, I decided to test the effect of Resatorvid at 5μM and FPS-ZM1 at 30nM in our experiments.
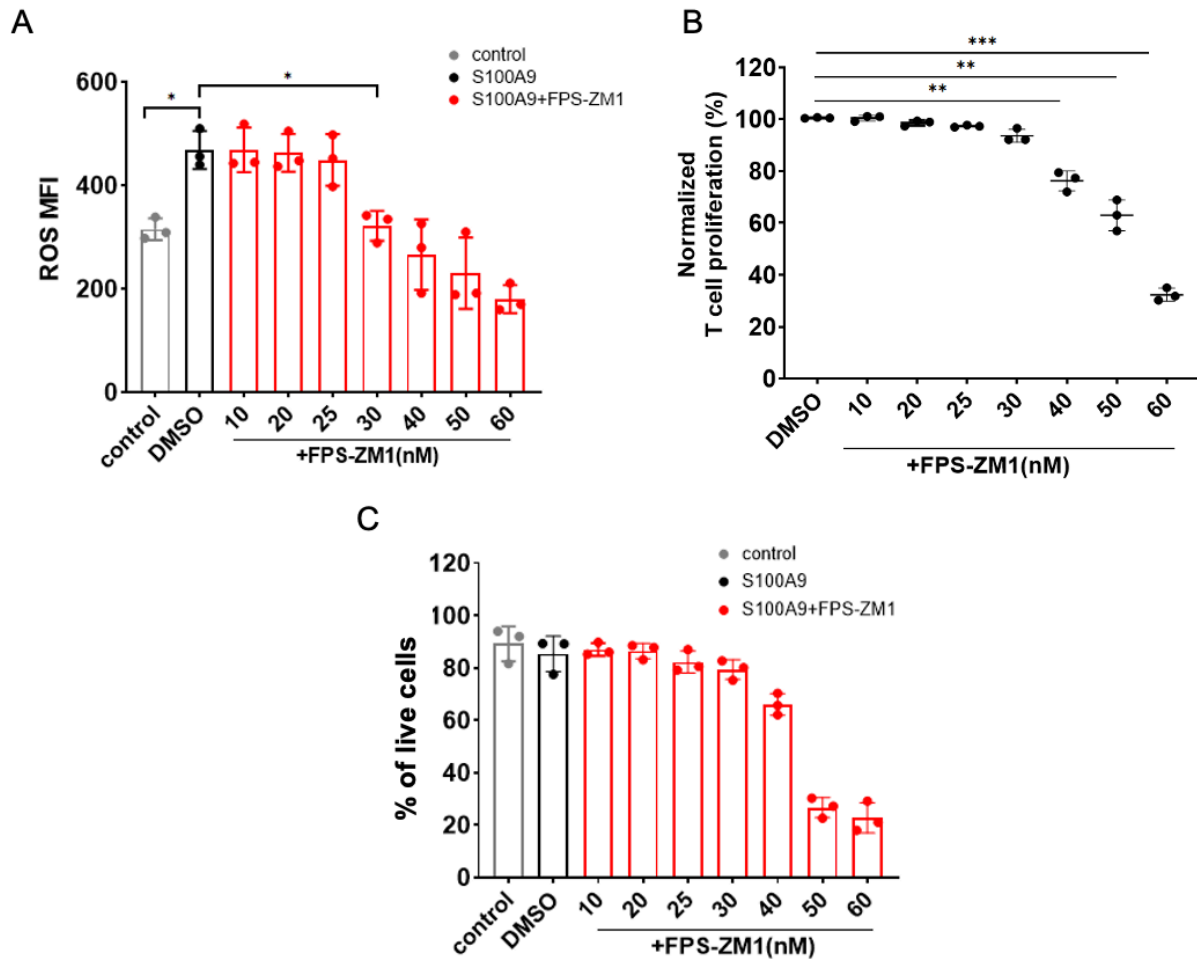
Figure 9. Investigating the optimal FPS-ZM1 concentration for further experiments. (A) Healthy donor-derived monocytes were treated with S100A9 (10 μg/mL) and FPS-ZM1 or DMSO at different concentrations for 72 h. Frequency of PD-L1$^+$ monocytes on LPS treated monocytes (LPS) and monocytes incubated for 24 h in complete RPMI medium (control) and are shown. (B) CD3$^+$ T cells from healthy donor peripheral blood were purified by MACS and labelled with cell proliferation dye eFluor450. They were further co-cultured in a 96 well-plate pre-coated with anti-CD3 and anti-CD28 antibodies in the presence of different concentrations of FPS-ZM1 (10-60 nM) or DMSO. Following 96h of incubation, T cell proliferation was determined by eFluor450 dilution measurement by flow cytometry. Proliferation of T cells was normalized to 100 %, and normalized values are shown. (C) Frequency of dead monocytes incubated for 72 h with GM-CSF (40 ng/mL) in the absence (control) or presence of S100A9 (10 μg/mL) (S100A9) with FPS-ZM1 (S100A9+FPS-ZM1) are shown. Data are presented as mean ± SD. n=3, *p<0.05, **p<0.01, ***p<0.001.

5.1.2 HSP90α converted normal monocytes into immunosuppressive cells through TLR4 signaling

Previous studies in our lab demonstrated that upon exposure to melanoma-derived HSP90α-bearing extracellular vesicles, normal human monocytes upregulated PD-L1 and were converted into immunosuppressive MDSC via TLR4 signaling (56). To further analyze a possible role of TLR4 signaling and soluble HSP90α in the suppressive functions of MDSC, normal monocytes were treated with recombinant HSP90α (rHSP90α) for 24 h. I found that rHSP90α-treated monocytes upregulated PD-L1 expression, and Resatorvid blocked this upregulation (Figure 10A). The microarray analysis demonstrated that several MDSC related markers including CD274 (PD-L1), IDO-1, S100A12, CCL2, and CXCL5 upregulated in monocytes upon the treatment with rHSP90α (Figure 10B). Moreover, such monocytes displayed a significant capacity to inhibit T cell proliferation (Figures 10C and 10D). The treatment with Resatorvid was able to attenuate this suppression (Figure 10E).

A — PD-L1

B — HSP90α vs control

C

D

E
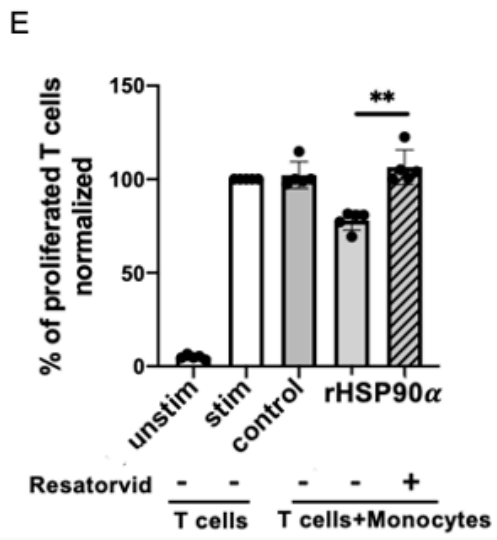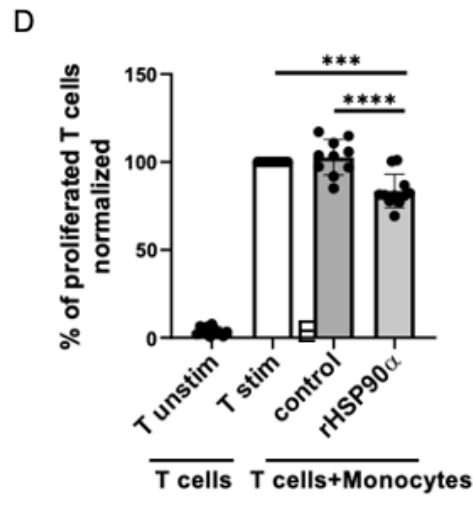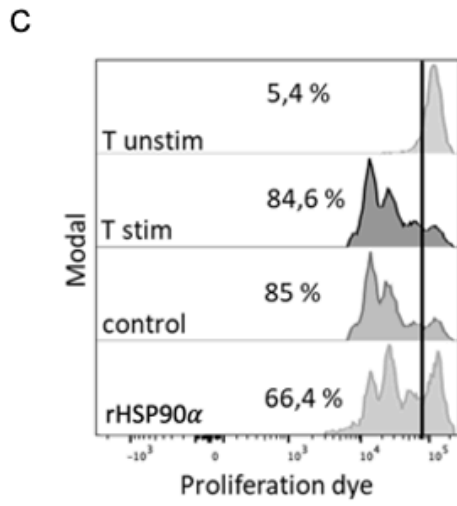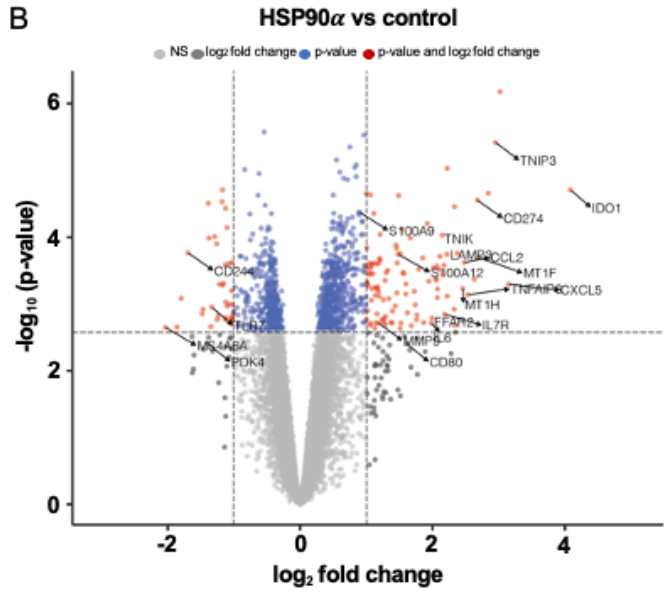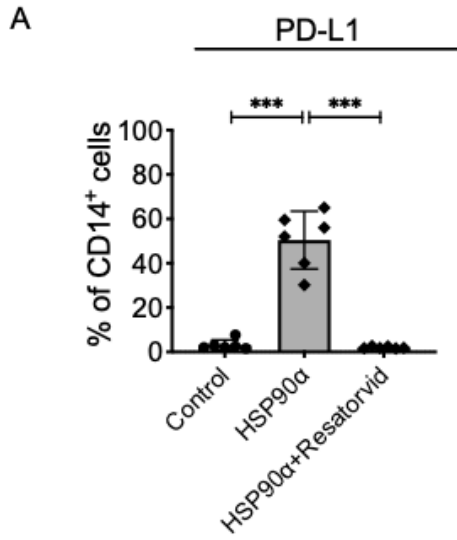
Figure 10. rHSP90α induced immunosuppressive monocytes via TLR4 signaling. (A) Healthy donor-derived monocytes were treated with 2 µg/mL rHSP90α $\pm$ Resatorvid (5 µM) or left untreated (control) for 24h. PD-L1 expression was analyzed by flow cytometry. (B) Microarray analysis of rHSP90α treated monocytes. Volcano plot representing differentially expressed genes. Horizontal dashed line indicates significance threshold (p<0.05). Vertical dashed line indicates 2-fold change. (C) Representative histograms and (D) bar graphs showing the proliferation of T cells stimulated with anti-CD3 and anti-CD28 antibodies and co-cultured with monocytes treated with rHSP90α or untreated (control) at 1:2 ratio in the presence of for 4 days. (E) Proliferation of T cells co-cultured with monocytes treated with rHSP90α (D) $\pm$ Resatorvid (5 µM). Data are presented as mean $\pm$ SD. n = 4-10, *p<0.05, **p<0.01, ***p<0.001).

5.1.3 rHMGB1 and rS100A9 induced MDSC-related marker expression on monocytes

Next, I stimulated monocytes with TLR4/RAGE ligands rHMGB1 and rS100A9. First, I checked the viability of monocytes after 72 h stimulation with rHMGB1 or rS100A9. rHMGB1 did not alter the survival of monocytes, whereas the addition of FPS-ZM1 reduced the survival (Figure 11A). In contrast, rS100A9, induced a cytotoxic effect on monocytes, which was further upregulated upon FPS-ZM1 treatment (Figure 11B).
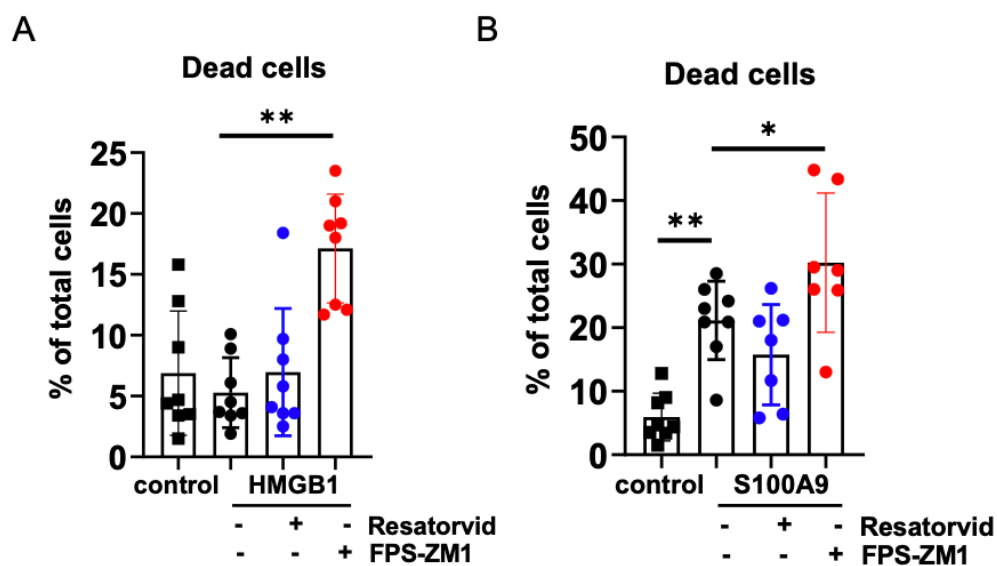
Figure 11. The viability of monocytes upon stimulation with rHMGB1 or rs100A9. Monocytes were pre-treated with Resatorvid (5μM) or FPS-ZM1 (30 nM) for 1 h, then stimulated with rHMGB1 (5 μg/mL) or S100A9 (10 μg/mL) in the presence of GM-CSF (40 ng/mL) for 72 h. Cumulative data for the frequency of dead cells in (A) HMGB1 or (B) S100A9 stimulated monocytes were shown. Monocytes treated for 72 h with GM-CSF only were shown as a control. Data are presented as mean $\pm$ SD. n=7-8, *p<0.05, **p<0.01.

The expression of PD-L1, HLA-DR, CD86, and CD80 on monocytes were further assessed. The gating strategy to determine the expression of these markers is shown in Figure 11. After 72 h stimulation with either rHMGB1 or rS100A9, PD-L1 expression on monocytes was upregulated in a TLR4-dependent manner (Figure 13A and 13B). Moreover, upon stimulation with rHMGB1 or rS100A9, HLA-DR, and CD86 expression were downregulated. Both RAGE and TLR4 inhibitors reversed HLA-DR (Figure 13C and 13D) and CD86 (Figure 13E and 13F) decreased on monocytes treated with rS1009 or rHMGB1. Additionally, CD80 expression on monocytes tended to downregulate upon their stimulation with rHMGB1 and to elevate again upon the treatment with Resatorvid and FPS-ZM1 (Figure 13G). However, rS100A9 promoted an upregulation of CD80 expression, which was even enhanced after FPS-ZM1 treatment (Figure 13H).
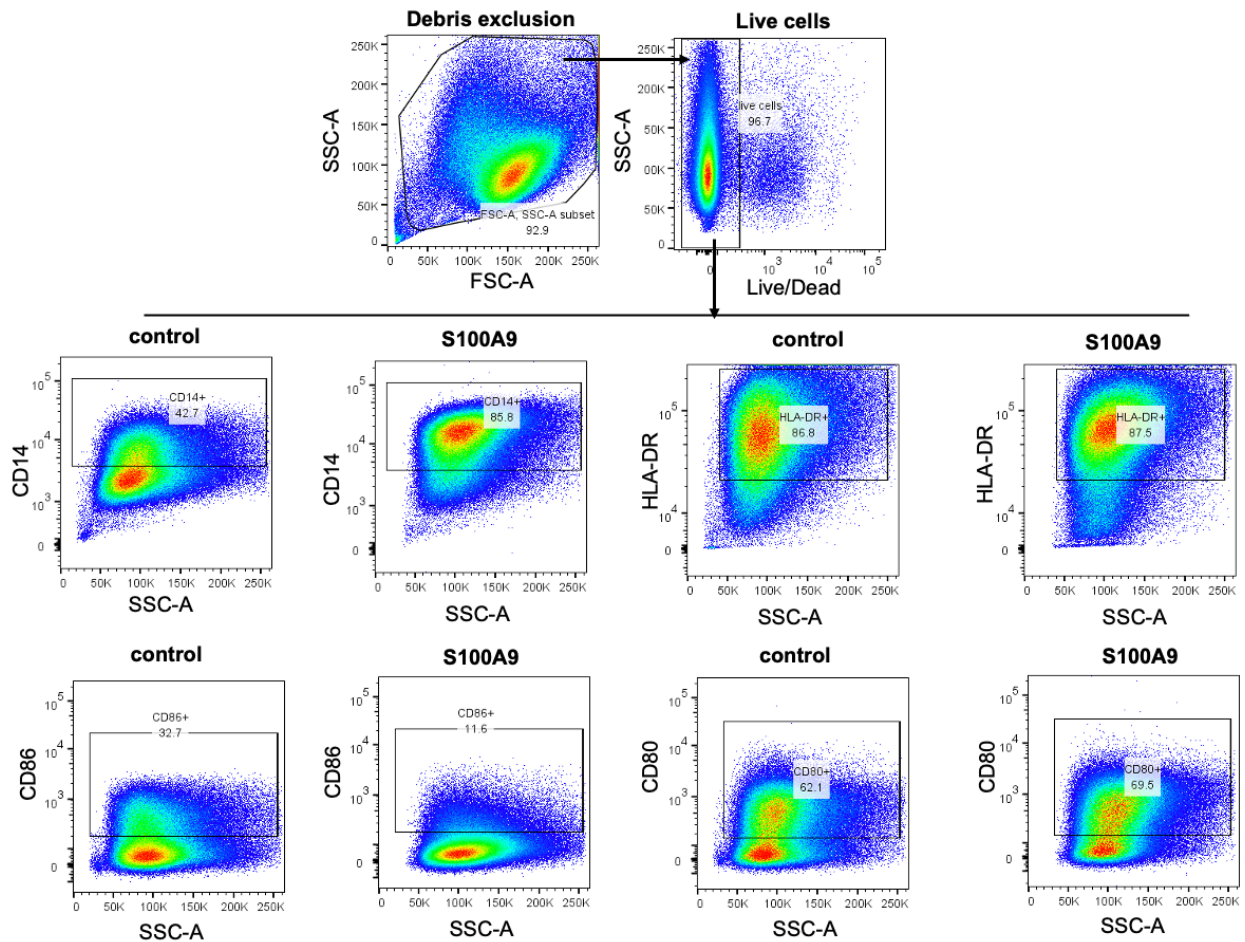
Figure 12. Gating strategies to determine the expression of CD14, HLA-DR, CD86, and CD80 on monocytes. CD14 monocytes were stained with fluorescently labelled antibodies and analyzed by flow cytometry. Single cells were gated, debris and dead cells were excluded. CD14^{+}, HLA-DR^{+}, CD86^{+}, and CD80^{+} cells were gated according to the respective isotype control.

Next, ROS production and IDO expression by monocytes were determined. rS100A9 and rHMGB1 induced ROS production on monocytes that was downregulated in the presence of both RAGE or TLR4 inhibitors (Figure 14A and 14B). IDO expression was also induced by rS100A9 in monocytes and was blocked by Resatorvid but not by FPS-ZM1 (Figure 14C).
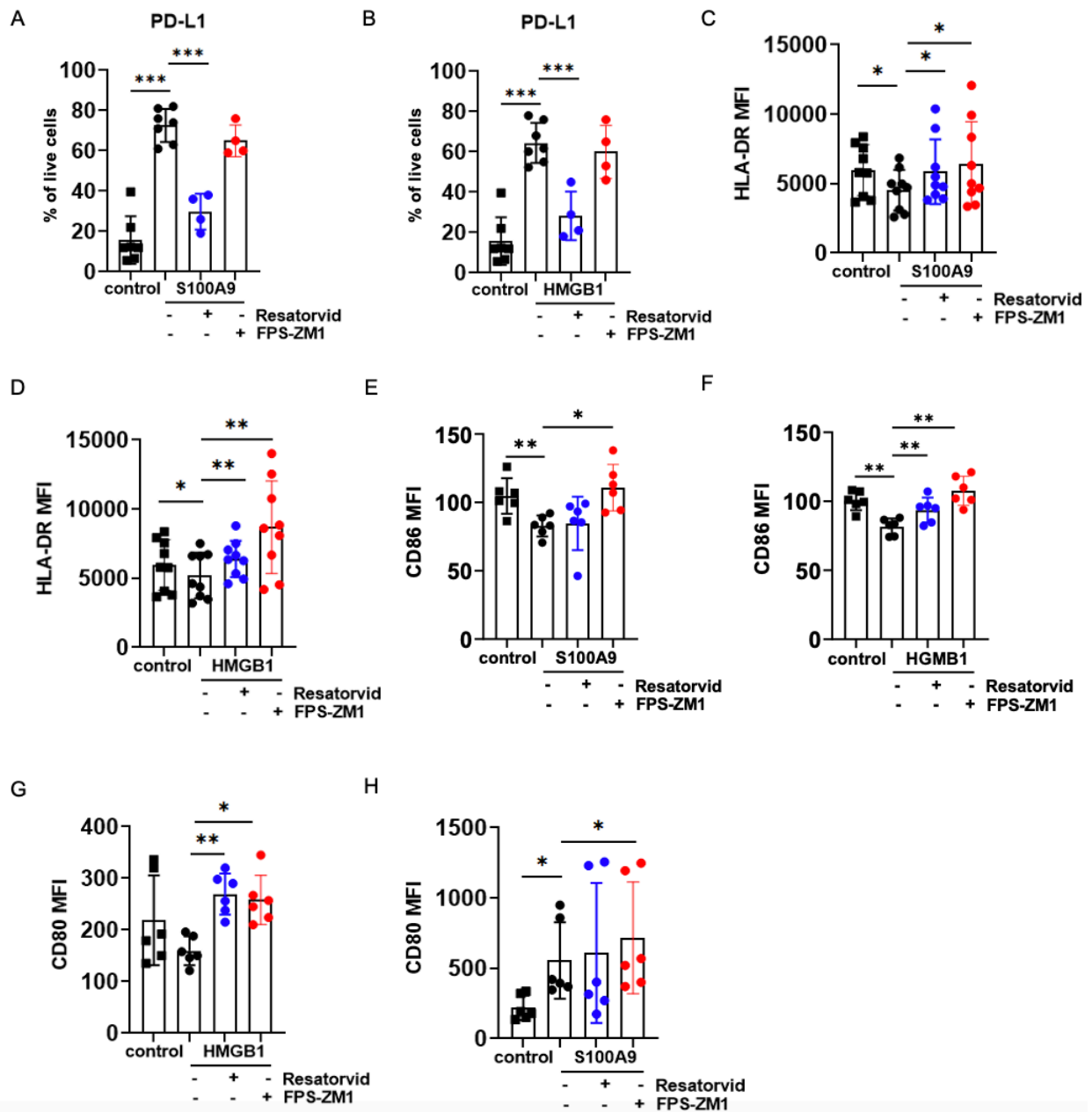
Figure 13. Effect of rHMGB1 and rS100A9 on the expression of markers related to immune functions of monocytes. Cumulative data for (A-B) PD-L1 expression, (C-D) HLA-DR mean fluorescence intensity (MFI), and (E-F) CD86 MFI, and (G-H) CD80 MFI of S100A9 or HMGB1 stimulated monocytes (for 72 h) pre-treated with Resatorvid or FPS-ZM1 in the presence of GM-CSF. Monocytes treated for 72 h with GM-CSF only are shown as a control. Data are presented as mean± SD. n=4-9, *p<0.05, **p<0.01, ***p<0.001.
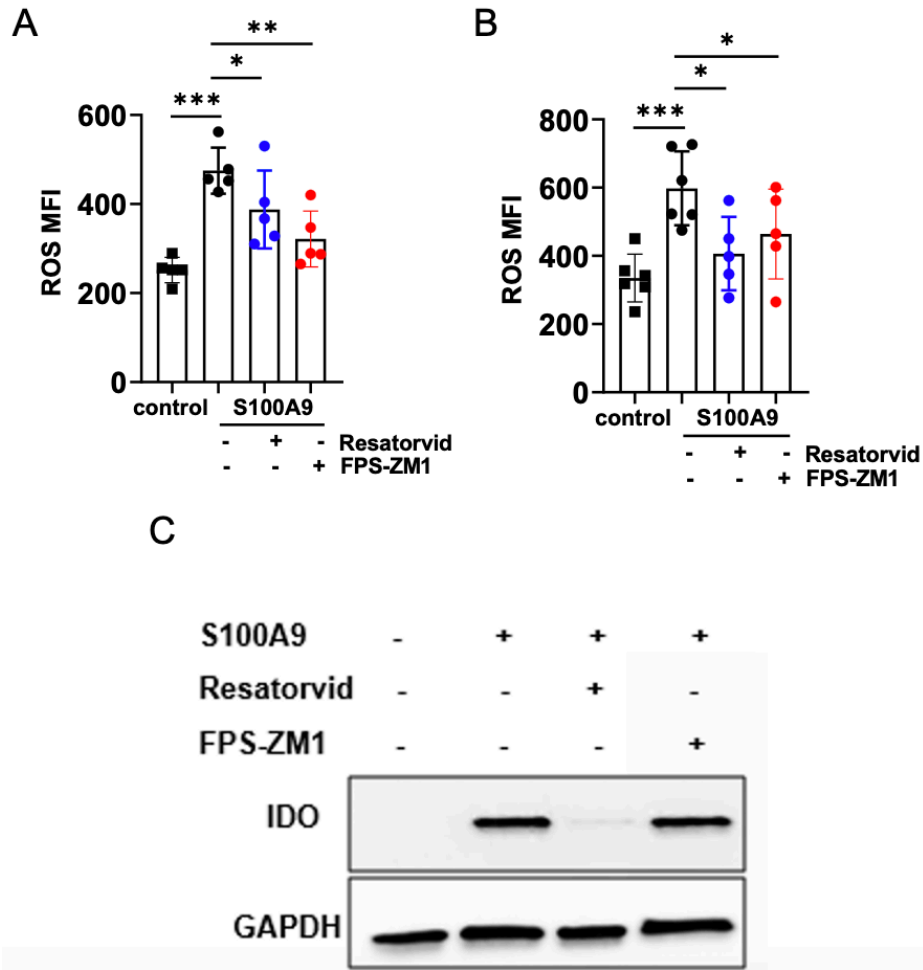
Figure 14. rHMGB1 and rS100A9 upregulated ROS production capacity of monocytes. Cumulative data for (A-B) ROS MFI and (C) Western blot analysis of IDO expression of S100A9 or HMGB1 stimulated monocytes (for 72 h) pre-treated with Resatorvid or FPS-ZM1 in the presence of GM-CSF. Monocytes treated for 72 h with GM-CSF only were shown as control. Data are presented as

To further investigate the mechanisms, by which rS100A9 and rHMGB1 enhance MDSC activation and generation, the expression of RAGE, TLR4, and CD14 on stimulated monocytes were assessed. The gating strategy for RAGE and TLR4 expression on monocytes is presented in Figure 15.
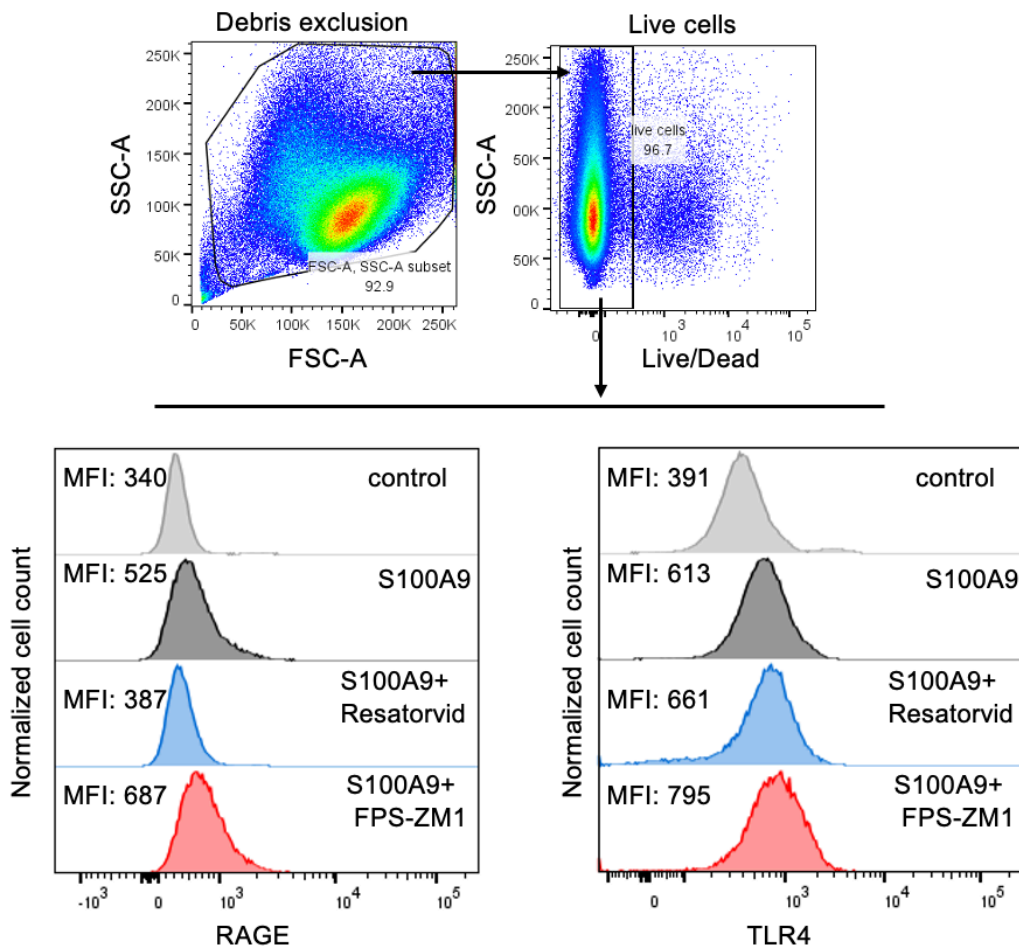
Figure 15. Gating strategies to determine the expression of TLR4 and RAGE on monocytes.

I found out that RAGE expression was upregulated upon the stimulation with rHMGB1 or rS100A9, which was downregulated upon the treatment with Resatorvid (Figures 16A and 16B). In contrast, RAGE inhibitor further upregulated the expression of RAGE on stimulated monocytes (Figure 16B). Similarly, TLR4 expression was enhanced on monocytes stimulated with rS100A9 and rHMGB1. However, no significant alteration of TLR4 expression on monocytes was detected after the exposition to inhibitors.
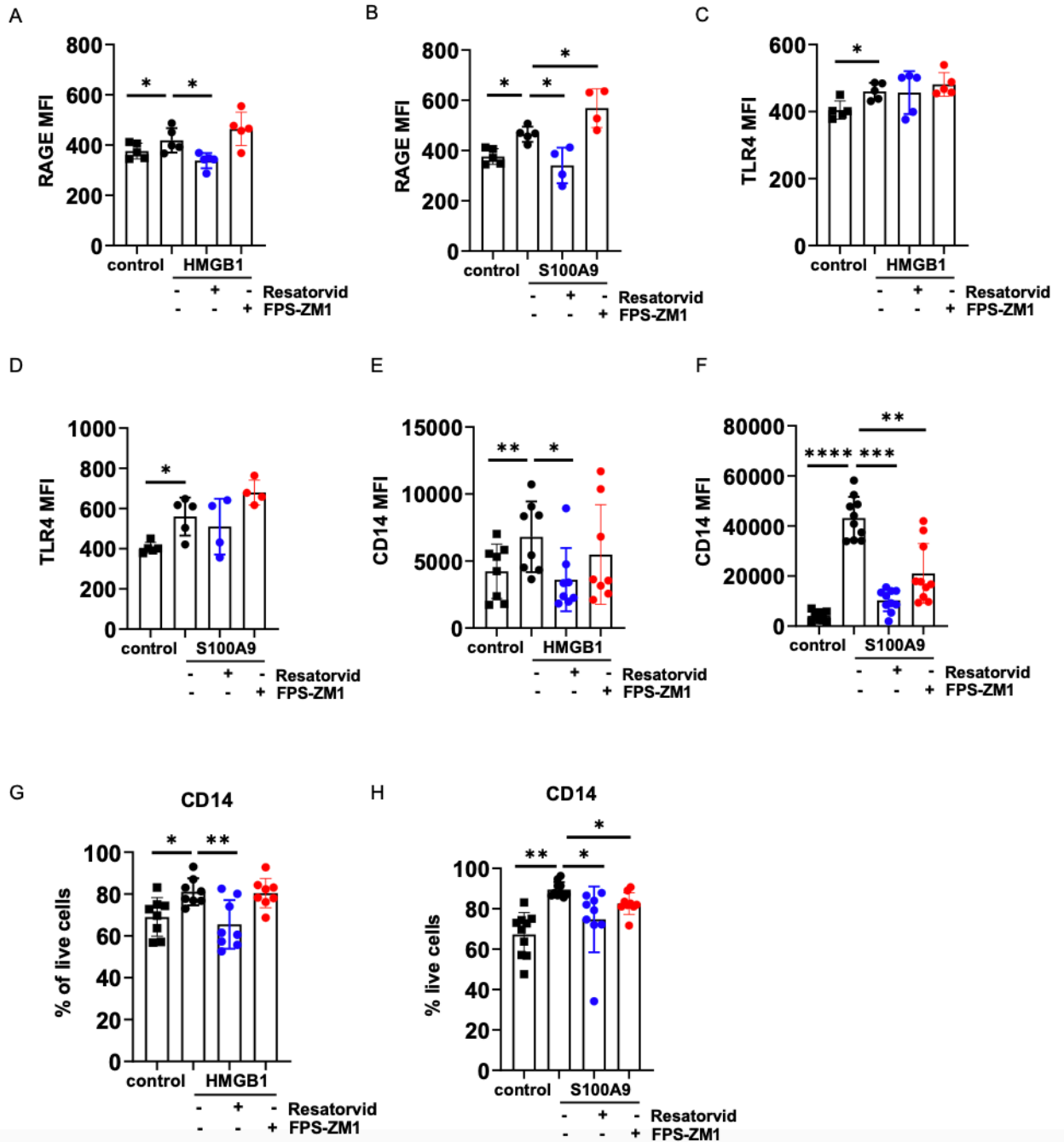
Figure 16. The influence of rHMGB1 and rS100A9 on RAGE, TLR4, and CD14 expression of monocytes. Cumulative data for MFI of (A-B) RAGE, (C-D) TLR4 and (E-F) CD14 as well as for the frequency of (G-H) CD14 expressing monocytes upon the stimulation with rS100A9 or rHMGB1 (for 72 h) and the pre-treatment with Resatorvid or FPS-ZM1 in the presence of GM-CSF. Monocytes treated for 72 h with GM-CSF only were shown as a control. Data are presented as mean± SD. n=4-10, *p<0.05, **p<0.01, ***p<0.001, ****p<0.0001.

Although monocytes treated with GM-CSF only (control) lost their CD14 expression, it was maintained in the rHMGB1 and rS100A9 stimulated monocytes (Figure 16E-16H). Whereas the addition of Resatorvid remarkably diminished CD14 expression on monocytes stimulated either with rHMGB1 or rS100A9, FPS-ZM1 only affected CD14 expression on rS100A9 treated monocytes (Figure 16E-16H).

5.1.4 TLR4 induced STAT3 and p38/MAPK activity, whereas RAGE involved mainly in NF-κB activation in monocytes by S100A9 or HMGB1

Activation of RAGE and TLR4 can induce multiple signaling pathways including MAPK, NF-κB pathways and STAT3 activation (153). Downstream pathway molecules involved in RAGE and TLR4 signaling were further investigated in monocytes stimulated with rS100A9 or rHMGB1 to find out their possible roles in S100A9 or HMGB1-mediated MDSC activation. I found out that p-p38 and p-p65 (NF-κB) levels were enhanced in rHMGB1 or rS100A9 treated monocytes (Figure 17A-17D). Whereas TLR4 inhibitor, but not RAGE inhibitor diminished the p-p38 expression in the S100A9 treated monocytes (Figure 17B), both inhibitors significantly reduced the p-NF-κB expression in both HMGB1 and S100A9 treated monocytes (Figure 17C and 17D).
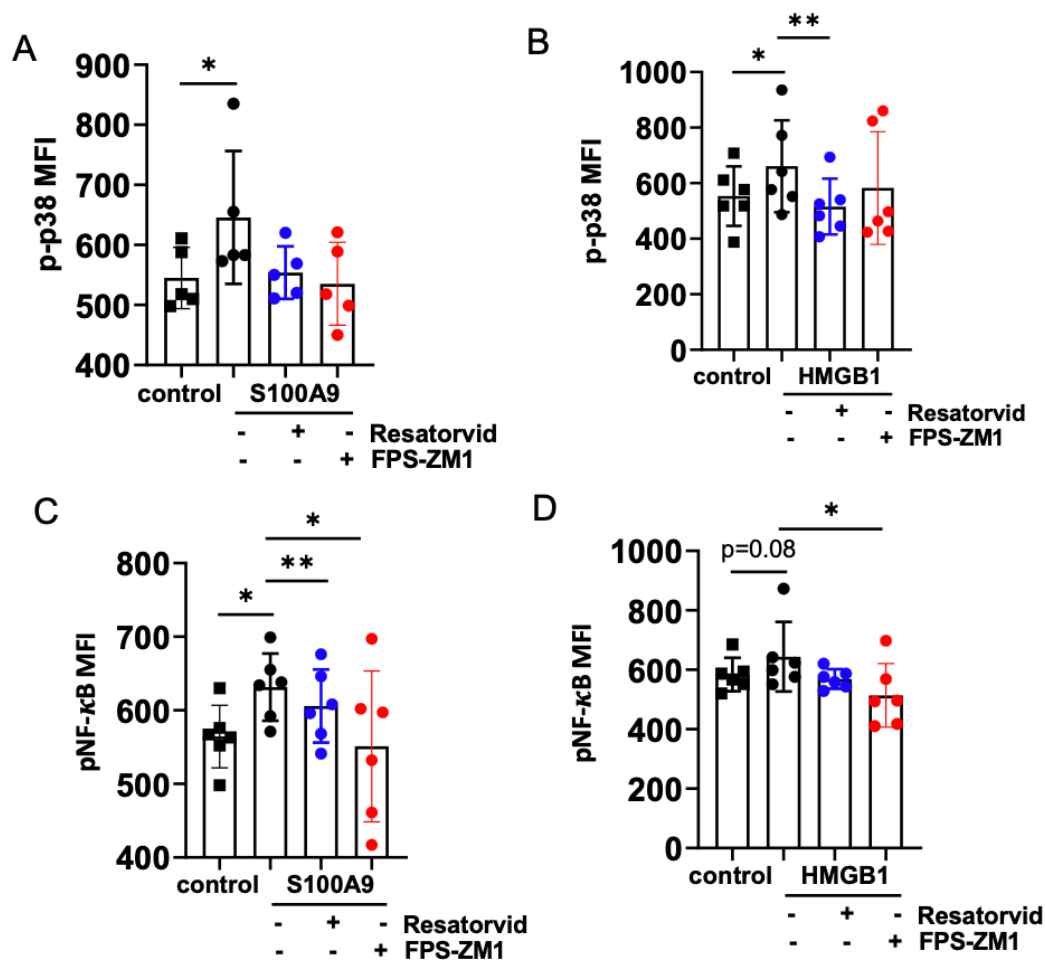
Figure 17. TLR4 induced p38/MAPK activity, whereas RAGE involved mainly in NF-κB activation in monocytes by S100A9 or HMGB1. Monocytes were stained with fluorescent-conjugated antibodies for surface markers, then they were fixed, permeabilized, and stained with antibodies for intracellular p-p38 and p-p65. Cumulative data for MFI of (A-B) p-p38 and (C-D) pNF-κB in monocytes stimulated with S100A9 or HMGB1 (for 72 h) and pre-treated with Resatorvid or FPS-ZM1 in the presence of GM-CSF. Monocytes treated for 72 h with GM-CSF only were shown as control. Data are presented as mean± SD. n=6, *p<0.05, **p<0.01.

STAT3 activity was enhanced in both HMGB1 (Figure 18A) and S100A9 (Figure 18B and 18C) stimulated monocytes. Interestingly, the TLR4 inhibitor Resatorvid, but not RAGE inhibitor FPS-ZM1, blocked HMGB1 or S100A9-induced STAT3 activation (Figure 18A-18C).
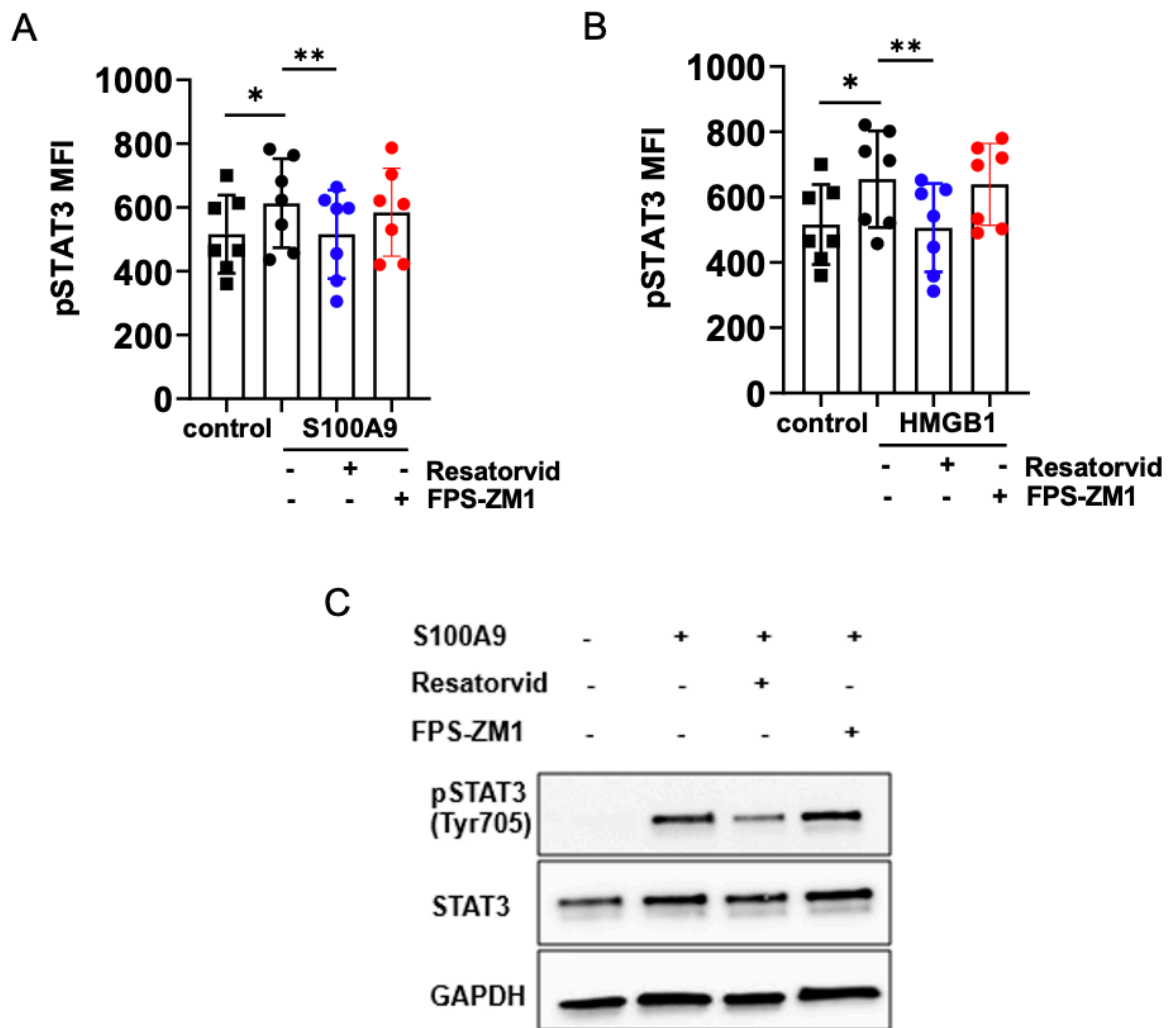
Figure 18. TLR4 mainly involved in the activation of STAT3 by rHMGB1 or rS100A9. Monocytes were stained with fluorescent-conjugated antibodies for surface markers, fixed, permeabilized and stained with antibodies for intracellular p-STAT3. Cumulative data for MFI of (A-B) p-STAT3 and (C) Western blot analysis of p-STAT3 expression in in monocytes stimulated with rS100A9 or rHMGB1 (for 72 h) and pre-treated with Resatorvid or FPS-ZM1 in the presence of GM-CSF. Monocytes treated for 72h with GM-CSF only were shown as control. Data are presented as mean± SD. n=3-7, *p<0.05, **p<0.01.

To gain a more profound understanding of the impact of S100A9 on monocytes, we performed microarray analysis comparing monocytes stimulated with rS100A9 and GM-CSF-stimulated and stimulated with GM-CSF only (S100A9 versus control), Resatorvid-treated and non-treated (S100A9+Resatorvid versus S100A9), and FPS-ZM1 treated and non-treated (S100A9+FPS-ZM1 versus S100A9) monocytes. In parallel to our previous findings, gene

expression profiling confirmed the increased expression of PD-L1 (CD274) and IDO1 in monocytes treated with rS100A9 (Figure 19A). In addition, several other MDSC-related genes such as IL6, IL10, ARG2, CXCL1, and CXCL2 were elevated (Figure 19A). Among the genes involved in the immunostimulatory function of myeloid cells, CD80 was slightly upregulated whereas CD86 was downregulated (data not shown). Additionally, I found an upregulation of S100A9 and S100A12 in monocytes stimulated with rS100A9. While Resatorvid treatment significantly reduced several MDSC-related genes including CD274, IDO1, CXCL1, CXL2, and IL-10 induced by rS100A9 (Figure 19B), the effect of FPS-ZM1 was not that drastic. FPS-ZM1 promoted the downregulation of S100A12 and CX3CR1. However, the expression of several MDSC-related genes was not altered (Figure 19C).
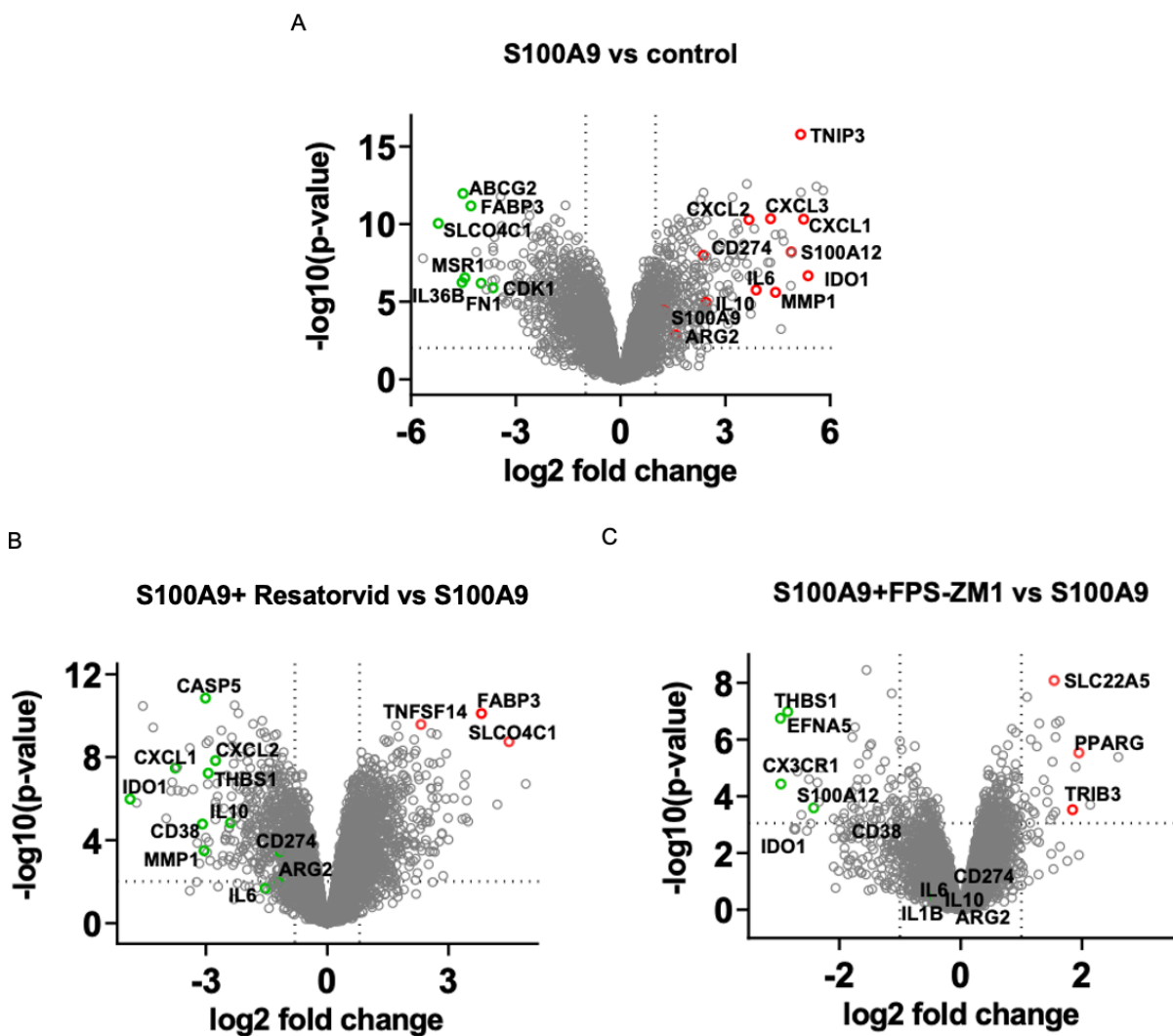
Figure 19. Microarray analysis of S100A9-stimulated monocytes. Monocytes stimulated with rS100A9 and GM-CSF for 72 h in the presence or absence of Resatorvid or FPS-ZM1 were analyzed by microarray technique (n=4). Volcano plot showing the differentially expressed genes between (A) monocytes treated with rS100A9 versus cells treated with GM-CSF only, (B) monocytes treated with rS100A9 in the presence of Resatorvid versus cells treated with S100A9, and (C) monocytes treated with rS100A9 in the presence of FPS-ZM1 versus those treated with S100A9. Horizontal dashed line indicates significance threshold (p<0.05). Selected differentially expressed genes were shown in red (upregulated) and green circles (downregulated). Vertical dashed line indicated two-fold change. Vertical dashed line indicated two-fold change.

5.1.5 S100A9 and HMGB1 converted monocytes into immunosuppressive MDSC mainly through TLR4 signaling

We demonstrated that S100A9 and HMGB1 induced the upregulation of MDSC gene signatures on monocytes. However, defining immunosuppressive MDSC still relies on determining their suppressive activity (179)**.** Therefore, the immunosuppressive activity of monocytes treated with S100A9 and HMGB1 were studied. We found that both rHMGB1 (Figure 20A and 20B) and rS100A9 (Figure 20C and 20D) stimulated normal monocytes to inhibit T cell proliferation. Whereas such suppression was reversed by the pre-treatment of monocytes with TLR4 inhibitor Resatorvid, the treatment with RAGE inhibitor FPS-ZM1 did not significantly alter the capacity of monocytes to inhibit T cell proliferation (Figure 20).
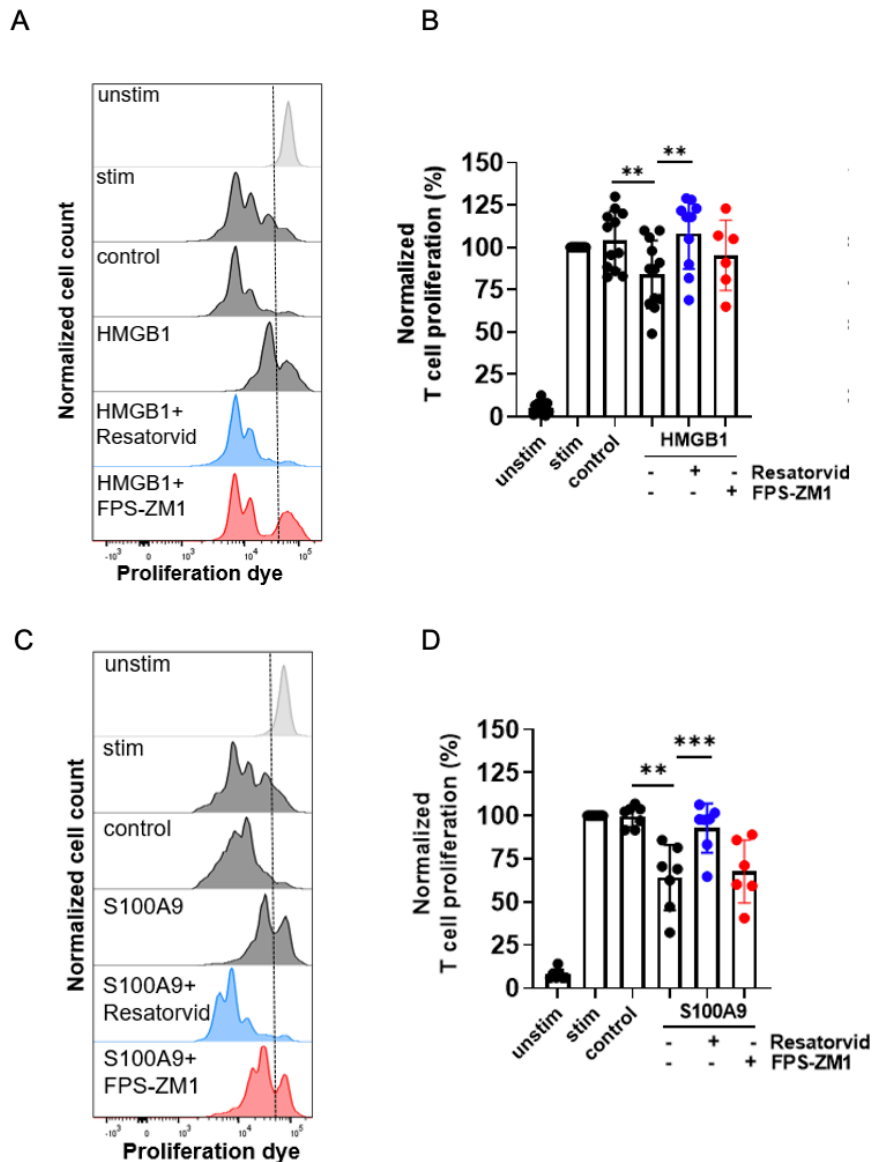
Figure 20. S100A9 and HMGB1 converted monocytes into immunosuppressive MDSC through TLR4 signaling. Monocytes were pre-treated with Resatorvid (5μM) or FPS-ZM1 (30nM) for 1h, then stimulated with rHMGB1 (5 μg/mL) or S100A9 (10μg/mL) in the presence of GM-CSF (40 ng/mL) for 72h. Monocytes treated for 72h with GM-CSF only were shown as control. After 72h, monocytes were harvested and co-cultured with allogenic CD3 T cells labelled with eFluor450 proliferation dye at 1:2 ratio in a 96-well plate pre-coated with anti-CD3 and anti-CD28 antibodies. (A, C) Representative histograms for proliferated T cells in the co-cultures with HMGB1- or S100A9-treated monocytes. (B, D) Cumulative data for proliferated T cells in the co-cultures with (A-B) HMGB1- or (C-D) S100A9-treated monocytes. Data are presented as the percentage of divided T cells normalized to the respective control of stimulated T cells (T stim). Data are presented as mean± SD. n=6-12, *p<0.05, **p<0.01, ***p<0.001.

5.2 Effect of TLR4 inhibitor on MDSC activity

5.2.1 Resatorvid abrogated suppression of T cell proliferation mediated by in vitro generated MDSC.

Since the TLR4 inhibitor Resatorvid showed a remarkable potential to block S100A9 or HMGB1-induced MDSC generation from healthy donor-derived monocytes, we wanted to investigate the effect of Resatorvid on the immunosuppressive capacity of already developed MDSC. First, I optimized an *in vitro* human MDSC generation protocol adapted from two different previously published protocols (180, 181). Monocytes were isolated from healthy donor-derived peripheral blood or buffy coat and treated with GM-CSF (50 ng/mL) and IL-6 (50 ng/mL) for 4 d. Then, *in vitro* generated MDSC were harvested and co-cultured with T cells (Figure 21A). I detected that generated MDSC significantly suppressed T cell proliferation, and the blockade of TLR4 signaling led to the attenuation of such effect mediated by *in vitro* generated MDSC (Figure 21B). Interestingly, Resatorvid was able also to significantly increase the frequency of total apoptotic cells within these MDSC (Figure 21C).
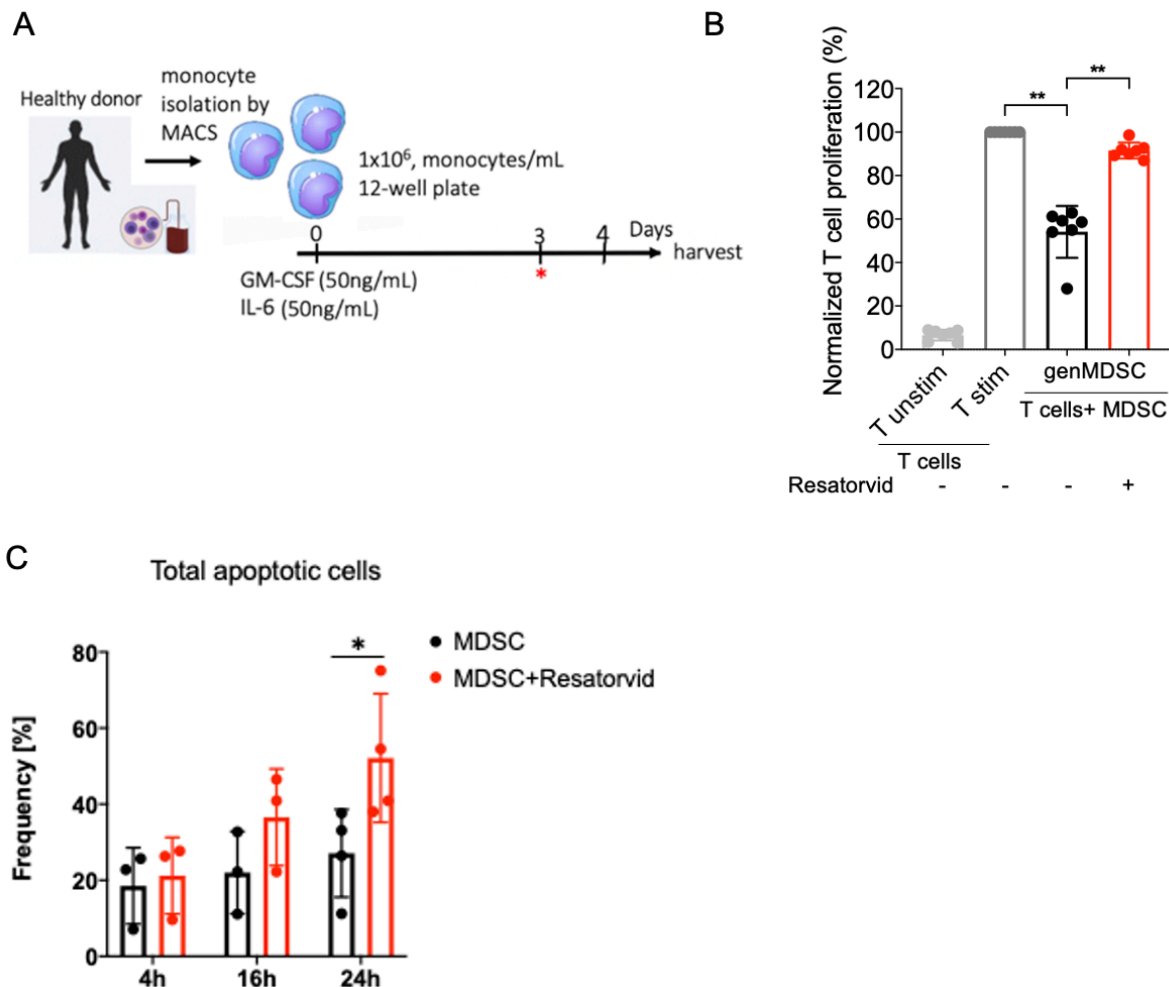
Figure 21. Resatorvid abrogated the suppression of T cell proliferation mediated by in vitro generated MDSC and promoted MDSC apoptosis. (A) Schematic presentation of the protocol for human MDSC generation from healthy donor-derived monocytes in vitro. (B) For the suppression of T cell proliferation assay, CD3+ T cells labelled with eFluor450 proliferation dye were co-cultured for 4 d with in vitro generated MDSC at the ratio 1:1 in a 96-well plate pre-coated with anti-CD3 and anti-CD28 antibodies in the presence of Resatorvid (5 μM) or DMSO (as control). T cell proliferation was assessed by flow cytometry. (C) In vitro generated MDSC were treated with Resatorvid for 24 h. The apoptotic cells were determined by Annexin V/7-AAD staining followed by flow cytometry. Cumulative data showing the frequency of total apoptotic cells within generated MDSC. Data are presented as mean± SD. n=4-7,

Next, we performed microarray analysis with *in vitro* generated MDSC treated with DMSO (as a control) or Resatorvid. Genes that were significantly downregulated upon Resatorvid treatment included CX3CR1, CD38, and CCR2 (Figure 22A). Analysis of KEGG pathways

revealed that among the genes with an increased expression in Resatorvid-treated MDSC, many were involved in apoptosis and cell metabolic activity (Figure 22B).
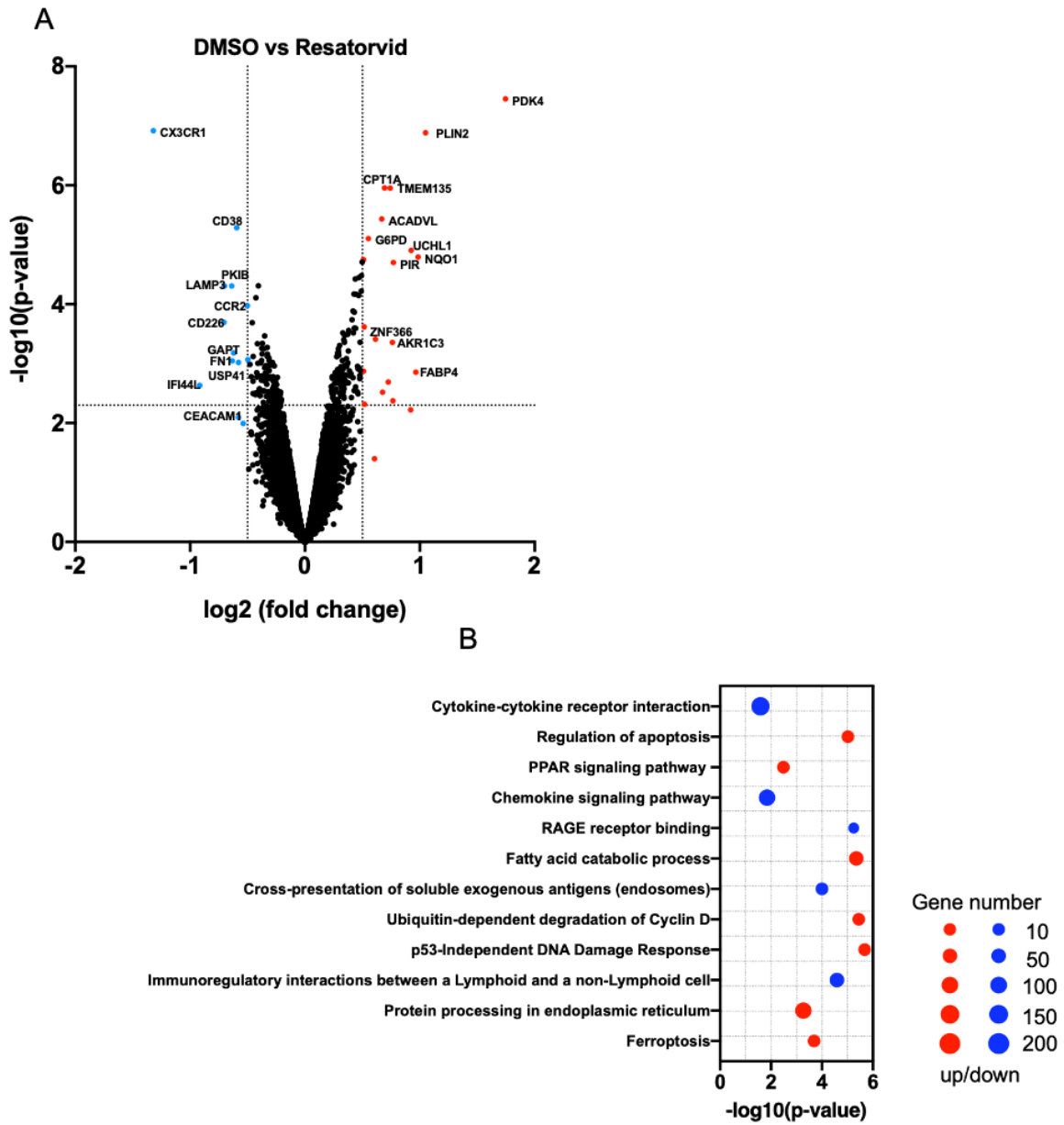
Figure 22. Microarray analysis of *in vitro* generated MDSC. (A) Volcano plot showing differentially expressed genes between MDSC treated with DMSO and Resatorvid (5μM) for 24 h (n=4). (B) Functionally enriched up and downregulated KEGG pathways found in the analysis of DMSO vs Resatorvid treated monocytes. Size of the circle indicates the number of genes that are up or downregulated in the pathways.

5.2.2 Effect of Resatorvid on the immunosuppressive capacity of melanoma patient-derived M-MDSC

Since we showed that Resatorvid attenuated the immunosuppressive activity of *in vitro generated* MDSC, we wanted to test the effect of both TLR4 and RAGE inhibitors on M-MDSC isolated from melanoma patients. I observed that both inhibitors did not change the suppressive activity of patient-derived M-MDSC (Figure 23A). Interestingly, not only HLA-DR$^{-/low}$CD33^{+} M-MDSC but also HLA-DR$^{+/high}$CD33^{+} monocytes exerted suppressive activity against allogenic T cells (Figure 23B).
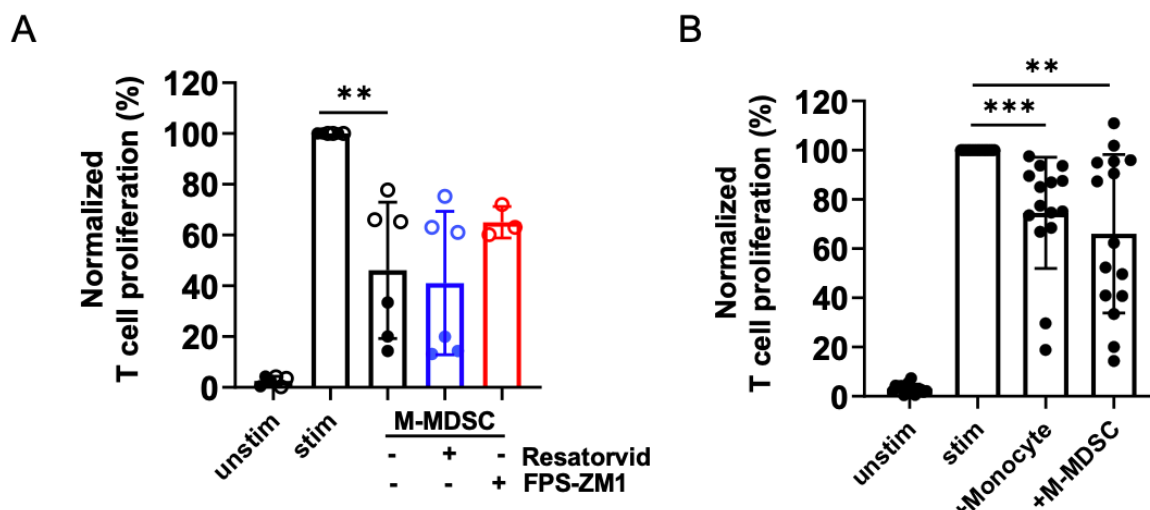
Figure 23. The effect of Resatorvid and FPS-ZM1 on the suppressive capacity of melanoma patient-derived MDSC. HLA-DR$^{-/low}$CD33$^+$ M-MDSC (M-MDSC) or (B) HLA-DR$^{+/high}$CD33$^+$ (monocytes) were isolated from the PBMC of advanced melanoma patients by flow cytometry. Then, they were co-cultured with autologous CD3 T cells labelled with eFluor450 proliferation dye at the ratio 1:1 in a 96-well plate pre-coated with anti-CD3 and anti-CD28 antibodies in the presence of Resatorvid (5μM), FPS-ZM1 (30nM) or DMSO. Cumulative data of T cell proliferation in the co-cultures with melanoma patient-derived (A) M-MDSC or (B) monocytes. Data are presented as mean± SD, n=3-15, **p<0.01, ***p<0.001.

To further understand why Resatorvid did not influence patient-derived M-MDSC, but abrogated the suppression mediated by *in vitro* generated MDSC, I analyzed the level of TLR4 ligands HSP90α, S100A8/9, and HMGB1 in the supernatant of the T cell and MDSC co-cultures. A higher level of TLR4 ligands were found in the co-cultures with *in vitro* generated MDSC compared to the patient-derived M-MDSC (Figure 24A). Additionally, we demonstrated that in vitro generated MDSC produced a significantly higher level of S100A8/9 and HMGB1 compared to the monocytes treated with GM-CSF alone (Figure 24B).
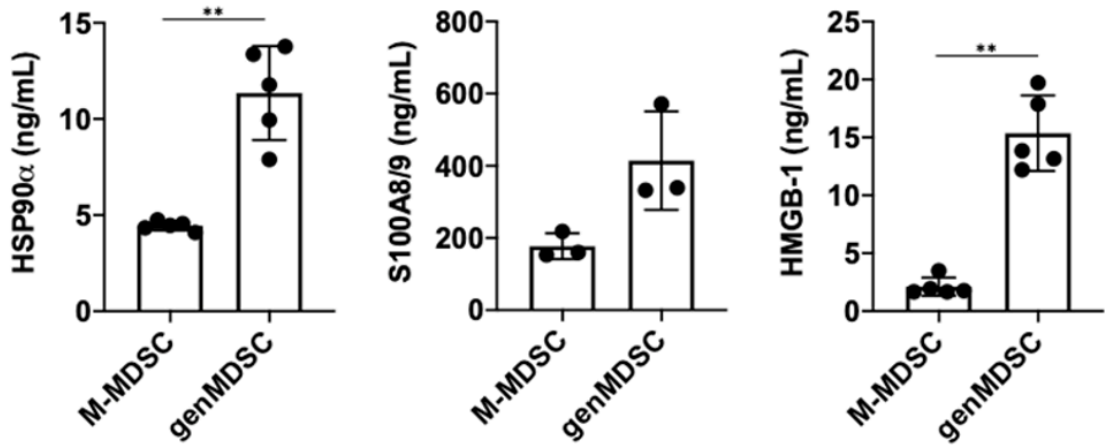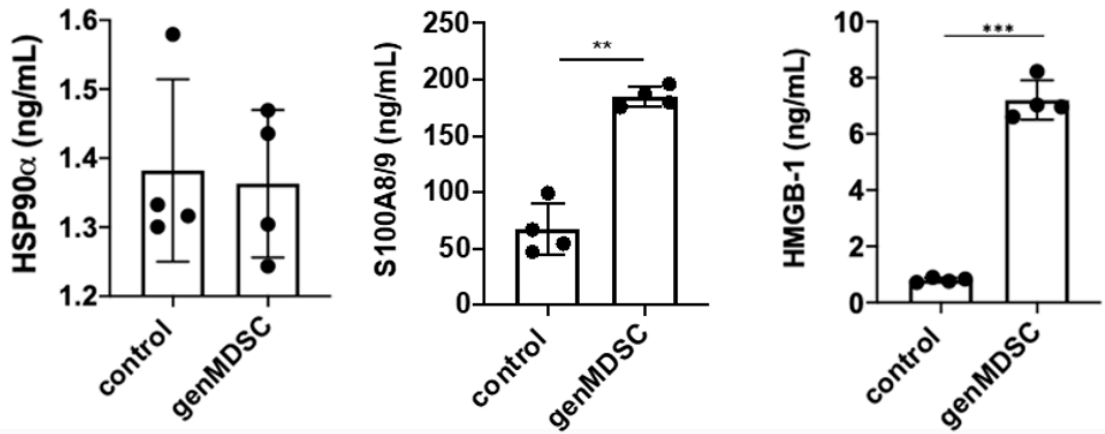
Figure 24. Investigating TLR4 ligands produced by M-MDSC or *in vitro* generated MDSC. Concentration of HSP90α, S100A8/9 and HMGB1 were measured by ELISA in the supernatant from the co-cultures containing MDSC and T cells or from the monocytes treated with GM-CSF alone or GM-CSF and IL-6. (A) M-MDSC were isolated from the PBMC of melanoma patients or *in vitro* generated MDSC (genMDSC). The level of HSP90α, S100A8/9, HMGB1 in the supernatant from the co-cultures of T cells and MDSC. (B) The level of HSP90α, S100A8/9, HMGB1 in the supernatant from monocytes treated with GM-CSF alone (control) or GM-CSF and IL6 (genMDSC). Data are presented as mean± SD. n= 3 −4, *p<0.05, **p<0.01).

5.3 Clinical relevance of S100A9 and HMGB1 in malignant melanoma

5.3.1 MDSC frequency and the level of S100A8/9 and HMGB1 in advanced melanoma patients

To address the question of the clinical relevance of S100A8/9 and HMGB1 in melanoma, we investigated their concentrations in the plasma of advanced melanoma patients. A correlation between an increased level of plasma S100A8/9 and an elevated frequency of PD-L1 expressing M-MDSC were shown in the peripheral blood of melanoma patients (Figure 25A). However, I failed to observe a similar correlation with HMGB1 (Figure 25B).

We further investigated the association between the level of TLR4/RAGE ligands in the plasma and the capacity of melanoma patient-derived HLA-DR$^{+/high}$CD33^{+} monocytes or HLA-DR$^{-/low}$CD33^{+} M-MDSC to inhibit T cell function. Although I did not detect any significant correlation between the plasma level of any TLR4/RAGE ligands and the immunosuppressive activity of M-MDSC (Figures 25C and 25E), there is a strong tendency for the correlation between elevated plasma levels of HMGB1 and S100A9 with the enhanced suppressive activity of HLA-DR$^{+/high}$CD33^{+} monocytes (Figure 25D and 25F).
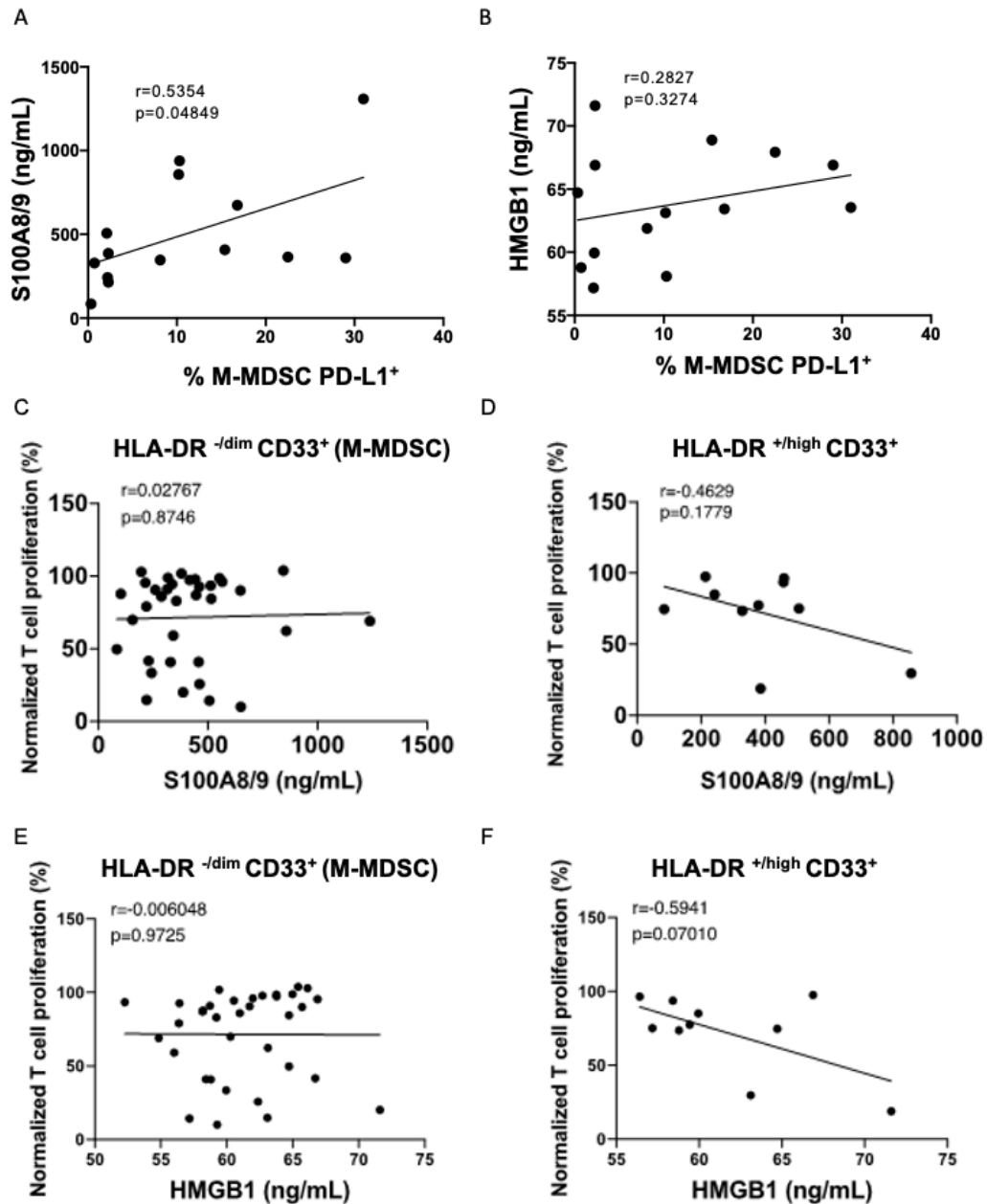
Figure 25. Investigating HMGB1 and S100A8/9 in the plasma of late-stage melanoma patients.
Concentration of HSP90α, S100A8/9 and HMGB1 were measured by ELISA in plasma of melanoma patients before the therapy starts. The frequency of PD-L1+ M-MDSC among total MDSC were plotted against the plasma levels of (A) S100A8/9 (ng/mL) or (B) HMGB1 (ng/mL). Normalized T cell proliferation in the co-cultures with (C) HLA-DR -/dim CD33+ (M-MDSC) and (D) HLA-DR +/high CD33+ were plotted against the plasma level of S100A8/9 (ng/mL). Normalized T cell proliferation in the co-cultures with (E) HLA-DR -/dim CD33+ (M-MDSC) and (F) HLA-DR +/high CD33+ were plotted against the plasma level of HMGB1 (ng/mL). The correlation was determined by a linear regression analysis.

5.3.2 Higher S100A8/A9 plasma level indicated worse PFS in melanoma patients

Several reports demonstrated that S100A8/9 and HMGB-1 expanded in the TME and serum of cancer patients and correlated with tumor progression (63, 165, 166). In agreement with these findings, patients with high levels of plasma S100A8/9 were shown to display significantly shorter PFS (Figure 26A). However, I did not observe similar results with HMGB1 (Figure 26B). TCGA data from the tumors of melanoma patients revealed that tumors expressing high S100A9 also express high MDSC-related markers including NOS1, ARG1, CXCR2, etc. (Figure 26C) In contrast, such association was not demonstrated for the tumors with high HMGB1 expression (Figure 26D).
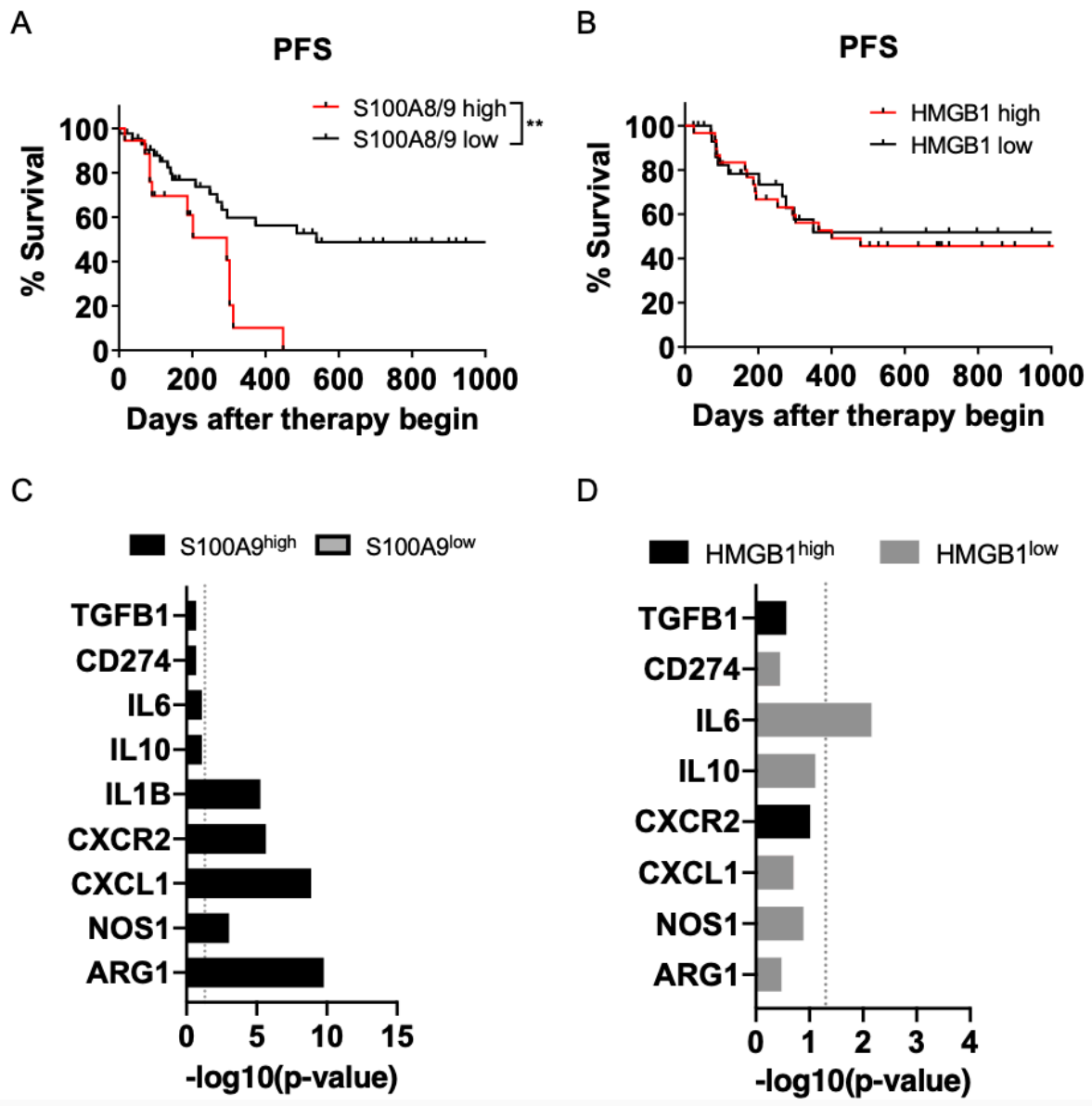
Figure 26. Clinical relevance of S100A8/9 and HMGB1 in late-stage melanoma patients. Concentration of S100A8/9 and HMGB1 were measured by ELISA in plasma before the therapy starts. (A) PFS of melanoma patients with high (>703.7 ng/mL; n=18) and low (<703.7 ng/mL; n=43) plasma levels of S100A8/9. (B) PFS of melanoma patients with high (>60.9 ng/mL; n=30) and low (<60.9 ng/mL; n=31) plasma level of HMGB1. S100A9 and HMGB1 expression levels were separated into two groups based on the top 25 percentile and bottom 25 percentile of gene expression within melanoma samples from TCGA dataset (n=111). Expression of TGFB1, CD274, IL6, IL10 IL1B, CXCR2, CXCL1, NOS1, and ARG1 in (C) S100A9 (low/high) or (D) HMGB1 (low/high) expressing tumors were analyzed. Dashed vertical line indicates the significance threshold (p<0.05). Analysis was performed by cBioPortal.com.

6 Discussion

6.1 HSP90α induced conversion of normal human monocytes into MDSC via TLR4 signaling

Previous studies in our lab showed that normal human monocytes are converted into immunosuppressive myeloid cells after their incubation with melanoma-derived HSP90α-bearing extracellular vesicles (56). Similarly, we found that soluble rHSP90α induced the immunosuppressive capacity of such monocytes. HSP90α stimulated the production of several MDSC-related markers such as PD-L1 and IDO-1 via TLR4 signaling, resulting in the inhibition of T cell proliferation. HSP90α was reported to be involved in tumor cell proliferation, survival, and angiogenesis (157). Inhibiting HSP90α was described as a promising therapeutic approach to inhibit tumor proliferation (182). Several HSP90 inhibitors emerged; yet none of them have shown satisfactory efficacy (182). However, based on its role in both MDSC generation and tumor cell growth, HSP90 could remain a promising target to improve cancer therapy.

6.2 S100A9 and HMGB1 induced conversion of normal human monocytes into MDSC

6.2.1 Acquisition of immunosuppressive properties

Long-term exposure to high concentrations of DAMPs like S100A9, HMGB1, and HSPs, which lead to chronic inflammation, was reported to promote MDSC accumulation (99). Chronic inflammation is considered to be a key hallmark in the initiation and progression of tumors (97). Apart from their generation from hematopoietic precursors by emergency myelopoiesis, MDSC can be also differentiated from mature myeloid cells in the TME (55). To mimic the conditions of the TME, I stimulated monocytes with rS100A9 or rHMGB1 at high concentrations and detected an increase in PD-L1 and IDO expression via TLR4 signaling. Moreover, under these conditions, a stimulation of ROS production, downregulation of CD86, and a significant inhibitory effect on T cell proliferation via TLR4 and RAGE signaling were demonstrated. The upregulation of PD-L1 and IDO-1 expression as well as elevated ROS

production represent the mechanisms, by which MDSC exert their suppressive effects on T cells (64). Activation of RAGE was reported to promote the production of ROS (153)

MDSC were reported to display a low expression of HLA-DR, CD80, and CD86 markers, which are involved in antigen presentation and co-stimulation (60). The downregulation of these molecules on antigen presenting cells (APCs) was shown to inhibit T cell activation (52). In our study, HMGB1 and S100A9 stimulation diminished the surface expression of CD86. CD80 expression, both at the protein and mRNA level, was not significantly altered in HMGB1-stimulated monocytes. In contrast, it was significantly upregulated on S100A9-stimulated monocytes. However, CD80 upregulation did not affect the co-stimulation capacity of S100A9 treated monocytes since they suppressed T cell proliferation, indicating that CD80 upregulation alone may not be sufficient to overcome the immunosuppressive function of MDSC.

S100A9 and HMGB1 were shown to induce the secretion of several inflammatory cytokines including IL-6, TNF-α, IL-1β, and production of ROS (153). S100A8/9 upregulation was also reported to be promoted by TLR4 or RAGE signaling-mediated activation of NF-κB (165). In agreement with these data, we found that IL-6, IL-10, IL-1β, S100A9, and S100A12 were elevated at mRNA level in S100A9-stimulated monocytes.

6.2.2 TLR4 mainly involved in the generation of MDSC

Next, I tested the expression of TLR4 and RAGE on monocytes stimulated by HMGB1 or S100A9. We demonstrated that the expression of both receptors was enhanced after the treatment with either S100A9 or HMGB1 at the protein level. This is in line with previous papers, reporting that NF-κB activation induced by TLR4 or RAGE signaling created a positive feedback loop by upregulating RAGE or TLR4 expression (153, 183). Interestingly, TLR4 and RAGE expression at the mRNA level was not significantly changed, indicating their transcription and translation were not affected but their trafficking was promoted.

CD14, a co-receptor for TLR4, acts as a chaperone, facilitating the delivery of LPS to the TLR4-MD-2 complex (184). LPS-induced increased CD14 expression was reported on monocytes (185). Similarly, our findings revealed that monocytes stimulated only with GM-CSF (control) showed a loss of CD14 expression, while it was preserved on monocytes stimulated with S100A9 and HMBG1. Additionally, inhibition of TLR4 and to a lesser extent RAGE signaling resulted in a downregulation of CD14 on monocytes.

Our findings indicated that mainly TLR4 to a lesser extent RAGE was involved in the upregulation of MDSC-related markers, including inflammatory cytokine expression. In contrast, other authors reported the involvement of RAGE signaling in the production of inflammatory cytokines in response to HMGB1 treatment since bone marrow-derived macrophages from RAGE-deficient mice were not able to produce these cytokines (151). This discrepancy with our results could be explained by species-specific differences between humans and mice.

TLR4 adaptor proteins MyD88 and TIRAP were previously reported to bind the phosphorylated RAGE and initiate activation of downstream molecules, suggesting the possible interaction between the RAGE and TLR4 (186). On the other side, RAGE-mediated MAPK signaling could affect TLR4 expression (186). Moreover, TLR4 knocked out mice were described to display a reduction in RAGE expression (187). Our experiments also showed that blocking of TLR4 signaling by its inhibitor-induced downregulation of RAGE expression. However, the expression of TLR4 was not significantly impaired by both RAGE and TLR4 inhibitors. These results may indicate that RAGE ligands could activate and interact with TLR4 and vice versa. It is plausible that in the absence of RAGE, those ligands can bind to TLR4, resulting in the production of several proinflammatory signals. The TLR4 inhibitor Resatorvid inhibits the interaction between downstream adaptor proteins and TLR4 (176), whereas FPS-ZM1 is a RAGE antagonist, blocking the interaction between RAGE and its ligands (177). Additionally, the TLR4 inhibitor was more effective in downregulating S100A9-induced MDSC-related marker expression than the RAGE inhibitor. It is plausible that Resatorvid could also inhibit RAGE signaling since it was. reported that TLR4 signaling is acting downstream of RAGE signaling.

Since TLR4 and RAGE signaling are sharing similar downstream signaling pathways (188), it is difficult to identify, which signaling pathway is mostly involved. Huang et al. (177) demonstrated that RAGE-mediated p38 was responsible for MDSC chemotaxis, whereas TLR4-mediated NF-κB was involved in MDSC activation (165). In contrast, I found that both RAGE and TLR4 were involved in NF-κB activation, while mainly TLR4 is responsible for p38 and STAT3 activation. I also demonstrated that monocyte stimulation via TLR4 is mainly responsible for the acquisition of their immunosuppressive activity. My results support the hypothesis that RAGE and TLR4 regulate S100A9 and HMGB1 mediated generation of MDSC through a complex network including feedback interactions.

6.3 Inhibition of TLR4 signaling restrained the immunosuppressive activity of in vitro generated but not patient-derived MDSC

We showed that blocking TLR4 signaling by Resatorvid abrogated inhibition of T cell proliferation mediated by *in vitro* generated MDSC. This might be due to the accumulation of TLR4 ligands (HSP90α, S100A8/9, and HMGB1) in the co-culture including generated MDSC and T cells. However, the concentration of these ligands in the co-culture of T cells with M-MDSC was significantly lower. It is plausible that TLR4 inhibitor worked effectively on genMDSC since they are still undergoing the transformation process and their immunosuppressive activity is more susceptible to modulation. In contrast, patient-derived M-MDSC have already reached a programmed state, in which their immunosuppressive activity is well-established. Therefore, TLR4 inhibitor may not have exerted a profound impact on altering their pre-established immunosuppressive activity. These findings suggest that the inhibition effectiveness of TLR4 signaling could be more effective for myeloid cells at the beginning of their transformation into MDSC.

Our microarray analysis demonstrated that the treatment with Resatorvid failed to induce a significant decrease in the expression of MDSC-related markers (PD-L1, ARG, iNOS, TGF-β IL-6, IL-10) on the generated MDSC. However, I observed an upregulation of genes involved in apoptosis and cell metabolic activity under these conditions. Interestingly, the expression of genes associated with the inflammatory response (189) and monocyte migration (52), including CX3CR1, CD38, and CCR2 was found to be downregulated. These observations suggest that Resatorvid may overcome immunosuppression mediated by MDSC and contribute to their apoptosis. In addition to its role in regulating immune responses, Resatorvid was shown to inhibit UV-induced skin tumorigenesis in preclinical models, suggesting its potential in cancer prevention (190). These findings indicated the potential of Resatorvid to target both tumor cells and MDSC. Although there is currently no clinical trial investigating the role of Resatorvid in cancer, an ongoing clinical trial is evaluating the safety and efficacy of Resatorvid in patients with severe sepsis (NCT00143611).

6.4 HLA-DR$^{+/high}$CD33$^+$ monocytic cells have suppressive activity against T cells

Multiple studies have demonstrated the suppressive activity of HLA-DR$^{-/low}$CD14$^+$ M-MDSC against T cells in cancer (54, 57, 99). However, to our knowledge, no suppressive activity of HLA-DR$^{+/high}$CD14$^+$ monocytes has been reported. Interestingly, in our study, I observed that not only melanoma patient-derived HLA-DR$^{-/low}$CD33$^+$ myeloid cells but also HLA-DR$^{+/high}$CD33$^+$CD14$^+$ monocytes were able to inhibit T cell proliferation, suggesting the involvement of the entire population of CD14$^+$ cells (independent from their HLA-DR expression) in immunosuppression in melanoma.

Further studies are needed to elucidate the mechanisms, by which these CD14$^+$ cells inhibit T cell responses in melanoma. In addition to HLA-DR, exploring TLR4 signaling-related gene signature and the expression of endogenous TLR4 ligands, such as S100A8/9 and HMGB1 may provide valuable insights into the characterization of MDSC.

Although I have used a well-established standardized protocol to test the immunosuppressive activity of MDSC, some challenges during their isolation and culture. Since MDSC have a limited lifespan in vitro and could be activated by various stimuli, including FACS sorting (54, 179), their immunosuppressive activity in vitro could be easily modulated (179). Moreover, the heterogeneity of MDSC makes it difficult to identify and isolate them (191). To avoid the potential pitfalls of a single test system, different methods evaluating MDSC function should be used.

6.5 Investigating S100A9 and HMGB1 in melanoma patients

6.5.1 Association between the levels of MDSC and S100A9 or HMGB1

Several reports have highlighted the expansion of S100A8/9 and HMGB1 in the TME and serum of cancer patients as well as their correlation with tumor progression (164, 165, 171). In our study, we identified a positive correlation between the frequency of PD-L1$^+$ M-MDSC and the concentrations of S100A8/9 and HSP90α in plasma of the same patients. However, I failed to observe the correlation between the suppressive activity of M-MDSC and the plasma

levels of S100A8/9 or HSP90α. Tumor-infiltrating MDSC were reported to possess higher suppressive capacities compared to circulating MDSC (68). Hence, it is possible that MDSC with enhanced suppressive activity could migrate into the TME of melanoma patients.

Furthermore, our TCGA analysis of tumors from melanoma patients revealed a correlation between the expression of MDSC-related markers and the level of S100A9 (but not HMGB1). However, previous studies demonstrated that HMGB1 was present in the TME, activated the NF-κB signaling pathway in MDSC and regulated their functions (153). The lack of correlation between HMGB1 concentrations and the expression of MDSC-related markers in our study warrants further investigation.

6.5.2 High plasma level of S100A8/9 correlated with poor PFS

S100A8 and A9 are found at minimal concentrations in the serum of healthy donors. However, their levels were enhanced in the diseases associated with inflammation and proposed as a biomarker for disease severity (164). Our lab previously demonstrated that elevated concentrations of S100A8/9 and HMGB1 in melanoma patients correlate with a poor response to ICI (192). In our study, patients with higher levels of S100A8/9 exhibited shorter PFS. In agreement with these findings, Wagner et al (193) demonstrated that elevated serum levels of S100A8/9 in advanced melanoma patients were associated with their poor PFS. Furthermore, it was reported that S100A8 and S100A9 can attract melanoma cells and facilitate the establishment of a pre-metastatic niche (193). Collectively, these findings highlight the clinical relevance of S100A8/9 and its high potential as a prognostic biomarker in melanoma patients. Additionally, targeting S100A8/9 may hold promise for the development of therapeutic strategies to improve the clinical outcome of melanoma patients.

Several preclinical studies with S100A8/9 inhibitors have been conducted, with a focus on targeting both cancer cells and MDSC (164, 165, 194). For instance, the S100A9 inhibitor Tasquinimod was demonstrated to block the immunosuppressive activity of MDSC, thereby enhancing anti-tumor immune responses (195). Moreover, targeting TLR4 and RAGE could be a therapeutic option to overcome immunosuppression in cancer (134, 142, 149). Deguchi et al (196) showed that a TLR4 inhibitor Eritoran effectively blocked S100A8-mediated cell migration and suppressed tumor progression in the Lewis lung carcinoma mouse model. Moreover, RAGE inhibitor TTP-488 was reported to reduce metastatic tumor burden and MDSC accumulation in melanoma and lung cancer mouse models (151). However, it is critical

to consider the potential drawbacks of blocking TLR4 and RAGE in the context of cancer immunotherapy. These receptors play important roles in immune system activation and pathogen recognition and their blockade could lead to the suppression of the immune response and an increased risk of infections (143, 197). Therefore, a delicate equilibrium must be maintained when considering the use of TLR4 and RAGE inhibitors as therapeutic agents.

In the current study, we did not observe any correlation between plasma HMGB1 levels and the clinical outcome of melanoma patients. However, it was previously published that an increased level of HMGB1 expression in tumors correlated with disease progression and worse OS in melanoma patients (198). The difference with our data could be due to the fact the level of HMGB1 in the TME of melanoma patients might be a better prognostic marker than its concentration in the circulation.

7 Conclusion

Taken together, this study highlights the crucial role of TLR4 stimulation and to a lesser extent of RAGE, by endogenous ligands S100A9 and HMGB1 in the acquisition of immunosuppressive properties by MDSCs in malignant melanoma. These findings suggest that targeting TLR4 signaling pathways may represent a promising therapeutic strategy to overcome MDSC-mediated immune suppression and enhance the efficacy of immunotherapeutic approaches in melanoma. Further investigations are warranted to explore the potential of TLR4 inhibitors and other targeted interventions including S100A8/9 in preclinical and clinical settings, with the goal of improving patient outcomes in melanoma treatment.

8 References

1.   Schreiber RD, Old LJ, Smyth MJ. Cancer immunoediting: integrating immunity's roles in cancer suppression and promotion. Science. 2011;331(6024):1565-70.

2.   Gubin MM, Vesely MD. Cancer Immunoediting in the Era of Immuno-oncology. Clin Cancer Res. 2022;28(18):3917-28.

3.   Dunn GP, Old LJ, Schreiber RD. The three Es of cancer immunoediting. Annu Rev Immunol. 2004;22:329-60.

4.   Liu S, Sun Q, Ren X. Novel strategies for cancer immunotherapy: counter-immunoediting therapy. J Hematol Oncol. 2023;16(1):38.

5.   Mittal D, Gubin MM, Schreiber RD, Smyth MJ. New insights into cancer immunoediting and its three component phases--elimination, equilibrium and escape. Curr Opin Immunol. 2014;27:16-25.

6.   Durgeau A, Virk Y, Corgnac S, Mami-Chouaib F. Recent Advances in Targeting CD8 T-Cell Immunity for More Effective Cancer Immunotherapy. Front Immunol. 2018;9:14.

7.   Sanmamed MF, Pastor F, Rodriguez A, Perez-Gracia JL, Rodriguez-Ruiz ME, Jure-Kunkel M, et al. Agonists of Co-stimulation in Cancer Immunotherapy Directed Against CD137, OX40, GITR, CD27, CD28, and ICOS. Semin Oncol. 2015;42(4):640-55.

8.   Medrano RFV, Hunger A, Mendonca SA, Barbuto JAM, Strauss BE. Immunomodulatory and antitumor effects of type I interferons and their application in cancer therapy. Oncotarget. 2017;8(41):71249-84.

9.   Anthony SM, Howard ME, Hailemichael Y, Overwijk WW, Schluns KS. Soluble interleukin-15 complexes are generated in vivo by type I interferon dependent and independent pathways. PLoS One. 2015;10(3):e0120274.

10.   Arango Duque G, Descoteaux A. Macrophage cytokines: involvement in immunity and infectious diseases. Front Immunol. 2014;5:491.

11.   Grivennikov SI, Greten FR, Karin M. Immunity, inflammation, and cancer. Cell. 2010;140(6):883-99.

12.   Vesely MD, Kershaw MH, Schreiber RD, Smyth MJ. Natural innate and adaptive immunity to cancer. Annu Rev Immunol. 2011;29:235-71.

13.   Vesely MD, Schreiber RD. Cancer immunoediting: antigens, mechanisms, and implications to cancer immunotherapy. Ann N Y Acad Sci. 2013;1284(1):1-5.

14.   Bhatia A, Kumar Y. Cancer-immune equilibrium: questions unanswered. Cancer Microenviron. 2011;4(2):209-17.

15.   Dunn GP, Bruce AT, Ikeda H, Old LJ, Schreiber RD. Cancer immunoediting: from immunosurveillance to tumor escape. Nat Immunol. 2002;3(11):991-8.

16.   Vinay DS, Ryan EP, Pawelec G, Talib WH, Stagg J, Elkord E, et al. Immune evasion in cancer: Mechanistic basis and therapeutic strategies. Semin Cancer Biol. 2015;35 Suppl:S185-S98.

17.   Khong HT, Restifo NP. Natural selection of tumor variants in the generation of "tumor escape" phenotypes. Nat Immunol. 2002;3(11):999-1005.

18.   Dutta S, Ganguly A, Chatterjee K, Spada S, Mukherjee S. Targets of Immune Escape Mechanisms in Cancer: Basis for Development and Evolution of Cancer Immune Checkpoint Inhibitors. Biology (Basel). 2023;12(2):218.

19.   Spranger S. Mechanisms of tumor escape in the context of the T-cell-inflamed and the non-T-cell-inflamed tumor microenvironment. Int Immunol. 2016;28(8):383-91.

20.   Wang Y, Zhang H, Liu C, Wang Z, Wu W, Zhang N, et al. Immune checkpoint modulators in cancer immunotherapy: recent advances and emerging concepts. J Hematol Oncol. 2022;15(1):111.

21.   Labani-Motlagh A, Ashja-Mahdavi M, Loskog A. The Tumor Microenvironment: A Milieu Hindering and Obstructing Antitumor Immune Responses. Front Immunol. 2020;11:940.

22.   Lindau D, Gielen P, Kroesen M, Wesseling P, Adema GJ. The immunosuppressive tumour network: myeloid-derived suppressor cells, regulatory T cells and natural killer T cells. Immunology. 2013;138(2):105-15.

23.   Sadeghi Rad H, Monkman J, Warkiani ME, Ladwa R, O'Byrne K, Rezaei N, et al. Understanding the tumor microenvironment for effective immunotherapy. Med Res Rev. 2021;41(3):1474-98.

24.   Restifo NP, Smyth MJ, Snyder A. Acquired resistance to immunotherapy and future challenges. Nat Rev Cancer. 2016;16(2):121-6.

25.   Naimi A, Mohammed RN, Raji A, Chupradit S, Yumashev AV, Suksatan W, et al. Tumor immunotherapies by immune checkpoint inhibitors (ICIs); the pros and cons. Cell Commun Signal. 2022;20(1):44.

26.   Jardim DL, Goodman A, de Melo Gagliato D, Kurzrock R. The Challenges of Tumor Mutational Burden as an Immunotherapy Biomarker. Cancer Cell. 2021;39(2):154-73.

27.   Chen DS, Mellman I. Elements of cancer immunity and the cancer-immune set point. Nature. 2017;541(7637):321-30.

28.   Maleki Vareki S. High and low mutational burden tumors versus immunologically hot and cold tumors and response to immune checkpoint inhibitors. J Immunother Cancer. 2018;6(1):157.

29.   Dai E, Zhu Z, Wahed S, Qu Z, Storkus WJ, Guo ZS. Epigenetic modulation of antitumor immunity for improved cancer immunotherapy. Mol Cancer. 2021;20(1):171.

30.   Trujillo JA, Sweis RF, Bao R, Luke JJ. T Cell-Inflamed versus Non-T Cell-Inflamed Tumors: A Conceptual Framework for Cancer Immunotherapy Drug Development and Combination Therapy Selection. Cancer Immunol Res. 2018;6(9):990-1000.

31.   Bonaventura P, Shekarian T, Alcazer V, Valladeau-Guilemond J, Valsesia-Wittmann S, Amigorena S, et al. Cold Tumors: A Therapeutic Challenge for Immunotherapy. Front Immunol. 2019;10:168.

32.   Liu YT, Sun ZJ. Turning cold tumors into hot tumors by improving T-cell infiltration. Theranostics. 2021;11(11):5365-86.

33.   Zhou X, Ni Y, Liang X, Lin Y, An B, He X, et al. Mechanisms of tumor resistance to immune checkpoint blockade and combination strategies to overcome resistance. Front Immunol. 2022;13:915094.

34.   Schadendorf D, van Akkooi ACJ, Berking C, Griewank KG, Gutzmer R, Hauschild A, et al. Melanoma. Lancet. 2018;392(10151):971-84.

35.   Weiskopf K, Schnorr PJ, Pang WW, Chao MP, Chhabra A, Seita J, et al. Myeloid Cell Origins, Differentiation, and Clinical Implications. Microbiol Spectr. 2016;4(5):10.1128.

36.   Trucco LD, Mundra PA, Hogan K, Garcia-Martinez P, Viros A, Mandal AK, et al. Ultraviolet radiation-induced DNA damage is prognostic for outcome in melanoma. Nat Med. 2019;25(2):221-4.

37.   Guo W, Wang H, Li C. Signal pathways of melanoma and targeted therapy. Signal Transduct Target Ther. 2021;6(1):424.

38.   Tyrell R, Antia C, Stanley S, Deutsch GB. Surgical resection of metastatic melanoma in the era of immunotherapy and targeted therapy. Melanoma Manag. 2017;4(1):61-8.

39.   Sood S, Jayachandiran R, Pandey S. Current Advancements and Novel Strategies in the Treatment of Metastatic Melanoma. Integr Cancer Ther. 2021;20:1534735421990078.

40.   Atkins MB, Hsu J, Lee S, Cohen GI, Flaherty LE, Sosman JA, et al. Phase III trial comparing concurrent biochemotherapy with cisplatin, vinblastine, dacarbazine, interleukin-2, and interferon alfa-2b with cisplatin, vinblastine, and dacarbazine alone in patients with metastatic malignant melanoma (E3695): a trial coordinated by the Eastern Cooperative Oncology Group. J Clin Oncol. 2008;26(35):5748-54.

41.   Robert C, Karaszewska B, Schachter J, Rutkowski P, Mackiewicz A, Stroiakovski D, et al. Improved overall survival in melanoma with combined dabrafenib and trametinib. N Engl J Med. 2015;372(1):30-9.

42.   Tanda ET, Vanni I, Boutros A, Andreotti V, Bruno W, Ghiorzo P, et al. Current State of Target Treatment in BRAF Mutated Melanoma. Front Mol Biosci. 2020;7:154.

43.   Marzagalli M, Ebelt ND, Manuel ER. Unraveling the crosstalk between melanoma and immune cells in the tumor microenvironment. Semin Cancer Biol. 2019;59:236-50.

44.   Eggermont AMM, Crittenden M, Wargo J. Combination Immunotherapy Development in Melanoma. Am Soc Clin Oncol Educ Book. 2018;38:197-207.

45.   Larkin J, Chiarion-Sileni V, Gonzalez R, Grob JJ, Rutkowski P, Lao CD, et al. Five-Year Survival with Combined Nivolumab and Ipilimumab in Advanced Melanoma. N Engl J Med. 2019;381(16):1535-46.

46.   Johnson DB, Nebhan CA, Moslehi JJ, Balko JM. Immune-checkpoint inhibitors: long-term implications of toxicity. Nat Rev Clin Oncol. 2022;19(4):254-67.

47.   Jenkins RW, Barbie DA, Flaherty KT. Mechanisms of resistance to immune checkpoint inhibitors. Br J Cancer. 2018;118(1):9-16.

48.   Ferrucci PF, Pala L, Conforti F, Cocorocchio E. Talimogene Laherparepvec (T-VEC): An Intralesional Cancer Immunotherapy for Advanced Melanoma. Cancers (Basel). 2021;13(6):1383.

49.   Kaufman HL, Shalhout SZ, Iodice G. Talimogene Laherparepvec: Moving From First-In-Class to Best-In-Class. Front Mol Biosci. 2022;9:834841.

50.   Kaufman HL, Bines SD. OPTIM trial: a Phase III trial of an oncolytic herpes virus encoding GM-CSF for unresectable stage III or IV melanoma. Future Oncol. 2010;6(6):941-9.

51.   Veglia F, Sanseviero E, Gabrilovich DI. Myeloid-derived suppressor cells in the era of increasing myeloid cell diversity. Nat Rev Immunol. 2021;21(8):485-98.

52.   Gabrilovich DI. Myeloid-Derived Suppressor Cells. Cancer Immunol Res. 2017;5(1):3-8.

53.   Marvel D, Gabrilovich DI. Myeloid-derived suppressor cells in the tumor microenvironment: expect the unexpected. J Clin Invest. 2015;125(9):3356-64.

54.   Bronte V, Brandau S, Chen SH, Colombo MP, Frey AB, Greten TF, et al. Recommendations for myeloid-derived suppressor cell nomenclature and characterization standards. Nat Commun. 2016;7:12150.

55.   Huber V, Vallacchi V, Fleming V, Hu X, Cova A, Dugo M, et al. Tumor-derived microRNAs induce myeloid suppressor cells and predict immunotherapy resistance in melanoma. J Clin Invest. 2018;128(12):5505-16.

56.   Fleming V, Hu X, Weller C, Weber R, Groth C, Riester Z, et al. Melanoma Extracellular Vesicles Generate Immunosuppressive Myeloid Cells by Upregulating PD-L1 via TLR4 Signaling. Cancer Res. 2019;79(18):4715-28.

57.   Cassetta L, Bruderek K, Skrzeczynska-Moncznik J, Osiecka O, Hu X, Rundgren IM, et al. Differential expansion of circulating human MDSC subsets in patients with cancer, infection and inflammation. J Immunother Cancer. 2020;8(2):e001223.

58.   Condamine T, Dominguez GA, Youn JI, Kossenkov AV, Mony S, Alicea-Torres K, et al. Lectin-type oxidized LDL receptor-1 distinguishes population of human polymorphonuclear myeloid-derived suppressor cells in cancer patients. Sci Immunol. 2016;1(2):aaf8943.

59.   Alshetaiwi H, Pervolarakis N, McIntyre LL, Ma D, Nguyen Q, Rath JA, et al. Defining the emergence of myeloid-derived suppressor cells in breast cancer using single-cell transcriptomics. Sci Immunol. 2020;5(44):eaay6017.

60.   Gabrilovich DI, Nagaraj S. Myeloid-derived suppressor cells as regulators of the immune system. Nat Rev Immunol. 2009;9(3):162-74.

61.   Condamine T, Mastio J, Gabrilovich DI. Transcriptional regulation of myeloid-derived suppressor cells. J Leukoc Biol. 2015;98(6):913-22.

62.   Condamine T, Gabrilovich DI. Molecular mechanisms regulating myeloid-derived suppressor cell differentiation and function. Trends Immunol. 2011;32(1):19-25.

63.   Umansky V, Blattner C, Gebhardt C, Utikal J. The Role of Myeloid-Derived Suppressor Cells (MDSC) in Cancer Progression. Vaccines (Basel). 2016;4(4):36.

64.   Groth C, Hu X, Weber R, Fleming V, Altevogt P, Utikal J, et al. Immunosuppression mediated by myeloid-derived suppressor cells (MDSCs) during tumour progression. Br J Cancer. 2019;120(1):16-25.

65.   Sinha P, Okoro C, Foell D, Freeze HH, Ostrand-Rosenberg S, Srikrishna G. Proinflammatory S100 proteins regulate the accumulation of myeloid-derived suppressor cells. J Immunol. 2008;181(7):4666-75.

66.   Kinoshita R, Sato H, Yamauchi A, Takahashi Y, Inoue Y, Sumardika IW, et al. Newly developed anti-S100A8/A9 monoclonal antibody efficiently prevents lung tropic cancer metastasis. Int J Cancer. 2019;145(2):569-75.

67.   Qin H, Lerman B, Sakamaki I, Wei G, Cha SC, Rao SS, et al. Generation of a new therapeutic peptide that depletes myeloid-derived suppressor cells in tumor-bearing mice. Nat Med. 2014;20(6):676-81.

68.   Kumar V, Patel S, Tcyganov E, Gabrilovich DI. The Nature of Myeloid-Derived Suppressor Cells in the Tumor Microenvironment. Trends Immunol. 2016;37(3):208-20.

69.   Li K, Shi H, Zhang B, Ou X, Ma Q, Chen Y, et al. Myeloid-derived suppressor cells as immunosuppressive regulators and therapeutic targets in cancer. Signal Transduct Target Ther. 2021;6(1):362.

70.   Noman MZ, Desantis G, Janji B, Hasmim M, Karray S, Dessen P, et al. PD-L1 is a novel direct target of HIF-1alpha, and its blockade under hypoxia enhanced MDSC-mediated T cell activation. J Exp Med. 2014;211(5):781-90.

71.   Kumar V, Gabrilovich DI. Hypoxia-inducible factors in regulation of immune responses in tumour microenvironment. Immunology. 2014;143(4):512-9.

72.   De Cicco P, Ercolano G, Ianaro A. The New Era of Cancer Immunotherapy: Targeting Myeloid-Derived Suppressor Cells to Overcome Immune Evasion. Front Immunol. 2020;11:1680.

73.   Lesokhin AM, Hohl TM, Kitano S, Cortez C, Hirschhorn-Cymerman D, Avogadri F, et al. Monocytic CCR2(+) myeloid-derived suppressor cells promote immune escape by limiting activated CD8 T-cell infiltration into the tumor microenvironment. Cancer Res. 2012;72(4):876-86.

74.   Blattner C, Fleming V, Weber R, Himmelhan B, Altevogt P, Gebhardt C, et al. CCR5(+) Myeloid-Derived Suppressor Cells Are Enriched and Activated in Melanoma Lesions. Cancer Res. 2018;78(1):157-67.

75.   Wang N, Feng Y, Wang Q, Liu S, Xiang L, Sun M, et al. Neutrophils infiltration in the tongue squamous cell carcinoma and its correlation with CEACAM1 expression on tumor cells. PLoS One. 2014;9(2):e89991.

76.   Kowalczuk O, Burzykowski T, Niklinska WE, Kozlowski M, Chyczewski L, Niklinski J. CXCL5 as a potential novel prognostic factor in early stage non-small cell lung cancer: results of a study of expression levels of 23 genes. Tumour Biol. 2014;35(5):4619-28.

77.   Groth C, Arpinati L, Shaul ME, Winkler N, Diester K, Gengenbacher N, et al. Blocking Migration of Polymorphonuclear Myeloid-Derived Suppressor Cells Inhibits Mouse Melanoma Progression. Cancers (Basel). 2021;13(4):726.

78.   Cheng JN, Yuan YX, Zhu B, Jia Q. Myeloid-Derived Suppressor Cells: A Multifaceted Accomplice in Tumor Progression. Front Cell Dev Biol. 2021;9:740827.

79.   Nagaraj S, Gupta K, Pisarev V, Kinarsky L, Sherman S, Kang L, et al. Altered recognition of antigen is a mechanism of CD8+ T cell tolerance in cancer. Nat Med. 2007;13(7):828-35.

80.   Rodriguez PC, Quiceno DG, Zabaleta J, Ortiz B, Zea AH, Piazuelo MB, et al. Arginase I production in the tumor microenvironment by mature myeloid cells inhibits T-cell receptor expression and antigen-specific T-cell responses. Cancer Res. 2004;64(16):5839-49.

81.   Ostrand-Rosenberg S, Sinha P. Myeloid-derived suppressor cells: linking inflammation and cancer. J Immunol. 2009;182(8):4499-506.

82.   Umansky V, Schirrmacher V. Nitric oxide-induced apoptosis in tumor cells. Adv Cancer Res. 2001;82:107-31.

83.   Siret C, Collignon A, Silvy F, Robert S, Cheyrol T, Andre P, et al. Deciphering the Crosstalk Between Myeloid-Derived Suppressor Cells and Regulatory T Cells in Pancreatic Ductal Adenocarcinoma. Front Immunol. 2019;10:3070.

84.   Mao Y, Sarhan D, Steven A, Seliger B, Kiessling R, Lundqvist A. Inhibition of tumor-derived prostaglandin-e2 blocks the induction of myeloid-derived suppressor cells and recovers natural killer cell activity. Clin Cancer Res. 2014;20(15):4096-106.

85.   Tumino N, Di Pace AL, Besi F, Quatrini L, Vacca P, Moretta L. Interaction Between MDSC and NK Cells in Solid and Hematological Malignancies: Impact on HSCT. Front Immunol. 2021;12:638841.

86.   Ugolini A, Tyurin VA, Tyurina YY, Tcyganov EN, Donthireddy L, Kagan VE, et al. Polymorphonuclear myeloid-derived suppressor cells limit antigen cross-presentation by dendritic cells in cancer. JCI Insight. 2020;5(15):e138581.

87.   Sinha P, Clements VK, Bunt SK, Albelda SM, Ostrand-Rosenberg S. Cross-talk between myeloid-derived suppressor cells and macrophages subverts tumor immunity toward a type 2 response. J Immunol. 2007;179(2):977-83.

88.   Siddiqui S, Glauben R. Fatty Acid Metabolism in Myeloid-Derived Suppressor Cells and Tumor-Associated Macrophages: Key Factor in Cancer Immune Evasion. Cancers (Basel). 2022;14(1):250.

89.   Yan D, Yang Q, Shi M, Zhong L, Wu C, Meng T, et al. Polyunsaturated fatty acids promote the expansion of myeloid-derived suppressor cells by activating the JAK/STAT3 pathway. Eur J Immunol. 2013;43(11):2943-55.

90.   Dang Q, Sun Z, Wang Y, Wang L, Liu Z, Han X. Ferroptosis: a double-edged sword mediating immune tolerance of cancer. Cell Death Dis. 2022;13(11):925.

91.   Jian SL, Chen WW, Su YC, Su YW, Chuang TH, Hsu SC, et al. Glycolysis regulates the expansion of myeloid-derived suppressor cells in tumor-bearing hosts through prevention of ROS-mediated apoptosis. Cell Death Dis. 2017;8(5):e2779.

92.   Li X, Zhong J, Deng X, Guo X, Lu Y, Lin J, et al. Targeting Myeloid-Derived Suppressor Cells to Enhance the Antitumor Efficacy of Immune Checkpoint Blockade Therapy. Front Immunol. 2021;12:754196.

93.   Ozbay Kurt FG, Lasser S, Arkhypov I, Utikal J, Umansky V. Enhancing immunotherapy response in melanoma: myeloid-derived suppressor cells as a therapeutic target. J Clin Invest. 2023;133(13):e170762.

94.   Petrova V, Arkhypov I, Weber R, Groth C, Altevogt P, Utikal J, et al. Modern Aspects of Immunotherapy with Checkpoint Inhibitors in Melanoma. Int J Mol Sci. 2020;21(7):2367.

95.   Navarini-Meury AA, Conrad C. Melanoma and innate immunity--aActive inflammation or just erroneous attraction? Melanoma as the source of leukocyte-attracting chemokines. Semin Cancer Biol. 2009;19(2):84-91.

96.   Falcone I, Conciatori F, Bazzichetto C, Ferretti G, Cognetti F, Ciuffreda L, et al. Tumor Microenvironment: Implications in Melanoma Resistance to Targeted Therapy and Immunotherapy. Cancers (Basel). 2020;12(10):2870.

97.   Kanterman J, Sade-Feldman M, Baniyash M. New insights into chronic inflammation-induced immunosuppression. Semin Cancer Biol. 2012;22(4):307-18.

98.   Zhao H, Wu L, Yan G, Chen Y, Zhou M, Wu Y, et al. Inflammation and tumor progression: signaling pathways and targeted intervention. Signal Transduct Target Ther. 2021;6(1):263.

99.   Umansky V, Sevko A, Gebhardt C, Utikal J. Myeloid-derived suppressor cells in malignant melanoma. J Dtsch Dermatol Ges. 2014;12(11):1021-7.

100.   Weide B, Martens A, Zelba H, Stutz C, Derhovanessian E, Di Giacomo AM, et al. Myeloid-derived suppressor cells predict survival of patients with advanced melanoma: comparison with regulatory T cells and NY-ESO-1- or melan-A-specific T cells. Clin Cancer Res. 2014;20(6):1601-9.

101.   Schilling B, Sucker A, Griewank K, Zhao F, Weide B, Gorgens A, et al. Vemurafenib reverses immunosuppression by myeloid derived suppressor cells. Int J Cancer. 2013;133(7):1653-63.

102.   Umansky V, Utikal J, Gebhardt C. Predictive immune markers in advanced melanoma patients treated with ipilimumab. Oncoimmunology. 2016;5(6):e1158901.

103. Daveri E, Vergani E, Shahaj E, Bergamaschi L, La Magra S, Dosi M, et al. microRNAs Shape Myeloid Cell-Mediated Resistance to Cancer Immunotherapy. Front Immunol. 2020;11:1214.

104. Gordy JT, Sandhu AK, Fessler K, Luo K, Kapoor AR, Ayeh SK, et al. IFNalpha and 5-Aza-2'-deoxycytidine combined with a dendritic-cell targeting DNA vaccine alter tumor immune cell infiltration in the B16F10 melanoma model. Front Immunol. 2022;13:1074644.

105. Shidal C, Singh NP, Nagarkatti P, Nagarkatti M. MicroRNA-92 Expression in CD133(+) Melanoma Stem Cells Regulates Immunosuppression in the Tumor Microenvironment via Integrin-Dependent Activation of TGFbeta. Cancer Res. 2019;79(14):3622-35.

106. Fleming V, Hu X, Weber R, Nagibin V, Groth C, Altevogt P, et al. Targeting Myeloid-Derived Suppressor Cells to Bypass Tumor-Induced Immunosuppression. Front Immunol. 2018;9:398.

107. Sevko A, Michels T, Vrohlings M, Umansky L, Beckhove P, Kato M, et al. Antitumor effect of paclitaxel is mediated by inhibition of myeloid-derived suppressor cells and chronic inflammation in the spontaneous melanoma model. J Immunol. 2013;190(5):2464-71.

108. Fultang L, Panetti S, Ng M, Collins P, Graef S, Rizkalla N, et al. MDSC targeting with Gemtuzumab ozogamicin restores T cell immunity and immunotherapy against cancers. EBioMedicine. 2019;47:235-46.

109. Ko JS, Rayman P, Ireland J, Swaidani S, Li G, Bunting KD, et al. Direct and differential suppression of myeloid-derived suppressor cell subsets by sunitinib is compartmentally constrained. Cancer Res. 2010;70(9):3526-36.

110. Gabrilovich D, Ishida T, Oyama T, Ran S, Kravtsov V, Nadaf S, et al. Vascular endothelial growth factor inhibits the development of dendritic cells and dramatically affects the differentiation of multiple hematopoietic lineages in vivo. Blood. 1998;92(11):4150-66.

111. Pan PY, Wang GX, Yin B, Ozao J, Ku T, Divino CM, et al. Reversion of immune tolerance in advanced malignancy: modulation of myeloid-derived suppressor cell development by blockade of stem-cell factor function. Blood. 2008;111(1):219-28.

112. Gargett T, Christo SN, Hercus TR, Abbas N, Singhal N, Lopez AF, et al. GM-CSF signalling blockade and chemotherapeutic agents act in concert to inhibit the function of myeloid-derived suppressor cells in vitro. Clin Transl Immunology. 2016;5(12):e119.

113. Gomez-Roca CA, Italiano A, Le Tourneau C, Cassier PA, Toulmonde M, D'Angelo SP, et al. Phase I study of emactuzumab single agent or in combination with paclitaxel in patients with advanced/metastatic solid tumors reveals depletion of immunosuppressive M2-like macrophages. Ann Oncol. 2019;30(8):1381-92.

114. Verza FA, Das U, Fachin AL, Dimmock JR, Marins M. Roles of Histone Deacetylases and Inhibitors in Anticancer Therapy. Cancers (Basel). 2020;12(6):1664.

115. Li X, Su X, Liu R, Pan Y, Fang J, Cao L, et al. HDAC inhibition potentiates anti-tumor activity of macrophages and enhances anti-PD-L1-mediated tumor suppression. Oncogene. 2021;40(10):1836-50.

116. Ny L, Jespersen H, Karlsson J, Alsen S, Filges S, All-Eriksson C, et al. The PEMDAC phase 2 study of pembrolizumab and entinostat in patients with metastatic uveal melanoma. Nat Commun. 2021;12(1):5155.

117. Serafini P, Carbley R, Noonan KA, Tan G, Bronte V, Borrello I. High-dose granulocyte-macrophage colony-stimulating factor-producing vaccines impair the immune response through the recruitment of myeloid suppressor cells. Cancer Res. 2004;64(17):6337-43.

118. Meyer C, Sevko A, Ramacher M, Bazhin AV, Falk CS, Osen W, et al. Chronic inflammation promotes myeloid-derived suppressor cell activation blocking antitumor immunity in transgenic mouse melanoma model. Proc Natl Acad Sci U S A. 2011;108(41):17111-6.

119. Hassel JC, Jiang H, Bender C, Winkler J, Sevko A, Shevchenko I, et al. Tadalafil has biologic activity in human melanoma. Results of a pilot trial with Tadalafil in patients with metastatic Melanoma (TaMe). Oncoimmunology. 2017;6(9):e1326440.

120. Pinton L, Solito S, Damuzzo V, Francescato S, Pozzuoli A, Berizzi A, et al. Activated T cells sustain myeloid-derived suppressor cell-mediated immune suppression. Oncotarget. 2016;7(2):1168-84.

121. Xin H, Zhang C, Herrmann A, Du Y, Figlin R, Yu H. Sunitinib inhibition of Stat3 induces renal cell carcinoma tumor cell apoptosis and reduces immunosuppressive cells. Cancer Res. 2009;69(6):2506-13.

122. Liu F, Cao J, Wu J, Sullivan K, Shen J, Ryu B, et al. Stat3-targeted therapies overcome the acquired resistance to vemurafenib in melanomas. J Invest Dermatol. 2013;133(8):2041-9.

123. Wong ALA, Hirpara JL, Pervaiz S, Eu JQ, Sethi G, Goh BC. Do STAT3 inhibitors have potential in the future for cancer therapy? Expert Opin Investig Drugs. 2017;26(8):883-7.

124. Bitsch R, Kurzay A, Ozbay Kurt F, De La Torre C, Lasser S, Lepper A, et al. STAT3 inhibitor Napabucasin abrogates MDSC immunosuppressive capacity and prolongs survival of melanoma-bearing mice. J Immunother Cancer. 2022;10(3):e004384.

125. Nandre R, Verma V, Gaur P, Patil V, Yang X, Ramlaoui Z, et al. IDO Vaccine Ablates Immune-Suppressive Myeloid Populations and Enhances Antitumor Effects Independent of Tumor Cell IDO Status. Cancer Immunol Res. 2022;10(5):571-80.

126. Kjeldsen JW, Lorentzen CL, Martinenaite E, Ellebaek E, Donia M, Holmstroem RB, et al. A phase 1/2 trial of an immune-modulatory vaccine against IDO/PD-L1 in combination with nivolumab in metastatic melanoma. Nat Med. 2021;27(12):2212-23.

127. Mirza N, Fishman M, Fricke I, Dunn M, Neuger AM, Frost TJ, et al. All-trans-retinoic acid improves differentiation of myeloid cells and immune response in cancer patients. Cancer Res. 2006;66(18):9299-307.

128. Kusmartsev S, Cheng F, Yu B, Nefedova Y, Sotomayor E, Lush R, et al. All-trans-retinoic acid eliminates immature myeloid cells from tumor-bearing mice and improves the effect of vaccination. Cancer Res. 2003;63(15):4441-9.

129. Tobin RP, Cogswell DT, Cates VM, Davis DM, Borgers JSW, Van Gulick RJ, et al. Targeting MDSC differentiation using ATRA: a phase I/II clinical trial combining pembrolizumab and all-trans retinoic acid for metastatic melanoma. Clin Cancer Res. 2023;29(7):1209-1219.

130. Veglia F, Tyurin VA, Blasi M, De Leo A, Kossenkov AV, Donthireddy L, et al. Fatty acid transport protein 2 reprograms neutrophils in cancer. Nature. 2019;569(7754):73-8.

131. Hossain F, Al-Khami AA, Wyczechowska D, Hernandez C, Zheng L, Reiss K, et al. Inhibition of Fatty Acid Oxidation Modulates Immunosuppressive Functions of Myeloid-Derived Suppressor Cells and Enhances Cancer Therapies. Cancer Immunol Res. 2015;3(11):1236-47.

132. Xia C, Yin S, To KKW, Fu L. CD39/CD73/A2AR pathway and cancer immunotherapy. Mol Cancer. 2023;22(1):44.

133. Goulopoulou S, McCarthy CG, Webb RC. Toll-like Receptors in the Vascular System: Sensing the Dangers Within. Pharmacol Rev. 2016;68(1):142-67.

134. Sfanos KS. Targeting Toll-like Receptors in Cancer Prevention. Cancer Prev Res (Phila). 2018;11(5):251-4.

135. Jang GY, Lee JW, Kim YS, Lee SE, Han HD, Hong KJ, et al. Interactions between tumor-derived proteins and Toll-like receptors. Exp Mol Med. 2020;52(12):1926-35.

136. O'Neill LA, Bowie AG. The family of five: TIR-domain-containing adaptors in Toll-like receptor signalling. Nat Rev Immunol. 2007;7(5):353-64.

137. Kawai T, Akira S. Signaling to NF-kappaB by Toll-like receptors. Trends Mol Med. 2007;13(11):460-9.

138. Honda K, Takaoka A, Taniguchi T. Type I interferon [corrected] gene induction by the interferon regulatory factor family of transcription factors. Immunity. 2006;25(3):349-60.

139. Wesche H, Henzel WJ, Shillinglaw W, Li S, Cao Z. MyD88: an adapter that recruits IRAK to the IL-1 receptor complex. Immunity. 1997;7(6):837-47.

140. Kawai T, Akira S. Regulation of innate immune signalling pathways by the tripartite motif (TRIM) family proteins. EMBO Mol Med. 2011;3(9):513-27.

141. Yamamoto M, Sato S, Hemmi H, Hoshino K, Kaisho T, Sanjo H, et al. Role of adaptor TRIF in the MyD88-independent toll-like receptor signaling pathway. Science. 2003;301(5633):640-3.

142. Li J, Yang F, Wei F, Ren X. The role of toll-like receptor 4 in tumor microenvironment. Oncotarget. 2017;8(39):66656-67.

143. Duan T, Du Y, Xing C, Wang HY, Wang RF. Toll-Like Receptor Signaling and Its Role in Cell-Mediated Immunity. Front Immunol. 2022;13:812774.

144. Zhou H, Jiang M, Yuan H, Ni W, Tai G. Dual roles of myeloid-derived suppressor cells induced by Toll-like receptor signaling in cancer. Oncol Lett. 2021;21(2):149.

145.   Bunt SK, Clements VK, Hanson EM, Sinha P, Ostrand-Rosenberg S. Inflammation enhances myeloid-derived suppressor cell cross-talk by signaling through Toll-like receptor 4. J Leukoc Biol. 2009;85(6):996-1004.

146.   Chuah YK, Basir R, Talib H, Tie TH, Nordin N. Receptor for advanced glycation end products and its involvement in inflammatory diseases. Int J Inflam. 2013;2013:403460.

147.   Palanissami G, Paul SFD. RAGE and Its Ligands: Molecular Interplay Between Glycation, Inflammation, and Hallmarks of Cancer-a Review. Horm Cancer. 2018;9(5):295-325.

148.   Origlia N, Arancio O, Domenici L, Yan SS. MAPK, beta-amyloid and synaptic dysfunction: the role of RAGE. Expert Rev Neurother. 2009;9(11):1635-45.

149.   Faruqui T, Khan MS, Akhter Y, Khan S, Rafi Z, Saeed M, et al. RAGE Inhibitors for Targeted Therapy of Cancer: A Comprehensive Review. Int J Mol Sci. 2022;24(1):266.

150.   Kang R, Hou W, Zhang Q, Chen R, Lee YJ, Bartlett DL, et al. RAGE is essential for oncogenic KRAS-mediated hypoxic signaling in pancreatic cancer. Cell Death Dis. 2014;5(10):e1480.

151.   Wuren T, Huecksteadt T, Beck E, Warren K, Hoidal J, Ostrand-Rosenberg S, et al. The receptor for advanced glycation endproducts (RAGE) decreases survival of tumor-bearing mice by enhancing the generation of lung metastasis-associated myeloid-derived suppressor cells. Cell Immunol. 2021;365:104379.

152.   Azizian-Farsani F, Abedpoor N, Hasan Sheikhha M, Gure AO, Nasr-Esfahani MH, Ghaedi K. Receptor for Advanced Glycation End Products Acts as a Fuel to Colorectal Cancer Development. Front Oncol. 2020;10:552283.

153.   Ostrand-Rosenberg S, Huecksteadt T, Sanders K. The Receptor for Advanced Glycation Endproducts (RAGE) and Its Ligands S100A8/A9 and High Mobility Group Box Protein 1 (HMGB1) Are Key Regulators of Myeloid-Derived Suppressor Cells. Cancers (Basel). 2023;15(4):1026.

154.   Somogyvari M, Khatatneh S, Soti C. Hsp90: From Cellular to Organismal Proteostasis. Cells. 2022;11(16):2479.

155.   Albakova Z, Mangasarova Y, Albakov A, Gorenkova L. HSP70 and HSP90 in Cancer: Cytosolic, Endoplasmic Reticulum and Mitochondrial Chaperones of Tumorigenesis. Front Oncol. 2022;12:829520.

156.   Pennisi R, Ascenzi P, di Masi A. Hsp90: A New Player in DNA Repair? Biomolecules. 2015;5(4):2589-618.

157.   Miyata Y, Nakamoto H, Neckers L. The therapeutic target Hsp90 and cancer hallmarks. Curr Pharm Des. 2013;19(3):347-65.

158.   Birbo B, Madu EE, Madu CO, Jain A, Lu Y. Role of HSP90 in Cancer. Int J Mol Sci. 2021;22(19):10317.

159. Huang B, Pan J, Liu H, Tang Y, Li S, Bian Y, et al. High Expression of Plasma Extracellular HSP90alpha is Associated With the Poor Efficacy of Chemotherapy and Prognosis in Small Cell Lung Cancer. Front Mol Biosci. 2022;9:913043.

160. Wang X, An D, Wang X, Liu X, Li B. Extracellular Hsp90alpha clinically correlates with tumor malignancy and promotes migration and invasion in esophageal squamous cell carcinoma. Onco Targets Ther. 2019;12:1119-28.

161. Ehrchen JM, Sunderkotter C, Foell D, Vogl T, Roth J. The endogenous Toll-like receptor 4 agonist S100A8/S100A9 (calprotectin) as innate amplifier of infection, autoimmunity, and cancer. J Leukoc Biol. 2009;86(3):557-66.

162. Vogl T, Gharibyan AL, Morozova-Roche LA. Pro-inflammatory S100A8 and S100A9 proteins: self-assembly into multifunctional native and amyloid complexes. Int J Mol Sci. 2012;13(3):2893-917.

163. Wang S, Song R, Wang Z, Jing Z, Wang S, Ma J. S100A8/A9 in Inflammation. Front Immunol. 2018;9:1298.

164. Srikrishna G. S100A8 and S100A9: new insights into their roles in malignancy. J Innate Immun. 2012;4(1):31-40.

165. Huang M, Wu R, Chen L, Peng Q, Li S, Zhang Y, et al. S100A9 Regulates MDSCs-Mediated Immune Suppression via the RAGE and TLR4 Signaling Pathways in Colorectal Carcinoma. Front Immunol. 2019;10:2243.

166. Wang L, Chang EW, Wong SC, Ong SM, Chong DQ, Ling KL. Increased myeloid-derived suppressor cells in gastric cancer correlate with cancer stage and plasma S100A8/A9 proinflammatory proteins. J Immunol. 2013;190(2):794-804.

167. Chen R, Kang R, Tang D. The mechanism of HMGB1 secretion and release. Exp Mol Med. 2022;54(2):91-102.

168. Tripathi A, Shrinet K, Kumar A. HMGB1 protein as a novel target for cancer. Toxicol Rep. 2019;6:253-61.

169. Wu T, Zhang W, Yang G, Li H, Chen Q, Song R, et al. HMGB1 overexpression as a prognostic factor for survival in cancer: a meta-analysis and systematic review. Oncotarget. 2016;7(31):50417-27.

170. Jin S, Yang Z, Hao X, Tang W, Ma W, Zong H. Roles of HMGB1 in regulating myeloid-derived suppressor cells in the tumor microenvironment. Biomark Res. 2020;8:21.

171. Li J, Sun J, Rong R, Li L, Shang W, Song D, et al. HMGB1 promotes myeloid-derived suppressor cells and renal cell carcinoma immune escape. Oncotarget. 2017;8(38):63290-8.

172. Smyth GK. Linear models and empirical bayes methods for assessing differential expression in microarray experiments. Stat Appl Genet Mol Biol. 2004;3:Article3.

173. Ritchie ME, Phipson B, Wu D, Hu Y, Law CW, Shi W, et al. limma powers differential expression analyses for RNA-sequencing and microarray studies. Nucleic Acids Res. 2015;43(7):e47.

174.	Wu D, Smyth GK. Camera: a competitive gene set test accounting for inter-gene correlation. Nucleic Acids Res. 2012;40(17):e133.

175.	Van Allen EM, Miao D, Schilling B, Shukla SA, Blank C, Zimmer L, et al. Genomic correlates of response to CTLA-4 blockade in metastatic melanoma. Science. 2015;350(6257):207-11.

176.	Matsunaga N, Tsuchimori N, Matsumoto T, Ii M. TAK-242 (resatorvid), a small-molecule inhibitor of Toll-like receptor (TLR) 4 signaling, binds selectively to TLR4 and interferes with interactions between TLR4 and its adaptor molecules. Mol Pharmacol. 2011;79(1):34-41.

177.	Deane R, Singh I, Sagare AP, Bell RD, Ross NT, LaRue B, et al. A multimodal RAGE-specific inhibitor reduces amyloid beta-mediated brain disorder in a mouse model of Alzheimer disease. J Clin Invest. 2012;122(4):1377-92.

178.	Yamada M, Ichikawa T, Ii M, Sunamoto M, Itoh K, Tamura N, et al. Discovery of novel and potent small-molecule inhibitors of NO and cytokine production as antisepsis agents: synthesis and biological activity of alkyl 6-(N-substituted sulfamoyl)cyclohex-1-ene-1-carboxylate. J Med Chem. 2005;48(23):7457-67.

179.	Bruger AM, Dorhoi A, Esendagli G, Barczyk-Kahlert K, van der Bruggen P, Lipoldova M, et al. How to measure the immunosuppressive activity of MDSC: assays, problems and potential solutions. Cancer Immunol Immunother. 2019;68(4):631-44.

180.	Heine A, Held SAE, Schulte-Schrepping J, Wolff JFA, Klee K, Ulas T, et al. Generation and functional characterization of MDSC-like cells. Oncoimmunology. 2017;6(4):e1295203.

181.	Lechner MG, Liebertz DJ, Epstein AL. Characterization of cytokine-induced myeloid-derived suppressor cells from normal human peripheral blood mononuclear cells. J Immunol. 2010;185(4):2273-84.

182.	Li ZN, Luo Y. HSP90 inhibitors and cancer: Prospects for use in targeted therapies (Review). Oncol Rep. 2023;49(1):6.

183.	Wang L, Wu J, Guo X, Huang X, Huang Q. RAGE Plays a Role in LPS-Induced NF-kappaB Activation and Endothelial Hyperpermeability. Sensors (Basel). 2017;17(4):722.

184.	Zanoni I, Ostuni R, Marek LR, Barresi S, Barbalat R, Barton GM, et al. CD14 controls the LPS-induced endocytosis of Toll-like receptor 4. Cell. 2011;147(4):868-80.

185.	Liu E, Tu W, Law HK, Lau YL. Changes of CD14 and CD1a expression in response to IL-4 and granulocyte-macrophage colony-stimulating factor are different in cord blood and adult blood monocytes. Pediatr Res. 2001;50(2):184-9.

186.	Sakaguchi M, Murata H, Yamamoto K, Ono T, Sakaguchi Y, Motoyama A, et al. TIRAP, an adaptor protein for TLR2/4, transduces a signal from RAGE phosphorylated upon ligand binding. PLoS One. 2011;6(8):e23132.

187.	Zhong H, Li X, Zhou S, Jiang P, Liu X, Ouyang M, et al. Interplay between RAGE and TLR4 Regulates HMGB1-Induced Inflammation by Promoting Cell Surface Expression of RAGE and TLR4. J Immunol. 2020;205(3):767-75.

188.   Prantner D, Nallar S, Vogel SN. The role of RAGE in host pathology and crosstalk between RAGE and TLR4 in innate immune signal transduction pathways. FASEB J. 2020;34(12):15659-74.

189.   Sutti S, Bruzzi S, Heymann F, Liepelt A, Krenkel O, Toscani A, et al. CX(3)CR1 Mediates the Development of Monocyte-Derived Dendritic Cells during Hepatic Inflammation. Cells. 2019;8(9).

190.   Blohm-Mangone K, Burkett NB, Tahsin S, Myrdal PB, Aodah A, Ho B, et al. Pharmacological TLR4 Antagonism Using Topical Resatorvid Blocks Solar UV-Induced Skin Tumorigenesis in SKH-1 Mice. Cancer Prev Res (Phila). 2018;11(5):265-78.

191.   Hegde S, Leader AM, Merad M. MDSC: Markers, development, states, and unaddressed complexity. Immunity. 2021;54(5):875-84.

192.   Gebhardt C, Sevko A, Jiang H, Lichtenberger R, Reith M, Tarnanidis K, et al. Myeloid Cells and Related Chronic Inflammatory Factors as Novel Predictive Markers in Melanoma Treatment with Ipilimumab. Clin Cancer Res. 2015;21(24):5453-9.

193.   Wagner NB, Weide B, Gries M, Reith M, Tarnanidis K, Schuermans V, et al. Tumor microenvironment-derived S100A8/A9 is a novel prognostic biomarker for advanced melanoma patients and during immunotherapy with anti-PD-1 antibodies. J Immunother Cancer. 2019;7(1):343.

194.   Deguchi A, Watanabe-Takahashi M, Mishima T, Omori T, Ohto U, Arashiki N, et al. Novel multivalent S100A8 inhibitory peptides attenuate tumor progression and metastasis by inhibiting the TLR4-dependent pathway. Cancer Gene Ther. 2023:1-12.

195.   Al-Khami AA, Zheng L, Del Valle L, Hossain F, Wyczechowska D, Zabaleta J, et al. Exogenous lipid uptake induces metabolic and functional reprogramming of tumor-associated myeloid-derived suppressor cells. Oncoimmunology. 2017;6(10):e1344804.

196.   Deguchi A, Tomita T, Ohto U, Takemura K, Kitao A, Akashi-Takamura S, et al. Eritoran inhibits S100A8-mediated TLR4/MD-2 activation and tumor growth by changing the immune microenvironment. Oncogene. 2016;35(11):1445-56.

197.   Riehl A, Nemeth J, Angel P, Hess J. The receptor RAGE: Bridging inflammation and cancer. Cell Commun Signal. 2009;7:12.

198.   Li Q, Li J, Wen T, Zeng W, Peng C, Yan S, et al. Overexpression of HMGB1 in melanoma predicts patient survival and suppression of HMGB1 induces cell cycle arrest and senescence in association with p21 (Waf1/Cip1) up-regulation via a p53-independent, Sp1-dependent pathway. Oncotarget. 2014;5(15):6387-403.

Acknowledgements